RNA interference approaches and assessment of new delivery systems to target heparanase in soft tissue sarcomas

Thesis

The Open University
Milton Keynes, United Kingdom

Affiliated Research Centre
Fondazione IRCCS **Istituto Nazionale dei Tumori**
Milano, Italia

RNA interference approaches and assessment of new delivery systems to target heparanase in soft tissue sarcomas

Thesis presented for the Degree of Doctor of Philosophy

The Open University, Milton Keynes (UK)

School of Life, Health and Chemical Sciences

Noemi Arrighetti
M.Sc. in Medical Biotechnology
Personal identifier: E4113458

March, 2019

The aim of science is not to open the door to infinite wisdom, but to set a limit to infinite error.

— Bertolt Brecht, Life of Galileo

ABSTRACT

Soft tissue sarcomas are rare tumours of mesenchymal origin characterised by high biomolecular complexity and heterogeneity. The clinical management of advanced diseases remains a major challenge which needs new therapeutic strategies.

Mounting evidence supports that the heparanase/heparan sulfate proteoglycan system plays a key role in sustaining tumour progression and dissemination and preclinical studies suggest its potential relevance as a therapeutic target.

To better understand the specific role of heparanase, we performed RNA interference in rhabdoid tumour and synovial sarcoma models, and assessed the functional effects of heparanase silencing. We tested both miRNA and siRNA targeting heparanase, but only siRNAs were able to silence mRNA and down-regulate the protein following transient transfection. The reduced expression and enzymatic activity of secreted heparanase observed upon siRNA transfection were consistent with a strong inhibition of cell migration and invasion capability. The expression of pro-angiogenic factors was also reduced both in rhabdoid tumour and synovial sarcoma cell lines. In contrast, we observed that heparanase localised in specific subcellular compartments was resistant to the siRNA effect.

The clinical application of siRNA-based therapeutic strategies faces significant challenges, mainly due to siRNA *in vivo* poor stability and inefficient delivery. In this work, we evaluated the use of different nanodelivery systems aimed at overcoming these limitations.

The first approach consisted of hybrid nanoparticles with a silica core and a pH-responsive hydrogel shell. These nanoparticles showed promising features, such as remarkable loading and efficient release of siRNA, endo-lysosomal escape and *in vivo* accumulation at the tumour site. Nevertheless, siRNA delivered through this approach did not inhibit heparanase expression. The second nanodelivery system was leukosome, a biomimetic nanoparticle with leukocyte proteins included in a phospholipidic bilayer. Leukosomes efficiently delivered siRNA into the cells avoiding the endo-lysosomal entrapment.

Moreover, these biomimetic nanoparticles mainly accumulated at the tumour primary and metastatic sites. Despite these promising features, also leukosomes were unable to deliver an active siRNA.

Overall, these findings demonstrate that specific inhibition of heparanase by gene silencing is a potential therapeutic approach for soft tissue sarcoma treatment. However, the siRNA delivery systems tested in this work, although promising in terms of tumour and metastasis targeting, still need further improvement to be suitable for nucleic acid delivery.

This study was conducted under the supervision of Drs. Cinzia Lanzi and Paola Perego at the Molecular Pharmacology Unit, headed by Dr. Nadia Zaffaroni, at the Department of Applied Research & Technological Development, Fondazione IRCCS Istituto Nazionale dei Tumori, Milano, Italy.

Part of the project was carried out under the supervision of Drs. Ennio Tasciotti, Alessandro Parodi, Francesca Taraballi and Roberto Molinaro at the Center for Biomimetic Medicine, Houston Methodist Research Institute, Houston, TX, USA.

TABLE OF CONTENTS

LIST OF FIGURES AND TABLES

ABBREVIATIONS

AFM	Atomic force microscopy
AT/RT	Atypical teratoid rhabdoid tumour
BCA	Bicinchoninic acid
BSA	Bovine serum albumin
CHOL	Cholesterol
Ct	Cycle threshold
CTLA-4	Cytotoxic T cell lymphocyte-associated protein 4
CXCL16	Chemokine (C-X-C motif) ligand 16
Dh	Hydrodynamic diameters
DLS	Dynamic light scattering
DOPC	1,2-dioleoyl-sn-glycero-3-phosphocholine
DPPC	Dipalmitoylphosphatidylcholine
DSPC	1,2-Distearoyl-sn-glycero-3-phosphocholine
ECM	Extracellular matrix
ELISA	Enzyme-linked immunosorbent assays
EZH2	Enhancer of zeste homolog 2
FACS	Fluorescence activated cell sorting
FBS	Fetal bovine serum
FGF	Fibroblast growth factor
FT-IR	Fourier transform infrared
HATs	Histone acetyltransferases
HDAC	Histone deacetylase
HGF	Hepatocyte growth factor
HMRI	Houston Methodist Research Institute
HNP	Hybrid nanogel particle
HPSE	Heparanase
HS	Heparan-sulfate
HSPGs	Heparan sulfate proteoglycans
IF	Immunofluorescence
IVM	Intravital microscopy
KBr	Potassium bromide
KRT	Rhabdoid tumour of the kidney
miRNA	MicroRNA
MMP-9	Matrix metallopeptidase 9
mRNA	Messenger RNA
MRT	Malignant rhabdoid tumour
MTT	3-(4,5-dimethylthiazol-2-yl)- 2,5-diphenyltetrazolium bromide
N/P	Amino/phosphate
Neg Ctr	Negative Control
O/N	Overnight
PB	Phosphate buffer
PBS	Phosphate-buffered saline
PD-1	Programmed death receptor 1
PDEAEM	Poly(diethylaminoethyl methacrylate)
PDGF	Platelet-derived growth factor

PDI	Polydispersity index
PDL-1	Programmed death receptor 1 ligand
PEGMA	Polyethylene glycol methacrylate
PEI	Polyethylenimine
PI	Propidium iodide
PRC	Polycomb repressive complex
pre-miRNA	Precursor microRNA
pri-miRNA	Primary microRNA
qRT-PCR	Quantitative reverse transcription polymerase chain reaction
RISC	RNA-induced silencing complex
RNAi	RNA interference
RQ	Relative quantification
RT	Rhabdoid tumour
RTKs	Receptor tyrosine kinases
SDS	Sodium dodecyl sulfate
SEM	Scanning electron microscope
siRNA	Small interfering RNA
SMARCB1	SWI/SNF-related matrix-associated actin-dependent regulator of chromatin subfamily B member
SRB	Sulforhodamine B
SS	Synovial sarcoma
STS	Soft tissue sarcoma
SWI/SNF	Switch/sucrose son-fermentable
TBS	Tris-buffered saline
TEGDMA	Triethylene glycol dimethacrylate
TEM	Transmission electron microscopy
TF	Tissue Factor/Coagulation Factor III
TLE	Thin layer evaporation
uPA	Urokinase-type Plasminogen Activator
VEGF	Vascular endothelial growth factor
WGA	Wheat germ agglutinin

1.INTRODUCTION

1.1. Soft tissue sarcomas

The word ‘sarcoma’ is derived from the Greek σάρξ (sárx, “flesh”) -ωμα (ōma, “process”). Soft tissue sarcomas (STSs) are rare malignancies accounting for 1% of all cancers in adults and nearly 10% in children and adolescents [Siegel R.L. et al., 2018]. STSs arise from the embryonic mesoderm tissue, usually from connective, muscle, adipose, neural, vascular, or lymphatic tissues [Gilbert N.F. et al., 2009]. The most common onset location of sarcoma is in the extremities (arms, legs, hands, or feet), but it can also occur in the trunk (chest, back, hips, shoulders or abdomen), in the retroperitoneum or in head and neck; the anatomic site of the primary disease is an important variable influencing treatment and outcome. STSs tend to invade surrounding tissues and give rise to metastases in 50% of patients, especially in lymph nodes and lungs, whereas tumours arising in the abdominal cavity commonly metastasise to the liver and peritoneum [Cormier J.N. and Pollock R.E., 2004]. STSs constitute a highly heterogeneous family of malignancies comprising more than 50 subtypes. They can be classified according to the 2013 World Health Organization Classification of Tumours of Soft Tissue and Bone in twelve main groups [Fletcher C.D., 2013]:

(1) Adipocytic tumours

(2) Fibroblastic/myofibroblastic tumours

(3) The so-called fibrohistiocytic tumours

(4) Smooth muscle tumours

(5) Pericytic (perivascular) tumours

(6) Skeletal muscle tumours

(7) Vascular tumours

(8) Gastrointestinal stromal tumours

(9) Nerve sheath tumours

(10) Chondro-osseous tumours

(11) Tumours of uncertain differentiation

(12) Undifferentiated/unclassified sarcomas

Depending on the biological behaviour, they are sub-categorised in: benign, intermediate locally aggressive, intermediate rarely metastasising, or malignant [Wei S. et al., 2017].

The aetiology of most STSs remains unknown. Genetic factors (*i.e.*, neurofibromatosis, retinoblastoma, Li-Fraumeni syndrome, Gardner's syndrome), environmental factors (exposure to environmental carcinogens such as dioxin and some herbicides, trauma, injury or previous ionising radiation exposure), and immunological factors such as immunosuppression after transplant surgery, have been identified as predisposing aetiological factors in STS development [Zahm S.H. and Fraumeni J.F. Jr., 1997; Thomas D.M. et al., 2012]. As in other malignancies, it is very unlikely that a single factor causes the disease, but a multifactorial aetiology is likely.

Based on genetic alterations, STSs can be divided into two major categories: the first one characterised by the presence of specific chromosomal translocations or mutations and a near-diploid karyotype, more frequent in young patients; the second one, which accounts for about 50% of STS, exhibiting complex karyotypes with non-specific chromosomal rearrangements, but presenting frequent genetic gain or losses characteristic of unstable genome [de Alava E., 2007].

Sarcoma specific translocations produce fusion genes that mainly encode aberrant transcription factors or transcription regulators, such as PAX3/7-FKHR in alveolar rhabdomyosarcomas, EWS-ETS in Ewing's sarcoma and SS18-SSX in synovial sarcoma (SS). The encoded hybrid oncoproteins induce aberrant transcription of target genes, stimulating various intracellular signaling pathways and resulting in cell proliferation, evasion from growth inhibition, escape from senescence, apoptosis and immune response, induction of angiogenesis, invasion and metastasis [Mitelman F. et al., 2007].

The experimental models used in this thesis included SS and rhabdoid tumour (RT), specifically, CME-1 SS cells and A204 RT cells.

1.1.1. Synovial sarcoma

SS is an aggressive tumour accounting for 10% to 20% of STSs, most prevalent in adolescent and young adults [Herzog C.E., 2005]. Despite its name, SS is unrelated to the synovial tissues. The disease arises in soft tissues of the extremities in 66% of cases, especially adjacent to large joints (thigh, knee, ankle, feet, and arms), but can occur anywhere in the body. SS is characterised by local invasiveness and propensity to metastasise, particularly to the lungs [Orbach D. et al., 2011]. The clinical behaviour varies from superficial indolent tumours to highly aggressive tumours that are capable of recurring locally or at distant sites years after surgical resection of the primary tumour.

Two main morphological tumour subtypes have been identified, *i.e.*, the biphasic and monophasic variants, although, in a few cases a poorly differentiated monophasic subtype has been reported [Begin L.R., 2003; Cascales P. et al., 2006; Rong R. et al., 2009]. The two subtypes are equally distributed in children, with 55% of monophasic subtypes and 45% of biphasic subtypes, whereas the monophasic subtype is more frequent in adults (72%). The biphasic SS morphology has been interpreted as a manifestation of aberrant mesenchymal to epithelial transition associated with interference by SS18-SSX oncogenes on E-cadherin repression [Saito T. et al., 2006]. However, the histological monophasic or biphasic subtypes have no prognostic impact [Orbach D. et al., 2011]. Distinction in monophasic or biphasic SS subtypes is based on the presence of spindle cells or both spindle and epithelial glandular cells, respectively. Monophasic SSs are entirely composed of packed spindle cells with no epithelial differentiation. Biphasic SSs are characterised by epithelial cells bearing ovoid nuclei and abundant cytoplasm areas of glandular differentiation in a background of spindle cells. The poorly differentiated variant is the

rarest and more aggressive SS subtype and presents dense cellularity, numerous mitotic figures, and areas of necrosis [Haldar M. et al., 2008].

Genetically, 95% of SSs are characterised by the chromosomal translocation t(X;18) which involves the SSX1, SSX2 or rarely SSX4 genes, closely related genes from chromosome Xp11, and the SS18 gene from chromosome 18q11. The translocation results in the formation of a chimeric gene encoding a chromatin remodeling fusion protein, which is able to induce transcriptional dysregulation [Brett D. et al., 1997] (Figure 1.1). Multiple studies concur to establish that the SS18-SSX translocation plays a role in this cancer: 1) most cases exhibit the translocation as the only cytogenetic abnormality and other mutations are rarely present [Panagopoulos I. et al., 2001; Joseph C.G. et al., 2014], 2) the translocation is maintained in metastatic and advanced lesions [Panagopoulos I. et al., 2001], 3) SS18-SSX knockdown causes SS cell death [Carmody Soni E.E. et al., 2014], and 4) the expression of the oncoprotein in immature myoblasts was shown to induce SS with 100% penetrance in a mouse model [Haldar M. et al., 2007]. This study strongly supports that the SS18-SSX translocation behaves as a driver in SSs.

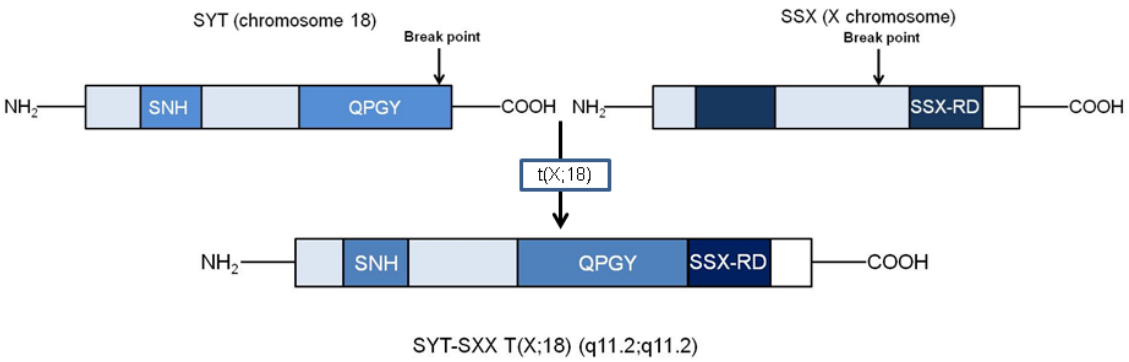

Figure 1.1. The SS18-SSX translocation.

The SS translocation involving the SS18 transcriptional activator on chromosome 18 and the SSX transcriptional repressor located on the X chromosome produces the fusion genes SS18–SSX1, SS18–SSX2, and rarely SS18–SSX4.

The crucial role for the fusion product in the pathogenesis of SS has been linked to its interference with the gene expression by epigenetic deregulation [Przybyl J. et al., 2012].

The current view is that SS18-SSX fusion proteins acquire novel functional properties accounting for oncogenic transformation, although the mechanism of the oncogenic activity has not been completely elucidated yet. Two recent studies proposed that the activity of SS18-SSX fusion proteins is mediated by protein-protein interactions that alter genetic programs through chromatin remodeling. In particular, SS18-SSX protein has been suggested to be incorporated into SWItch/sucrose non-fermentable (SWI/SNF/BAF) complexes replacing wild type SS18 and expelling SWI/SNF-related matrix-associated actin-dependent regulator of chromatin subfamily B member 1 (SMARCB1/BAF47). In this way, BAF complexes counteract polycomb repressive complex (PRC)2-mediated repression of transcription [McBride M.J. et al., 2018] (Figure 1.2, A). In addition, SS18-SSX containing BAF complexes have been shown to interact with the histone demethylase KDM2B within the PRC1.1 and to aberrantly activate the transcription of target genes involved in sarcoma cell transformation [Banito A. et al., 2018] (Figure 1.2, B). As a result, the epigenetic antagonism between BAF complexes (transcription promoters) and PCR2 (repressive complexes) would be altered leading to an abnormal transcriptional pattern that drives malignant transformation.

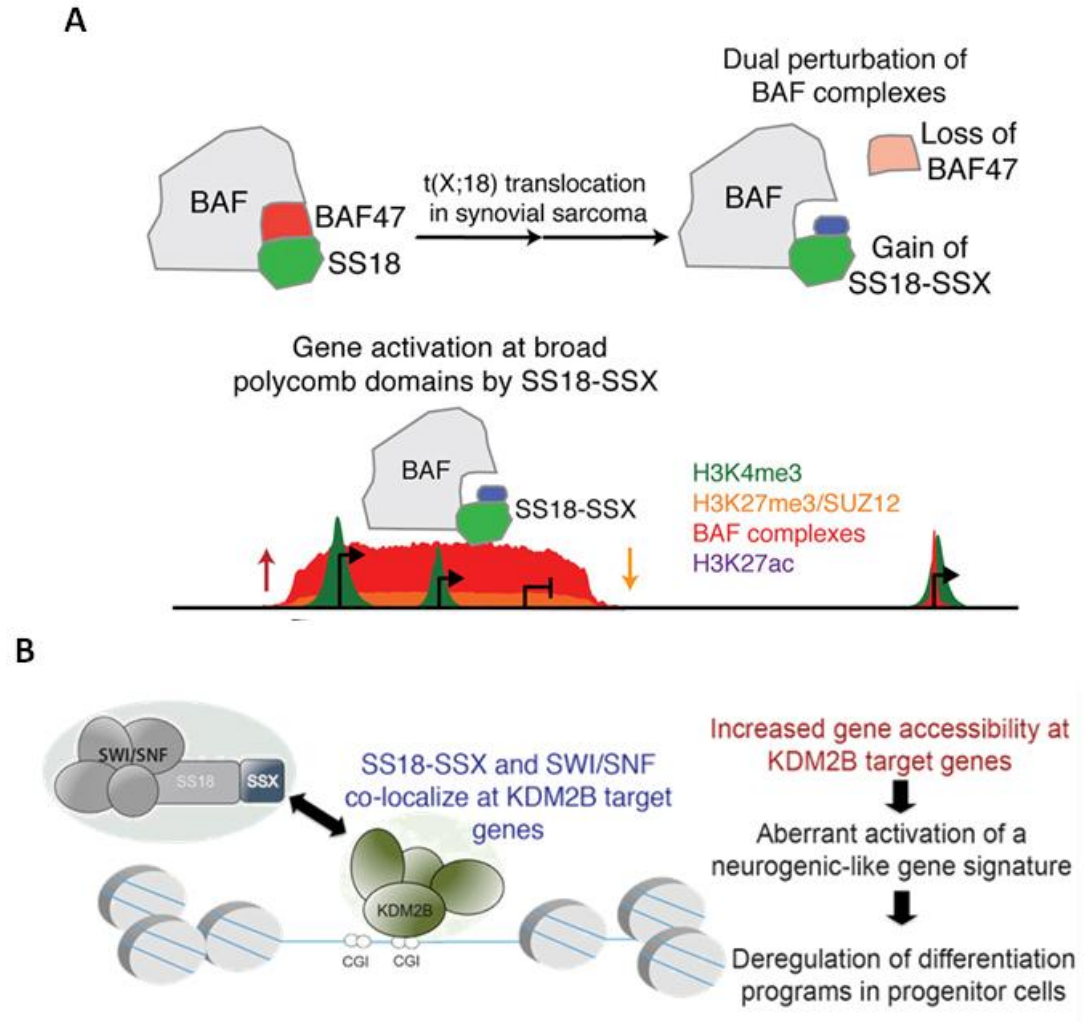

Figure 1.2. SS18-SSX fusion protein.

(A) Graphic representation of the interaction between SS18-SSX protein and BAF complexes and subsequent transcription activation [McBride M.J. et al., 2018]. (B) Graphic representation of the SWI/SNF activation mediated by SS18-SSX/KDM2B interaction, and subsequent aberrant transcription activation [Banito A. et al., 2018].

The fusion SS18-SSX genes are unique to SS and considered diagnostic markers for these tumours. Fluorescence *in situ* hybridisation and quantitative reverse transcription polymerase chain reaction (qRT-PCR) are used as diagnostic techniques to detect the chromosomal translocation and the fusion transcript, respectively [Takenaka S. et al., 2008; Saito T., 2013].

1.1.1.1 Synovial sarcoma therapy

Commonly, the first approach to SSs involves complete surgical resection of the tumour, which may be preceded or followed by radiotherapy. Post-operative radiotherapy and local excision can control local recurrence [Shwartz D.L. et al., 2002]. For metastatic SSs, the conventional front-line chemotherapy regimen containing anthracyclines and alkylating agents, exhibits limited advantages because of toxicity and eventual progression of the disease [Lange S.E.S. et al., 2014]. Moreover, prolonged treatment may induce severe adverse consequences, such as cardiotoxicity, infertility, and late effects affecting growth and development as well as the onset of secondary malignancies [Sultan I. et al., 2009]. The probability of recurrence of SS is approximately 50%, usually within 2 years, but there are cases of recurrence up to 30 years after diagnosis. About 40% of the tumours display metastatic spread, most commonly to the lungs with regional lymph node involvement. Advanced stage at presentation, positive surgical resection margins, larger tumour size (>5 cm) and non-extremity tumour site are all negative prognostic factors for SSs [Lewis J.J. et al., 2000]. The 5-year overall survival rate for the patients without metastases is about 80% whereas it is lower (10-25%) in case of metastatic disease [Wu Y. et al., 2017]. The poor prognosis for recurrent and metastatic SS highlights the need for new therapeutic approaches to improve treatment outcomes.

Besides conventional chemotherapy, targeted therapy has been explored extensively for SS treatment in an attempt to hit tumour features essential for tumour growth and progression. Multiple receptor tyrosine kinase (RTK)-mediated signaling pathways are active in SS and are implicated in angiogenesis [*e.g.*, vascular endothelial growth factor (VEGF), platelet-derived growth factor (PDGF), fibroblast growth factor (FGF) and their receptors] [El Beaino M. et al., 2017]. Therefore, agents against these factors are among the commonly investigated targeted therapeutics. Several anti-angiogenic therapies have been tested in clinical trials, including multi-RTKs inhibitors (*i.e.*, pazopanib, sorafenib, sunitinib,

regorafenib, imatinib and gefitinib), and the monoclonal antibodies bevacizumab (anti-VEGF) and olaratumab (anti-PDGFRα) [https://clinicaltrials.gov]. Among these, only pazopanib (votrient), a RTK inhibitor targeting VEGFR and PDGFR family members and c-kit, and olaratumab gained approval in 2012 and 2016, respectively, for the treatment of advanced STS, including SS, in patients who received prior chemotherapy [Desar I.M.E. et al., 2018].

The insulin-like growth factor (IGF) system, which regulates downstream pathways involved in cell proliferation and apoptosis inhibition, is another target for SS therapy. In detail, IGF-II and the receptor IGF-1R have been found up-regulated in SSs due to IGF-II induction mediated by SS18-SSX fusion proteins. Moreover, IGF-1R over-expression has been associated with higher metastatic dissemination in SSs [Xie Y. et al., 1999; de Bruijn D. R. et al., 2006; Sun Y. et al., 2006]. Clinical trials of cixutumumab, an anti-IGF-1R monoclonal antibody, have been carried out and obtained stable disease as the best response in a few SS patients [https://clinicaltrials.gov].

The PI3K/Akt/mTOR signaling pathway, which promotes cell proliferation and anti-apoptotic survival responses, is dysregulated in SS and associated with aggressive clinical behaviour [Setsu N. et al., 2013]. Inhibitors of mTOR, such as temsirolimus and everolimus, have been included in clinical trials for patients with advanced sarcoma, including SS [https://clinicaltrials.gov].

The WNT-β catenin signaling pathway is activated in a subset of SS and its inhibitors have been found to have anti-tumour effects in preclinical studies [Trautmann M. et al., 2014; Barham W. et al., 2013]. ^{90}Y-OTSA 101, a radiolabeled monoclonal antibody directed against the WNT receptor FZD10, is under investigation in a clinical trial in patients with progressive advanced SS [Giraudet A.L. et al., 2018].

The Hedgehog pathway, a major regulator of stem cell maintenance, cell differentiation and proliferation, is aberrantly activated in a variety of human cancers including soft tissue

and bone sarcomas [Almazan-Moga A. et al., 2017; Kumar R.M. and Fuchs B., 2015]. GLI is a transcription factor that, activated by the Hedgehog signaling, induces target gene transcription; it is known that the inappropriate activation of Hedgehog signaling leads to the growth, proliferation, and invasion of tumour cells [Skoda A.M. et al., 2018]. Vismodegib, an inhibitor of this pathway, has been evaluated in combination with RO4929097, a Notch signaling pathway inhibitor, in a Phase II clinical trial in advance STS patients, including SS patients, and obtained a stable disease in about half of the patients [https://clinicaltrials.gov].

Since the fusion protein SS18-SSX is a peculiar feature of SS and acts as the disease driver, it is attractive for investigation of the possibility to develop a specific target therapy. Natarajan V. and colleagues evaluated the use of small molecules that bind the junction region of the SS18-SSX1 fusion protein by applying an *in silico* drug screening based on molecular docking. In this study, the authors identified a compound (FPTI) able to inhibit SS cell proliferation with some selectivity [Natarajan V. et al., 2018].

Other epigenetic regulators involved in cancer progression have been investigated as potential targets in preclinical and clinical studies; particular attention has been paid to histone deacetylases (HDACs) and the methyltransferase enhancer of zeste homolog 2 (EZH2). The HDAC inhibitor vorinostat and the EZH2 inhibitor tazemetostat have been tested in clinical trials in STS patients. No objective responses were achieved but a stable disease was obtained as the best response [Desar I.M.E. et al., 2018].

One of the most promising new therapeutic approaches for SS involves the targeting of the tumour microenvironment and will be discussed in chapter 3.1.1.

1.1.2. Rhabdoid tumours

Rhabdoid tumour (RT) is a rare aggressive malignant tumour that may affect brain [Atypical teratoid rhabdoid tumour (AT/RT)], kidney [Rhabdoid tumour of the kidney

(KRT)], or extrarenal soft tissues [Malignant rhabdoid tumour (MRT)]. The most common soft tissues affected by MRT are liver, skin and lung, but it can arise almost in all soft tissues [Wu X. et al., 2008]. The incidence of RT is higher in children between 1 and 4 years, although it can occur also in adults [Leong F.J. and Leong A.S., 1996]. Rhabdoid cells exhibit filamentous cytoplasmic inclusions, large nucleoli and eosinophilic cytoplasm. Histology of RT is characterised by heterogeneous morphology with neural, epithelial, mesenchymal, or ependymal patterns, making diagnosis difficult [Parham D.M. et al., 1994].

All RTs present homozygous loss or expression mutations of the tumour suppressor SMARCB1/INI1/hSNF5/BAF47 gene [Versteege I. et al., 1998; Biegel J.A. et al., 1999]. Thereby, diagnosis is usually confirmed by loss of nuclear staining of SMARCB1 protein by immunohistochemistry. SMARCB1 is a core subunit of the SWI/SNF chromatin remodeling complex, the same epigenetic regulator of gene transcription implicated in SSs. The SWI/SNF complex remodels chromatin by regulating the positions of nucleosomes and reducing the density of DNA, therefore allowing gene transcription activation. Mutations of SMARCB1 are sufficient and necessary to cause cancer [Geller J.I. et al., 2015]. The SWI/SNF complex competes for chromatin binding with the PRC2, whose catalytic subunit EZH2 is a histone methyltransferase which carries out the trimethylation of histone 3 at lysine 27, inducing gene expression repression (Figure 1.3). The inactivation of SMARCB1 leads to an elevated expression of EZH2 and consequently the down-regulation of various tumour suppressors' expression [Wilson B.G. et al., 2010].

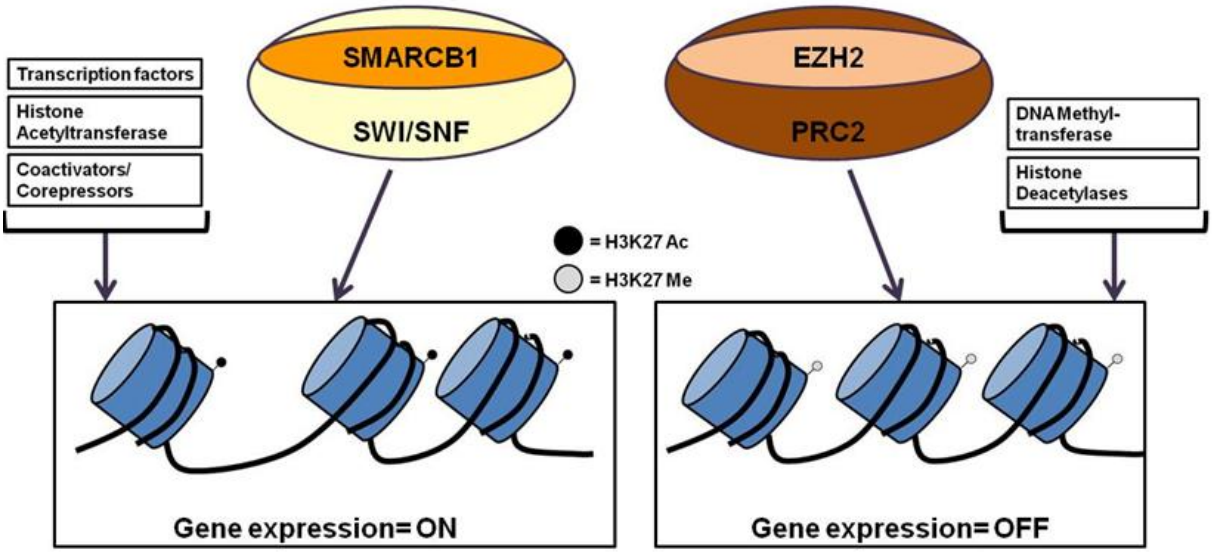

Figure 1.3. Epigenetic antagonism between PRC2 and SWI/SNF chromatin remodeling complexes.

As catalytic subunit of the PRC2, EZH2 carries out the trimethylation of histone 3 at lysine 27 (H3K27Me3), leading to gene expression repression. PRC2 competes for binding to the chromatin with the SWI/SNF chromatin remodeling complex, which allows gene transcription activation. SMARCB1 is a component of the SWI/SNF complex.

1.1.2.1 Rhabdoid tumour therapy

RT is often diagnosed at high stage and patients present early metastases to lung, liver, and lymph nodes, leading to poor prognosis. Overall survival of RT patients at 5-years, is about 30%, independently of the tumour site, and is lower in younger patients (about 9% for patients aged 0-5 months) [Sultan I. et al., 2010].

Commonly, the treatment for RT includes surgical resection of the tumour, chemotherapy and radiotherapy. Total resection of tumour is a favourable prognostic factor; however, it is not always feasible, particularly for AT/RT [Chi S.N. et al., 2009; Madigan C.E. et al., 2007].

There is no gold standard therapy for RT due to the rarity of the disease and heterogeneity of origin site; in the past, RTs were treated on the basis of the tumour location (*i.e.*, KRT as Wilms Tumour, AT/RT as medulloblastoma). Recently, the identification of common molecular features and the subsequent treatment of RTs as an independent entity improved the prognosis of patients. Chemotherapy regimen includes combinations of vinca alkaloids,

alkylating agents, platinum compounds and anthracyclines [Chi S.N. et al, 2009]. In some patients, the use of high-dose chemotherapy followed by autologous stem cell transplantation or, for AT/TR patients, the use of intrathecal chemotherapy (methotrexate, cytarabine, mafosfamide, and hydrocortisone) may lead to favourable outcome [Gilman A.L. et al., 2011; Koga Y. et al., 2009; Athale U.H. et al., 2009; Blaney S.M. et al., 2012]. Some studies have related radiotherapy treatment with improved clinical outcomes [Tekautz T.M. et al., 2005; Zhuge Y. et al., 2010]. Unfortunately, the long term side-effects of all these treatments have a strong impact on children growth and development, affecting the quality of life.

Several targeted therapeutics are currently under preclinical and clinical evaluation either alone or in combination with conventional chemotherapy. SMARCB1 loss causes altered activation of signaling pathways. Effector molecules of these pathways, such as CDKs, EZH2, Aurora kinase A, GLI1, HDACs and Wnt/β-catenin, have been investigated as therapeutic targets (Figure 1.4).

For instance, GLI1, a member of Sonic-Hedgehog pathway involved in cell differentiation and oncogenesis, has been described as up-regulated in RT primary tumours [Kerl[a] K. et al., 2013]. Inhibition of GLI1, through administration of arsenic trioxide, reduced MRT cells proliferation *in vitro* and tumour growth in a mouse xenograft model [Kerl K. et al., 2014; Tang Y. et al., 2014]. Hedgehog signaling pathway inhibitors have entered a new ongoing clinical trial on brain tumour patients, including AT/RT, which proposes the evaluation of rational combination therapies based on tumour type and molecular characteristics of the diseases [https://clinicaltrials.gov].

In a preclinical study, promising results have been obtained with the inhibition of WNT by RNA interfering (RNAi) molecules, which resulted in strong reduction of AT/RT cell viability [Chakravadhanula M. et al., 2015].

C-MYC is highly expressed in RTs. The mechanism by which the loss of SMARCB1 induces MYC activity in RT cells has not been clarified. A recent study in AT/TR preclinical models demonstrated that MYC inhibition, obtained through transgenic expression of a MYC dominant negative or inhibition of MYC transcriptomic programs with the BET inhibitor JQ1, reduces tumour cell self-renewal, induces senescence, and inhibits tumour growth *in vivo* [Rosson G.B. et al., 1998; Cheng S.W. et al., 1999; Alimova I. et al., 2018].

Alisertib (MLN8237) is an inhibitor of Aurora A kinase, which regulates the formation and stability of the mitotic spindle; this compound has been tested in 4 paediatric AT/RT patients and, as single-agent, induced a strong and durable regression of the disease [Wetmore C. et al., 2015]. It was previously demonstrated that usually Aurora A is repressed by SMARCB1 and the use of MLN8054, a selective small-molecule inhibitor of Aurora A kinase, reduced cell proliferation, followed by apoptosis induction *in vitro*, and reduced tumour growth in xenograft models [Carol H. et al., 2011; Lee S. et al., 2011].

SMARCB1 loss can promote cell cycle progression resulting from up-regulation of the EZH2 pathway. Inhibitors of component of this pathway (CDK4/CDK6/CyclinD), which is involved in cell cycle progression via Rb phosphorylation, have already been tested in clinical trials for different malignancies. Among them, the CDK4/6 inhibitor ribociclib (LEE001) has been tested in paediatric MRT patients displaying acceptable safety and pharmacokinetics [https://clinicaltrials.gov]. In preclinical studies palbociclib (PD-0332991), another CDK4/6 inhibitor, showed promising results in terms of anti-tumour activity in both *in vitro* and *in vivo* experiments [Geoerger B. et al., 2017; Hashizume R. et al., 2016].

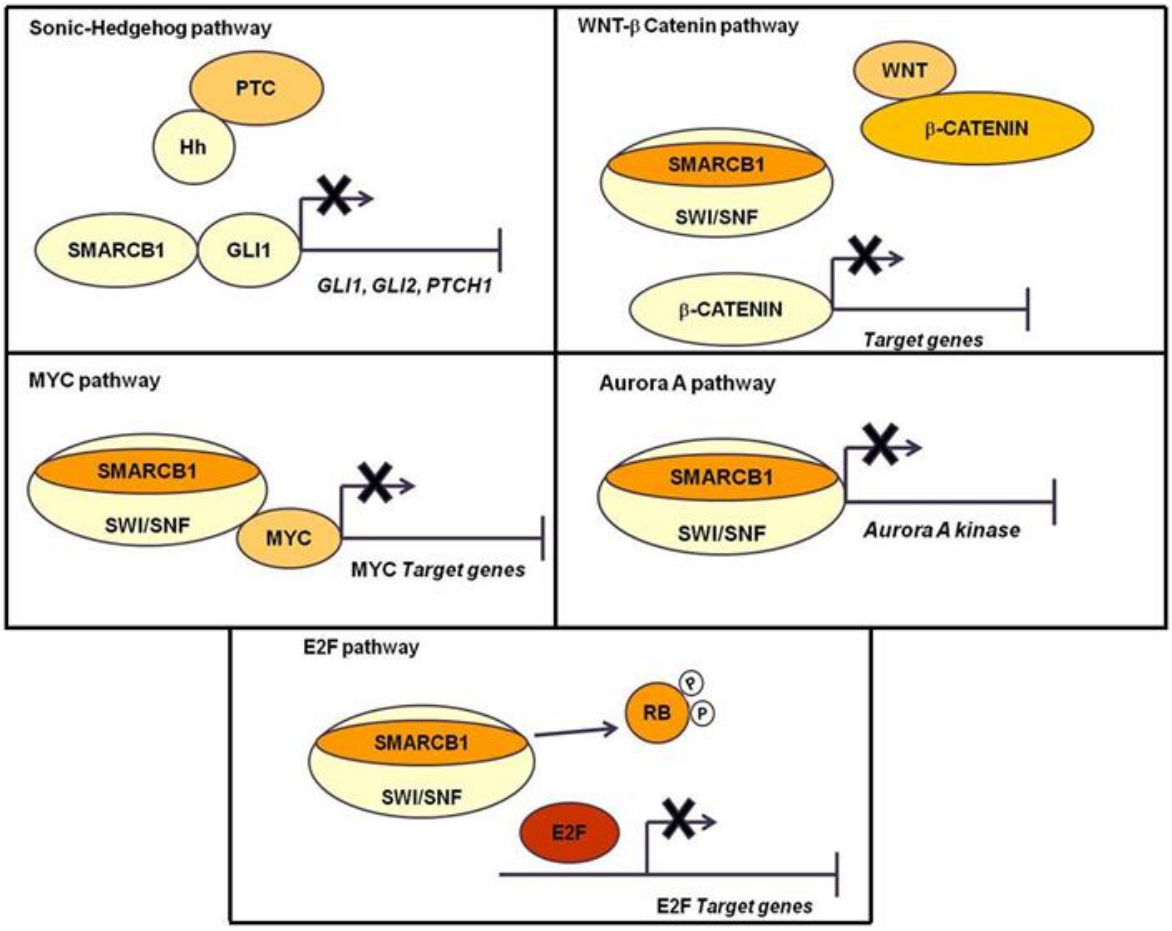

Figure 1.4. Pathways regulated by SWI/SNF complex.

The SWI/SNF complex, with the core subunit SMARCB1, plays a critical role in regulating expression of genes implicated in key signalling pathways, such as the Hedgehog, WNT-β catenin, MYC, Aurora A kinase and E2F.

As previously mentioned, SWI/SNF and PRC complexes have opposite functions at transcription levels and compete for binding to the chromatin. SMARCB1-deficient tumours express higher levels of EZH2, whose transcription is directly repressed by SMARCB1 [Wilson B.G. et al., 2010]. Lack of SMARCB1 in RT leads to repression of gene transcription caused by aberrant H3K27me3 mediated by EZH2 and oncogenic dependence on this methyltransferase. The EZH2 inhibitor tazemetostat, has shown promising activity in an undergoing Phase I clinical trial in paediatric patients with SMARCB1-negative tumours [https://clinicaltrials.gov]. In preclinical *in vivo* studies, the use of tazemetostat showed anti-tumour activity in RT models [Kurmasheva R.T. et al., 2017].

The epigenetic status of chromatin is regulated also by histone acetyltransferases (HATs) and HDACs, which are often aberrantly expressed in RTs. HDAC inhibitors showed anti-tumour effect in combination with chemotherapeutic agents and radiosensitisation in preclinical *in vitro* and *in vivo* studies [Kerl[b] K. et al., 2013; Thiemann M. et al., 2012; Moreno N. and Kerl K., 2016]. HDAC inhibitors (*i.e.*, Vorinostat and Valproic Acid) have also been used in clinical trials in paediatric AT/RT patients alone or in combination treatments showing high tolerability [Fouladi M. et al., 2010; Hummel T.R. et al., 2013; Su J.M. et al., 2011].

1.1.3. Sarcoma microenvironment targeting

The reciprocal interaction of tumour with microenvironment, including stroma cells, extracellular matrix (ECM) and signaling molecules, such as growth factors, chemokines and cytokines, is indeed fundamental for tumour sustenance. In such cross-talk, CXCL12 and its cell-surface receptor, CXCR4, are key factors promoting tumour growth and metastasis dissemination [Domanska U.M. et al., 2013]. AMD3100, a CXCR4 inhibitor, effectively suppressed tumour growth when used in combination with anti-angiogenic agents and/or ifosfamide in both *in vitro* and *in vivo* SS models [Wakamatsu T. et al., 2014].

Immune-based therapies have been explored in SS and RT patients. The cancer-testis antigen NY-ESO-1, highly expressed in the majority (80%) of SS, is one of the most analysed immune-targets. Adoptive immunotherapy with $CD8^+$ T cells, genetically engineered to recognise the NY-ESO-1 antigen, was shown to induce significant tumour regressions in 67% patients with metastatic SS [Robbins P.F. et al., 2011]. Another approach to target NY-ESO-1 is vaccination. The dendritic cell-targeting viral vector expressing the NY-ESO-1 gene CMB305 induced NY-ESO-1 specific T cell responses in SS patients and is currently in initial Phase I study [Pollack S.M., 2018]. On the other

hand, immune checkpoint inhibition by ipilimumab, a monoclonal antibody specific for cytotoxic T cell lymphocyte-associated protein 4 (CTLA-4), did not provide clinical benefit in a clinical trial for SS patients [Maki R.G. et al., 2013].

Immune checkpoint inhibitors targeting programmed death receptor 1 (PD-1) or its ligand (PDL-1), and CTLA-4 have raised interest in the treatment of RTs [Nemes K. and Frühwald M.C., 2018]; in particular, a Phase I/II clinical trial with the anti-PDL-1, atezolizumab, is ongoing in paediatric and young adult patients with solid tumours, including MRT [https://clinicaltrials.gov]. T cells, expressing chimeric CD-specific antigen receptors (CARs), which target tumour-associated antigens directly on the tumour cell surface, represent an additional immunotherapeutic approach of potential interest for RT. CAR-T cells have shown promising results in patients with haematological malignancies. It has been recently demonstrated that glypican 3-positive MRT cells *in vitro* are responsive to CAR-T cells [Li W. et al., 2017]. Paediatric patients with AT/RT exhibited good response to anti-tumour immunotherapy with autologous dendritic cell vaccination and three out of seven patients became long-term survivors [van Gool S.W. et al., 2016].

Because of the heterogeneity and rarity of STSs, the treatment of these pathologies remains a major challenge. Despite the improvement of systemic treatments, including the use of targeted therapy and immunotherapy, patients with advanced or recurrent disease still have poor prognosis. In fact, chemotherapy gives low response rates in most STS subtypes with acute and long-term toxicities, particularly relevant in paediatric patients. Further treatment strategies will require a better understanding of the STS biomolecular complexity to elucidate mechanisms involved in tumour progression and to understand the interplay between the tumour and its microenvironment. Thus, innovative therapies should conceivably envision multi-targeted approaches able to counteract multiple pathways and the tumour-microenvironment reciprocal dependency.

The heparanase/HSPG system, which acts at the tumour-microenvironment interface, is an emerging therapeutic target in several pathological conditions and prominently in cancer [Secchi M.F. et al., 2015; Vlodavsky I. et al., 2016]. A few recent studies also support a potential relevance in sarcomas [Shafat I. et al., 2011; Cassinelli G. et al., 2013].

1.2. The heparanase/heparan sulfate proteoglycan system

Heparanase is the only mammalian endo-β-D-glucuronidase cleaving heparan-sulfate (HS) side chains of heparan sulfate proteoglycans (HSPGs). HS is a glycosaminoglycan synthesised in the Golgi apparatus and composed of glucuronic acid and N-acetylglucosamine disaccharide units. Owing to their flexibility, HS polysaccharides display high variability in conformation and orientation of functional groups that allows the binding to a variety of different proteins. HS is synthesized in a non-template driven process on specific serine residues located on a restricted group of core proteins, the HSPGs associated with the cell surface (i.e., syndecan and glypican) or the ECM (i.e., perlecan, agrin, and collagen XVIII). The chain is firstly synthesized as an N-acetylated polymer, which then undergoes a series of modifications, including sulfation, epimerisation and deacetylation. Variable modifications encode information for different functions. Extracellularly, HS are modified by two endosulfatases, Sulfatase 1 and Sulfatase 2, which selectively remove 6-O-sulfate groups from mature HS. Heparin is a more completely modified version of HS, displaying also a higher negative charge density. Alterations of the HS synthesis or modifications processes have been associated with several diseases, such as cancer, amyloid disease, infectious disease or inflammatory conditions [Gallagher J.T., 2001].

HSPGs are ubiquitous glycoproteins localised at the cell surface, basement membrane and ECM; in addition, they can translocate into the nucleus in a regulated manner [Kovalszky

I. et al., 2014]. On the basis of their main location, they have been divided in three main groups:

1) membrane HSPGs (*i.e.*, syndecans and glypicans);
2) ECM HSPGs (*i.e.*, agrin, perlecan, type XVIII collagen);
3) intracellular secretory vesicle HSPG (*i.e.*, serglycin in mast cells).

HSPGs play a wide variety of structural, biochemical and regulatory functions under both physiological and pathological conditions. Membrane HSPGs are involved in cell-cell and cell-ECM interactions, favouring cell adhesion and motility. Moreover, they play a key role in cell signaling acting as co-ligands and co-receptors for growth factors, chemokines and cytokines. HSPGs are involved in receptors endocytosis, helping ligands uptake and receptors internalisation for degradation or recycling [Sarrazin S. et al., 2011]. HSPGs contribute to the organisation and homeostasis of ECM providing mechanical support. Furthermore, thanks to their structural heterogeneity, they are able to sequestrate a wide variety of HS-binding bioactive molecules, including growth factors, cytokines and enzymes in an inactive reservoir form, from which they can be released by HS degradation mediated by heparanase (Figure 1.5) [Dreyfuss J.L. et al., 2009].

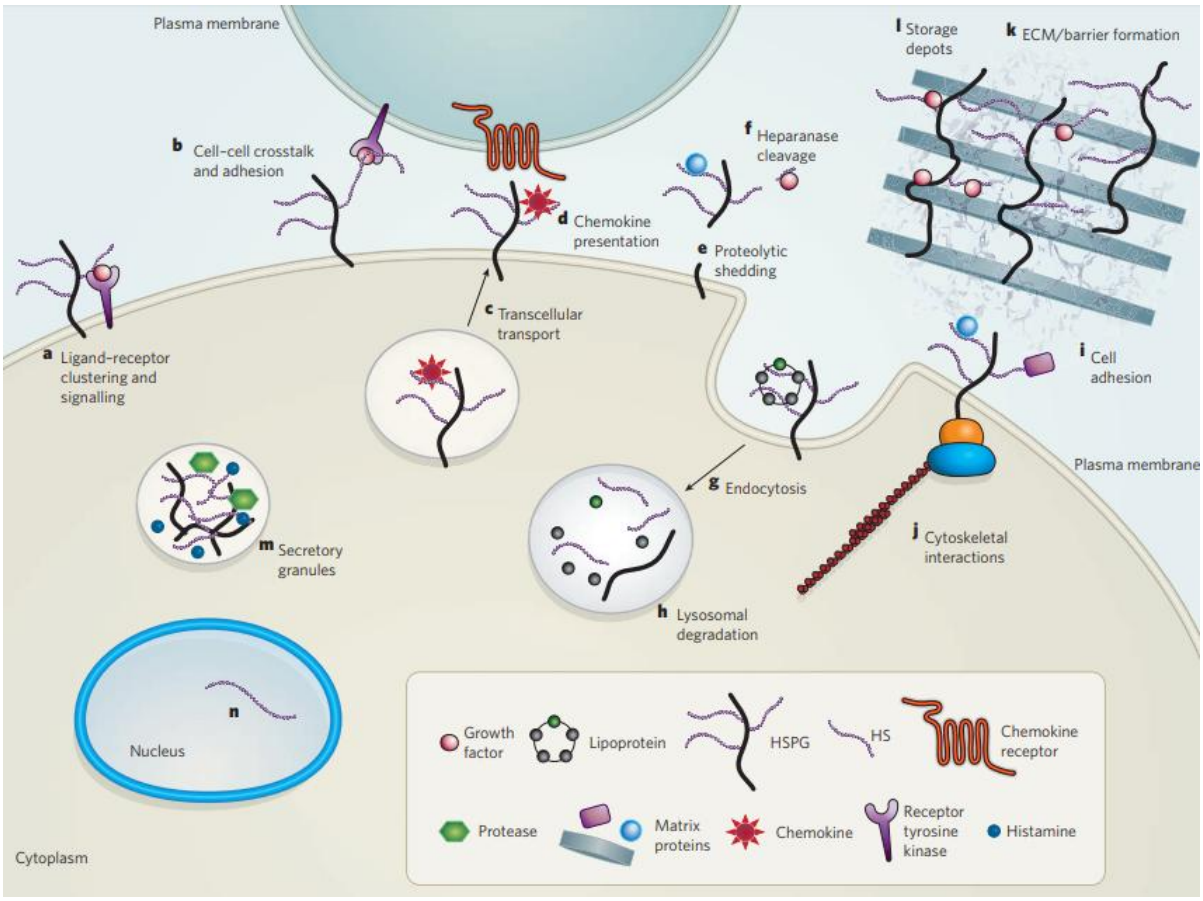

Figure 1.5. HSPGs role in cells.

HSPGs act as co-receptors for growth factors and their receptors on the same cell (**a**) or on neighbouring cells (**b**). They transport and present chemokines at the cell surface (**c-d**). By cleaving HS on proteoglycans, heparanase leaves the core protein exposed to attack by proteases, leading to proteolytic shedding (**e-f**). Cell-surface HSPGs are recycled or degraded in lysosomes after endocytosis (**g-h**). Moreover, HSPGs facilitate cell adhesion to the ECM (**i**) and form bridges to the cytoskeleton (**j**). Extracellular HSPGs are involved in the formation of matrices that form physiological barriers and concentrate bioactive molecules in the extracellular space (**k-l**). A specific HSPG, serglycin, carries heparin and is packaged into secretory granules of mast cells (**m**). Finally, HS chains are also found in the nucleus (**n**) [Bishop J.R. et al., 2007].

The cleavage activity of heparanase produces discrete HS fragments leading to ECM disassembly in processes requiring tissue remodeling such as inflammation, angiogenesis, and metastasis. Moreover, it induces the mobilisation of HS-binding molecules and, through the activation of protease-mediated processes, the release of soluble bioactive HSPG ectodomains [Manon-Jensen T. et al., 2010; Arvatz G. et al., 2011]. Preclinical studies have documented the pro-angiogenic and pro-metastatic activity of heparanase. Clinically, an association between heparanase levels and tumour progression or patient prognosis has been described in several different tumours types [Barash U. et al., 2010].

Heparanase pro-angiogenic activity is in part ascribed to its ability to release from the ECM HS-binding pro-angiogenic factors (*e.g.* VEGF, FGF, hepatocyte growth factor (HGF), PDGF, heparin-binding EGF-like, IL-8) involved in paracrine and/or autocrine stimulation of signaling pathways mediated by receptor tyrosine kinases (RTKs) (*e.g.* PDGFR, FGFR, c-Met, EGFR) [Vreys V. and David G., 2007]. Therefore, targeting the heparanase/HS axis may have an impact on signaling pathways that support tumour growth and survival.

1.2.1. Heparanase

Heparanase activity as HS endoglycosidase was described for the first time in murine models in 1975 [Hook M. et al., 1975; Ogren S. and Lindahl U., 1975] and the name "heparanase" was introduced 9 years later [Nakajima M. et al., 1984]; the heparanase coding gene (*HPSE1*) was cloned in 1999 [Vlodavsky I. et al., 1999; Hulett M.D. et al., 1999; Toyoshima M. and Nakajima M., 1999; Kussie P.H. et al., 1999] and, more recently, a model of the protein structure was obtained by X-ray crystallography (Figure 1.6). Heparanase 3D structure presents a characteristic (β/α)8 domain with two conserved acidic residues (Glu^{225} and Glu^{343}) critical for the catalytic activity. The C-terminal domain is required for heparanase activity and regulates protein secretion [Wu L. et al., 2015].

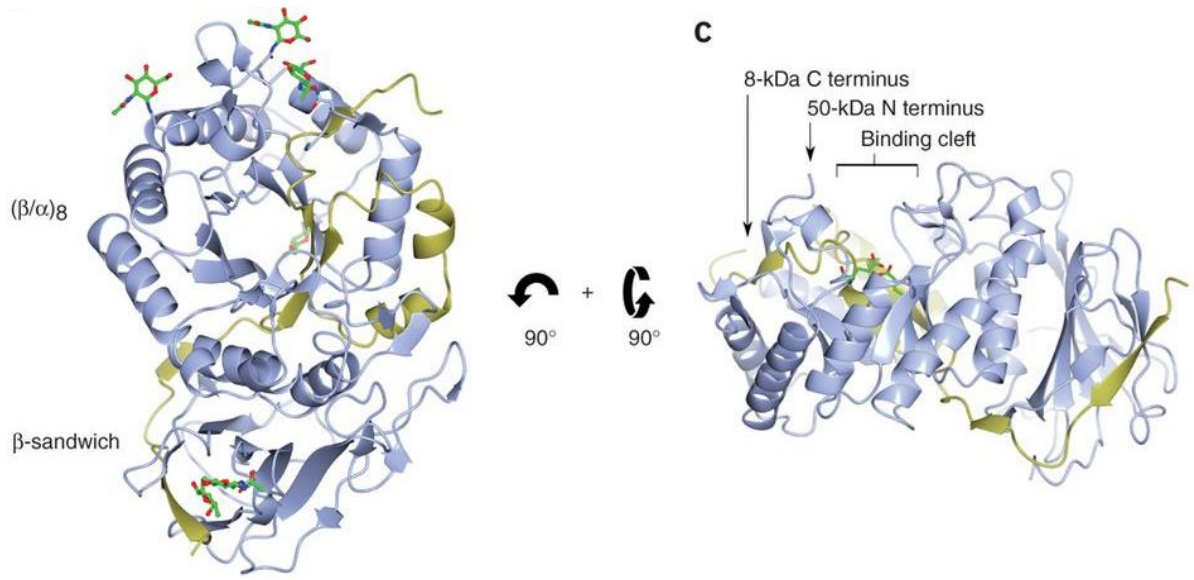

Figure 1.6. Heparanase crystal 3D view.

Front (left) and side (right) views of heparanase. Subunits are coloured yellow (8 kDa) and blue (50 kDa). There are five sites of N-glycosylation coloured in green and red in the front view. The two catalytic residues are coloured in green and red in the side view [Wu L. et al., 2015].

Physiologically, expression of heparanase is restricted primarily to the placenta, the skin tissues and blood-borne cells, including platelets and activated cells of the immune system [Vreys V. and David G., 2007], whereas it is detected in almost all tumours, including sarcomas [Ilan N. et al., 2006; Masola V. et al., 2009; Shafat I. et al., 2011; Kazarin O. et al., 2014].

The heparanase gene is localised on chromosome 4q21.3, which encodes a precursor of 543 amino acids (pre-proheparanase). The pre-proheparanase is processed into an inactive 65 kDa precursor enzyme by the removal of the N-terminal signal peptide in the Golgi apparatus, where the proheparanase is glycosylated. Then the protein is secreted into the extracellular space, where it binds several membrane molecules, such as glycoproteins (*e.g.*, HSPGs). The binding to these molecules favours the re-internalisation of the proenzyme by endocytosis and the storage into lysosomes. The activation of the enzyme is mediated by cathepsin L by the proteolytic cleavage and excision of a 6 kDa linker region. The resulting mature enzyme is a heterodimer consisting of non-covalently associated 8 and 50 kDa protein subunits (Figure 1.7) [Vlodavsky I. et al., 2016].

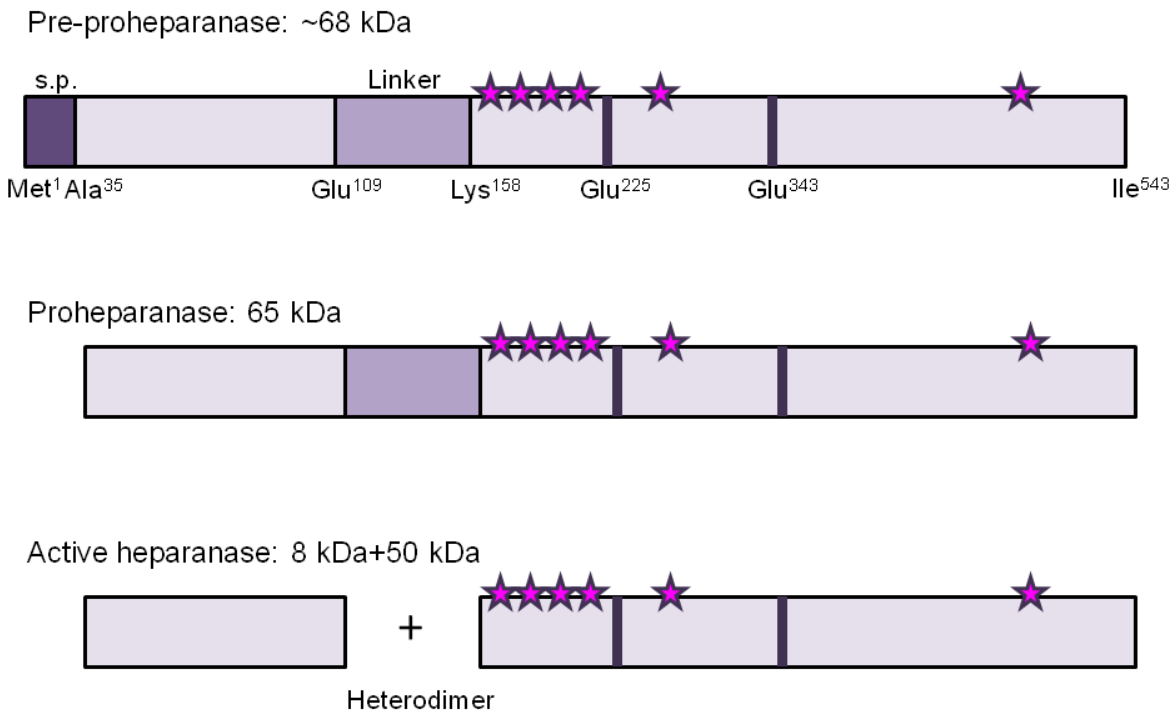

Figure 1.7. Heparanase processing.

Pre-proheparanase harbours 35 amino acids signal peptide (Met1–Ala35) which is removed in the Golgi apparatus. The protein is then glycosylated and secreted as a latent 65 kDa protein. Proteolytic processing occurring into lysosomes removes the linker domain (Ser110–Gln157), resulting in a heterodimer composed of 8 kDa (Gln36–Glu109) and 50 kDa (Lys158–Ile543) subunits. Stars represent glycosilation sites.

Upon activation, heparanase can be secreted or can translocate into the nucleus. The mechanism underlying the nuclear transport of heparanase has not been elucidated yet, but three different hypotheses have been proposed: 1) two putative nuclear localisation signals could mediate its nuclear localisation [Schubert S.Y. et al., 2004]; 2) heparanase could use HS as vehicle [Schubert S.Y. et al., 2004]; or 3) heat shock protein 90 may function as a chaperone for nuclear translocation of heparanase [Nobuhisa T. et al., 2007].

The mature endoglycosidase stored in the lysosomes is secreted into the extracellular space in response to specific physiologic or pathologic stimuli that may vary among cell types and biological settings (*e.g.*, inflammatory cytokines, fatty acids, protein kinase A and C) [Chen, G. et al., 2004; Shafat I. et al., 2006]. The acidic lysosomal environment provides optimal conditions for heparanase storage and enzymatic activity. In fact, it has been demonstrated that its enzymatic activity is optimal between pH 5.5 and 6.0 [Gilat D. et al., 1995]. The acidic tumour microenvironment also favours heparanase activity. In fact, the

production of acidic metabolites (*e.g.* lactic acid) is caused by anaerobic glycolysis under hypoxic conditions [Cairns R.A. et al., 2011]; this condition may also explain the enhanced activity of other enzymes such as proteases, which together with heparanase can favour cancer progression [Mason S.D. and Joyce J.A., 2011]. Inside the nucleus, active heparanase has been shown to degrade HS side chains of nuclear HSPGs, leading to the regulation of gene expression. Heparanase can interfere with gene expression via different mechanisms: 1) enhancing HATs activity by the cleavage of syndecan-1 HS, which is a HAT inhibitor. The activation of HATs induces the transcription of genes driving tumour progression [*e.g.* VEGF, Matrix metallopeptidase 9 (MMP-9), HGF] [Purushothaman A. et al., 2011]; 2) directly interacting with the nucleic acid [Yang Y. et al., 2015].

Heparanase has both enzymatic and non-enzymatic functions. Enzymatic activity, exerted by the active 50 kDa molecule, induces the cleavage of HS and the subsequent release of HS-binding molecules stored onto the HSPGs and the remodeling of ECM and basement membrane; all together these phenomena contribute to facilitate cell motility in tumour progression critical processes such as angiogenesis and inflammation [Vlodavsky I. et al., 2011]. Heparanase non-enzymatic activity is mediated by the binding to still not well defined receptors on the cell surface activating signaling cascades intracellularly, such as Akt, ERK, p38 and Src pathways, ultimately leading to up-regulation of pro-angiogenic factors, such as VEGF and HGF [Fux L. et al., 2009].

1.2.2. Heparanase role in cancer progression

The available evidence supports a role for heparanase in cancer progression in a large number of malignancies. Aberrant heparanase activity and expression correlates with increased micro-vessel density, metastatic potential of tumour cells and patients reduced post-operative survival [Kelly T. et al., 2003; Vlodavsky I. and Friedmann Y., 2001; Sanderson R.D. et al., 2017]. By degrading HS, heparanase participates in ECM

remodeling and promotes the concomitant release of several HS binding molecules, allowing cell dissemination, promoting the establishment of a new vascular network that supports tumour growth and provides a gateway for invading metastatic cells. Also, the signaling capacity of heparanase, which is mediated by the binding to cell surface receptors and the activation of intracellular pathways, sustains tumour growth and invasion [Riaz A. et al., 2013]. Furthermore, heparanase ability to regulate gene expression supports the tumour's aggressive behaviour by enhancing the transcription of pro-angiogenic and pro-metastatic factors, such as VEGF, HGF and MMP-9 (Figure 1.8) [Sanderson R.D. et al., 2017].

In multiple myeloma, it has been shown that heparanase also contributes to metastasis and angiogenesis by promoting syndecan-1 shedding; in fact, by cleaving HS on syndecan-1, heparanase leaves the core protein exposed to attack by proteases, among which MMP-9 is up-regulated by heparanase. Shedding syndecan-1 can bind specific receptors (*i.e.*, VLA-4 and VEGFR2) and stimulate invasion. Moreover, the cleavage and the release of syndecan-1 extracellular domain in a soluble form acts as a paracrine signal co-factor that ensures tumour/stroma cell cross-talk thereby enhancing the activity of HS-binding growth factors [Ramani V.C. et al., 2013].

It is known that inflammation plays a role in the neoplastic process, fostering proliferation, survival and migration [Mantovani A. et al., 2008]. Heparanase is a key player in inflammation; indeed, HS remodeling may affect the inflammatory response at multiple levels, such as the release of different chemokines and cytokines in the extracellular space, the promotion of leukocyte binding to the endothelium and transmigration through EMC and basement membrane, and the activation of macrophages through modulation of toll-like receptors signaling pathway [Goldberg R. et al., 2013; Meirovitz A. et al., 2013; Hermano E. et al., 2014; Vlodavsky I. et al., 2016]. Also non-enzymatic activity of heparanase sustains inflammation by the activation of intracellular signaling pathways and

the promotion of cell-adhesion [Riaz A. et al., 2013]. During inflammation, heparanase expression increases in lymphocytes and its secretion contributes to the enhanced vascularisation and cell invasion characteristic of tumour-associated inflammation [Meirovitz A. et al., 2013].

Heparanase has been proposed to participate in autophagy, known to sustain tumour cell survival by providing metabolites obtained from the recycling of proteins and damaged organelles. This phenomenon contributes to provide growth advantages under stress conditions as well as resistance to chemotherapy [Rosenfeldt M.T. and Ryan K.M., 2011]. In the autophagocytic process, autophagosomes fuse with lysosomes, where the intracellular material can be degraded for recycling. Lysosomal-stored heparanase has been implicated in the autophagy process. The enzyme colocalises with the autophagy marker LC3-II (associated with autophagosomes) and its expression correlates with autophagy extent. The mechanism underlying autophagy induction by heparanase has not been clarified yet, but likely involves mTOR1, whose expression is inversely correlated with heparanase level (Figure 1.8) [Sanderson R.D. et al., 2017]. Up-regulation of heparanase and increased autophagy have been related with chemotherapy resistance [Shteingauz A. et al., 2015].

Besides, heparanase has been shown to participate in the biogenesis, composition and secretion of tumour-derived exosomes (Figure 1.8). These vesicles are considered important for the communication between neighbouring cells and for long-distance cell communication. By delivering proteins and nucleic acids, they are believed to play a role in tumour progression. Heparanase, which can also be a cargo of exosomes and be released at distant sites, has been implicated in the establishment of the metastatic niche [Thompson C.A. et al., 2013].

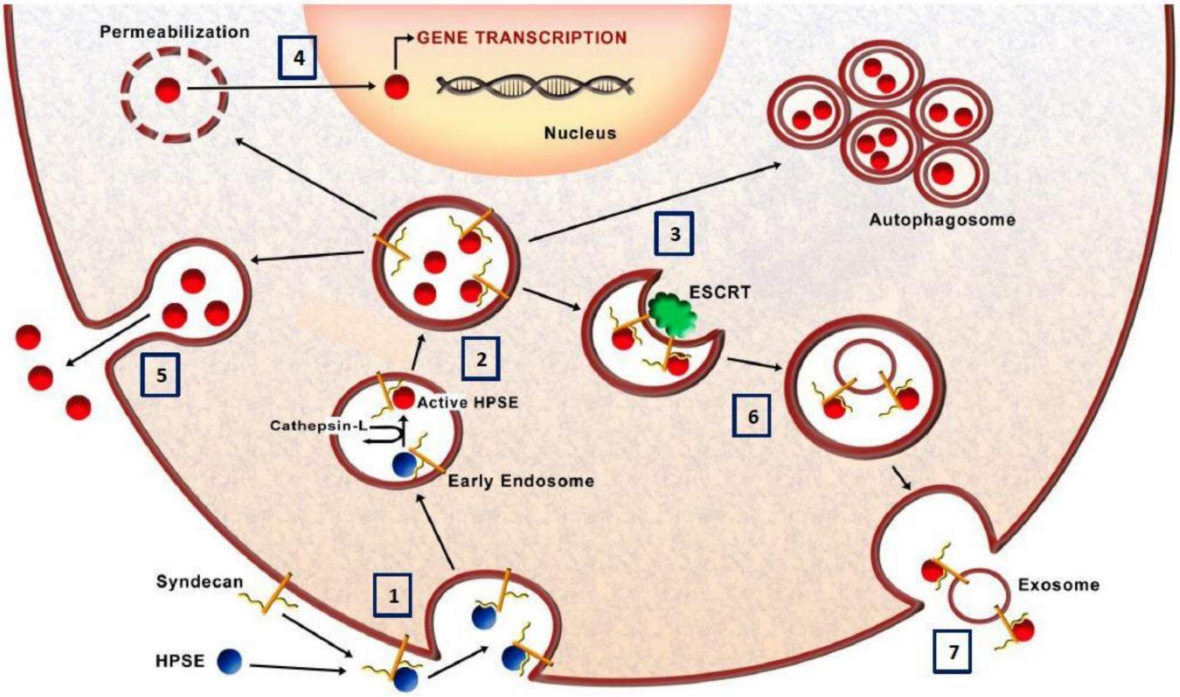

Figure 1.8. Schematic model of heparanase trafficking.

(1) The proheparanase is secreted in the extracellular spaces after synthesis. Here, it interacts with HSPGs, such as syndecan-1, and the complex is endocytosed. (2) Endosomes fuse with lysosomes, with the subsequent acidification and induction of heparanase cleavage by cathepsin-L. (3) In lysosomes heparanase participates in the formation of autophagosome. (4) Active heparanase translocates into the nucleus where it modulates gene transcription. (5) Active heparanase can be secreted in the extracellular space. (6) Heparanase modulates the formation and the release of exosomes and (7) it can be anchored to syndecan on exosome surfaces; heparanase, HPSE [Masola V. et al., 2018].

1.2.3. Heparanase/heparan sulfate axes as a therapeutic target

The support provided by heparanase/HSPG to several aspects of malignancy makes this system an attractive target for therapeutic intervention. The heparanase/HSPG system represents an intriguing nodal point for targeting tumour growth, angiogenesis, metastatic spread and drug resistance [Vlodavsky I. et al., 2016; Couchman J.R. et al., 2016; Sanderson R.D. et al., 2017; Lanzi C. et al., 2017]. Moreover, heparanase is over-expressed in essentially all tumours examined, including bladder, brain, breast, colon, liver, ovarian, pancreatic and haematological malignancies in addition to sarcomas [Ilan N. et al., 2006; Cassinelli[a] G. et al., 2016]. Interestingly, knock-out mice develop normally and exhibit no apparent anatomical or functional deficiencies and heparanase is the only mammalian

endoglycosidase able to cleave HS [Zcharia E. et al., 2009; Vlodavsky I. et al., 2012]. Taken together, these observations make heparanase a desirable target for cancer therapy.

So far, various approaches have been developed to achieve heparanase blockade:

1) **Heparin derivatives** bind heparanase as competitive substrate inhibitors, thus preventing access to the enzyme catalytic site. Heparin, that is a specialised form of HS produced exclusively by mast cells, was the first discovered heparanase substrate and it has been employed to inhibit heparanase enzymatic activity [Yahalom J. et al., 1984]. Unfortunately, due to thrombocytopenia and bleeding side effects, heparin cannot be administered at high concentrations or for prolonged treatments; so intensive synthesis studies have been conducted to obtain analogues with reduced anti-coagulant activity and increased heparanase affinity [Casu B. et al., 2008]. To reduce the unwanted anticoagulant activity of heparin, derivatives have been obtained through chemical modifications including oversulfation or partial desulfation, selective alteration of the residues that are involved in the biding to the antithrombin, or the development of low molecular weight heparin derivatives. Heparin derivatives act not only as heparanase inhibitors and HS mimetics preventing the binding of bioactive molecules to HS in the ECM and at the cell surface [Lanzi C. and Cassinelli G., 2018]. **PI-88** (muparfostat) is a phosphosulfomannoligosaccharide (a mixture of highly sulfated oligosaccharides) non-cleavable by the endo-β-D-glucuronidase. It inhibits heparanase activity and competes with HS for the binding of angiogenic and growth factors [Parish C.R. et al., 1999]. PI-88 was the first HS mimetic to enter clinical trials and it is currently under Phase II investigation for various cancer types [https://clinicaltrials.gov]. A Phase III trial in patients with hepatocellular carcinoma was prematurely terminated because the drug failed to reach the fixed disease-free survival endpoint. Recent evidence however suggests a possible clinical benefit in subgroups of patients with worse prognosis [Liu C.J. et al., 2014]. Among the most promising second-generation PI-88 analogues, the

tetrasaccharide fully-sulfated **PG545** (pixatimod) showed improved anti-tumour efficacy and reduced anti-coagulant activity, compared to PI-88 [Hammond E. et al., 2012]; moreover, it exhibited a remarkable immunomodulatory activity in preclinical studies [Weissmann M. et al., 2018]. Currently, PG545 is undergoing a Phase I clinical trial in combination with the immunocheckpoint inhibitor nivolumab (anti-PD-1 antibody) in patients with advanced solid tumours [https://clinicaltrials.gov]. **SST0001** (roneparstat) is a modified 100% N-acetylated and 25% glycol split heparin. N-acetylation confers to SST0001 a non anti-coagulant feature, whereas the glycol splitting enhances heparanase affinity. SST0001 is the only heparanase inhibitor tested in sarcoma models so far. Early studies carried out in our laboratory demonstrated a down-regulation of angiogenesis-related factors, such as MMP-9, VEGF, and inhibition of cell invasion in sarcoma cells treated with the drug [Cassinelli G. et al., 2013]. SST0001 exhibited *in vivo* anti-tumour activity in several solid and haematological tumour models. A synergistic interaction was observed when used in combination with anti-angiogenic drugs (*i.e.*, bevacizumab or sunitinib) in a Ewing's sarcoma model, and with the camptothecin irinotecan in a RT model [Shafat I. et al., 2011; Cassinelli G. et al., 2013; Cassinelli[b] G. et al., 2016]. In addition, SST0001 was shown to counteract the activation of several RTKs involved in the malignant phenotype of STS models [*e.g.*, Epidermal growth factor receptor (EGFR), PDGFR, ERBB4 and IGF-1R] [Cassinelli[b] G. et al., 2016]. In a recently completed Phase I clinical evaluation in advanced multiple myeloma patients, this drug showed an excellent safety profile and signals of activity [https://clinicaltrials.gov]. Another glycol-split low molecular weight heparin, **M402** (necuparanib), which is N-sulfated, binds HS-binding molecules, including heparanase, with high affinity [Zhou H. et al., 2011]. In preclinical studies, M402 showed an efficient anti-tumour and anti-metastatic activity in murine models of breast and pancreatic cancer [Zhou H., et al., 2011; Chu

C.L., et al., 2012]. A Phase II clinical trial in combination with gemcitabine and nab-paclitaxel in patients with metastatic pancreatic cancer has been recently terminated due to insufficient level of efficacy despite promising preclinical activity [https://clinicaltrials.gov].

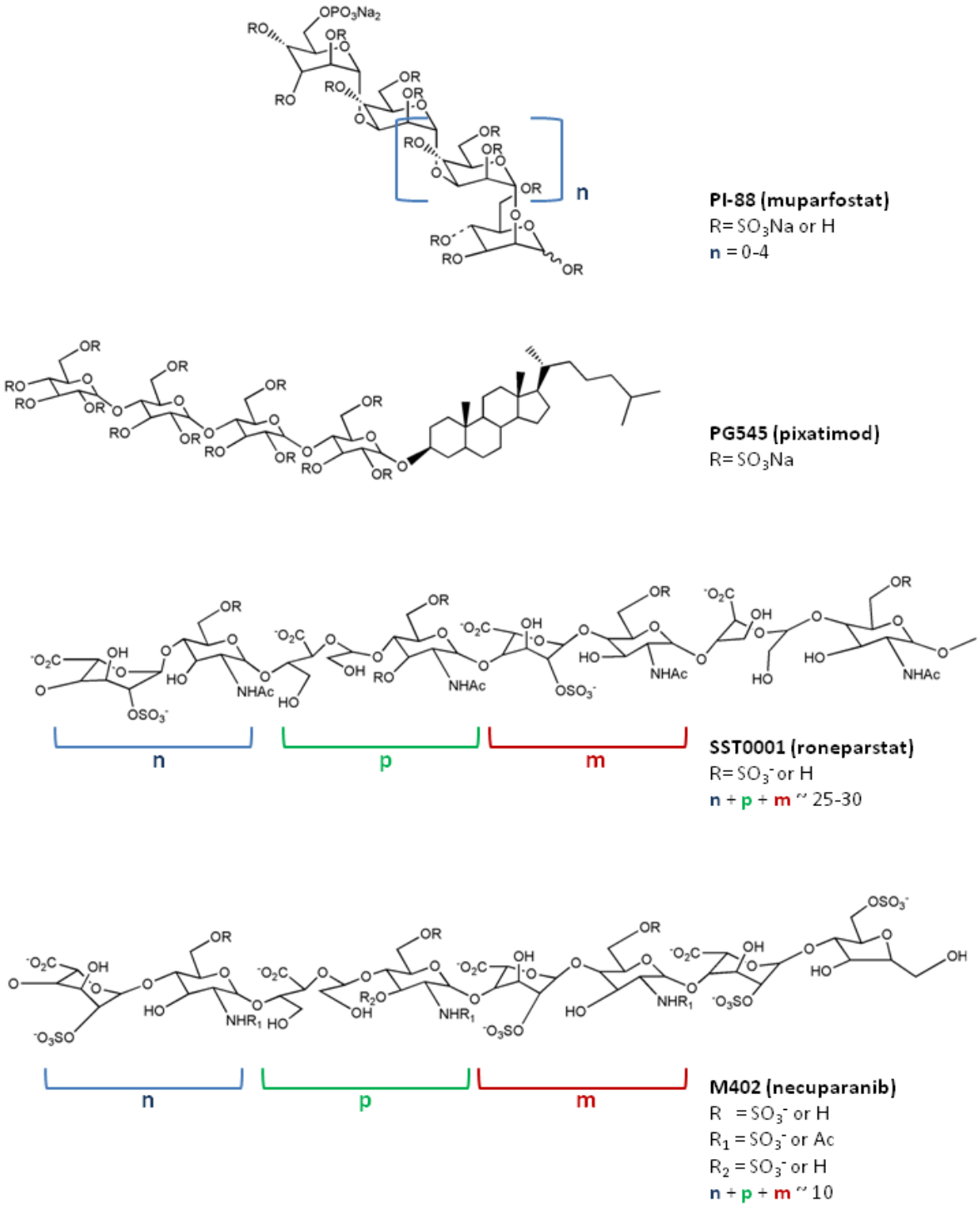

Figure 1.9. Schematic representation of heparin derivatives.

Schematic representation of PI-88, PG545, SST0001 and M402.

2) **Small molecules,** of both natural and synthetic origin, have been identified as heparanase inhibitors and are undergoing preclinical investigation [Lanzi C. et al., 2017]. Small molecules derivatives of benzalole and benzazolyl showed potent anti-heparanase activity in preclinical STS models, resulting in the inhibition of invasion and decrease of pro-angiogenic factors (*i.e.*, FGF-1 and 2, VEGF and MMP-9) [Madia V.N. et al., 2018; Messore A. et al., 2018]. The recently reported heparanase crystal structure is expected to be of great utility for the rational design of improved inhibitors.
3) **Monoclonal antibodies.** Recently, Weissmann and collaborators developed two different anti-heparanase antibodies, one against the KKDC peptide, a 14-aminoacid sequence comprising the substrate-binding domain of heparanase, and the other against the full-length protein. In preclinical *in vivo* studies, they were both able to neutralise heparanase, decreasing its intracellular content, and they inhibited lymphoma tumour growth and metastasis in preclinical models [Weissmann M. et al., 2016].
4) **Nucleic acid**-based inhibitors. Several attempts have been carried out to silence heparanase expression using different RNA interfering molecules, including microRNAs (miRNAs), small interfering RNA (siRNAs) and short hairpin RNAs (shRNA). MiR-1258 has been shown to down-regulate heparanase by targeting the 3′ UTR as demonstrated by luciferase assay in brain metastatic breast cancer cells [Zhang L. et al., 2011]. It has been shown in different preclinical studies that the over-expression of miR-1258 reduces *in vitro* invasion of cells, and the number of experimentally induced metastases *in vivo* [Liu H. et al., 2012; Shi J. et al., 2017; Zhang L. et al., 2011]. MiR-429 has been described to decrease the invasion ability of gastric cancer cells by targeting heparanase [Sheng N. et al., 2018]. Other RNAi-based systems, such as transient transfection of siRNAs, have been used to silence heparanase in different preclinical tumour models. Heparanase siRNA-mediated silencing resulted in the inhibition of migration and invasion in various cellular models [Mikami S. et al.,

2008; Zheng L.D. et al., 2010; Fan L. et al., 2011; Dong W. et al., 2014] and stable transfection reduced the tumourigenesis of an *in vivo* model of hepatocellular cancer [Xiong Z. et al., 2012]. Another strategy was the stable transfection of shRNA targeting heparanase that induced the decrease of tumour invasiveness, metastasis and angiogenesis in a gastric cancer preclinical model [Zheng L.D. et al., 2009].

1.3. RNA interference approaches

Conventional chemotherapy generally affects vital cellular processes such as DNA replication and cell division. For example, it blocks enzymes involved in replication and transcription, or interferes with the cytoskeleton. The main weaknesses of classical cancer therapy are the lack of specificity, the consequent occurrence of toxicity and drug resistance development. Even targeted therapies present limitations due to inadequate specificity and onset of drug resistance.

The use of RNA-based approaches aimed at interfering with cellular translational processes should lead to the generation of therapeutics with advantages in terms of specificity and efficacy compared to standard approaches.

RNAi was discovered in 1998 by the scientists Andrew Fire and Craig Mello in *C. elegans* and it earned them the Nobel Prize for Medicine in 2006 [Fire A. et al., 1998]. MiRNAs and siRNAs are small non-coding RNAs with important roles in gene regulation. In the last decades, they have been widely investigated as potential novel classes of therapeutic agents for the treatment of a wide range of disorders including cancer. RNA interfering molecules are able to silence gene expression at the post-transcriptional level by targeting messenger RNA (mRNA). In particular, a miRNA has multiple targets bound with incomplete complementarity, whereas a siRNA has one specific target at a homologue sequence.

1.3.1. MicroRNA

MiRNAs are composed of approximately 19-25 nucleotides and are naturally occurring post-transcriptional gene regulatory elements. These evolutionary conserved sequences, derived from non-coding regions, have been found in numerous species and have been shown to take part in the regulation of almost all cellular processes including developmental timings, stem cell functions, cellular differentiation, proliferation, and cell death [Calin G.A. and Croce C.M. 2006]. To date, 1917 different miRNAs have been discovered in humans [http://www.mirbase.org, March, 27th 2019].

About half of miRNAs are transcribed from non-protein coding transcripts, while the rest are located principally in the introns of coding genes and are co-transcribed with their host genes; they can also be grouped in clusters transcribed as poly-cistronic primary transcripts [Kim W.N., 2005].

MiRNAs are initially transcribed in the nucleus by RNA polymerase II, or more rarely by RNA polymerase III, as long primary miRNAs (pri-miRNAs). The pri-miRNAs have the typical shape of hairpins and are then processed into precursor miRNAs (pre-miRNAs, ~70 to 120 nucleotides) by Drosha, a RNase III enzyme which, with the DiGeorge syndrome critical region gene 8 (DGCR8 or Pasha), belongs to a multiprotein complex named Microprocessor. Next, exportin 5, which recognises the 2-nt overhanging at 3`end of pre-miRNAs, mediates their transport into the cytoplasm where they are cleaved by another RNase III enzyme Dicer into miRNA duplexes. The transactivation response RNA binding protein binds Dicer and helps the entry of the nucleic acid into the RNA-induced silencing complex (RISC), where the duplexes are divided and the “guide strand” associates with catalytic argonaute proteins. The other strand, “passenger strand” is usually degraded or, more rarely, associates with argonaute proteins, acting as active miRNA itself. The “guide strand” drives the RISC to the target mRNA through sequence complementarity and induces its translational repression. Recently, it has been found that RISC, with miRNA

and its target mRNA, is stored in processing bodies (P-bodies). The subsequent gene silencing is mediated by translational repression, due to imperfect sequence pairing, or mRNA deadenylation and subsequent degradation [Bhaskaran M. and Mohan M., 2014].

Alteration in miRNAs expression or activity can contribute to several diseases including tumour initiation and cancer progression. Altered miRNA expression in tumours compared to normal tissues can be linked to specific clinical and biological features [Bartel D.P., 2004]. Given that expression of certain miRNAs influence tumour treatment responses they can also be used as prognostic factors and biomolecules for patient treatment stratification. Since their discovery, miRNAs have, therefore, attracted interest as potential therapeutic targets as well as new therapeutic tools [Osada H. and Takahashi T., 2007; Oliveto S. et al., 2017]. The use of miRNAs offers the opportunity of simultaneously regulating a wide range of genes. Moreover, since they are naturally synthesised by cells, they display lower toxicity and immune response compared to other therapies [Chen Y. et al., 2015].

Several miRNA mimetics and antagonists have already been formulated and tested in preclinical studies for different diseases, including cancer. MiRNA-based therapeutics are designed to achieve miRNA inhibition or miRNA replacement depending on whether the miRNA provides a survival advantage to tumour cells or it behaves as a tumour suppressor. For the inhibition strategy, cells are transfected with a synthetic single-strand RNA, which acts as miRNA antagonists (*i.e.*, antagomirs, locked nucleic acid, etc.) and inhibits the action of the endogenous miRNAs. For the replacement strategy, synthetic double strand miRNAs (*i.e.*, miRNA mimics) are used to mimic the function of the endogenous miRNAs [Petrovic N. and Ergun S., 2018]. Two miRNAs have entered clinical trials. Miravirsen, a short locked nucleic acid directed against miR-122 has been developed by Santaris Pharma for the treatment of hepatitis C virus. It is administered by subcutaneous injection in Phase II clinical trials and no long-term safety issues were

developed by patients [van der Ree M.H. et al., 2016; Chakraborty C. and Das S., 2016]. A Phase I clinical study of a liposomal synthetic miR-34a mimic (MXR34) was carried out in patients with advanced solid tumours, but the trial was terminated because of a high incidence of adverse events [Beg M.S. et al., 2017]. In line with this, further efforts to devise proper formulation and precise delivery to cancer cells are required to avoid undesirable side effects.

1.3.2. Small interfering RNA

SiRNAs are short (19–30 nucleotides) double-strand RNAs capable of degrading mRNAs in the cytoplasm. The mechanism relies on the complementarity between a siRNA and its target mRNA, resulting in a specific inhibition of target translation [Torres-Martínez S. and Ruiz-Vázquez R.M., 2017].

SiRNAs can be introduced into cells using vectors allowing the expression of shRNA, which are exported by exportin 5 into the cytoplasm and then processed by Dicer into active siRNAs [Brummelkamp T.R. et al., 2002], or transfecting cells with synthetic siRNA duplexes. The concentration of siRNA transiently transfected is progressively decreased upon cell division and RNase mediated degradation [Bumcrot D. et al., 2006].

In the cytoplasm, long dsRNAs interact with Dicer that processes the strands into short (~20 to 30 nucleotides) double stranded oligonucleotides with 2-nt overhanging at the 3`end. Then, siRNAs interact with argonaute proteins, which cleave the "passenger strand" while the "guide strand" remains associated with the RISC. Next, the siRNA guides the RISC to its target mRNA and, as siRNAs are designed to be perfectly complementary to the target, causes site-specific cleavage via argonautes [Lam J.K. et al., 2015].

In principle, therapeutic approaches based on siRNA can be delivered either locally or systemically. For local administration, siRNAs can be injected directly into the target tissue, for example via the intravitreal and intranasal routes. In this way, siRNAs have

higher bioavailability and reduced side effects [Whitehead K.A. et al., 2009]. There are several siRNAs locally administered for various diseases in clinical trials, including two siRNAs developed for cancer treatment [https://clinicaltrials.gov] (Table 1.1).

Drug	Target gene	Disease	Administration	Status
CEQ508	β-catenin	FAP	Oral	Phase I/II, ongoing
SIG12D	KRAS	PDAC	Intratumour	Phase II, ongoing

Table 1.1. Clinical trials of siRNAs locally administered.

Familial adenomatous polyposis (FAP), Kirsten rat sarcoma (KRAS), pancreatic ductal adenocarcinoma (PDAC).

Systemic delivery of siRNA is the best option for targeting a specific mRNA in sites with limited accessibility. Currently, there are several systemically administered siRNAs under clinical trials and, among them, 6 are employed for treating neoplastic diseases (Table 1.2) [https://clinicaltrials.gov]. The systemic delivery of siRNAs encounters several limitations, such as dose-limiting toxicity, adverse effects due to off-target binding, and activation of an immune response [Nikam R.R. and Gore K.R., 2018].

Drug	Target gene	Disease	Status
CALAA-01	RRM2	Solid tumours	Phase I, terminated
Atu-027	PKN3	Solid tumours	Phase II, ongoing
ALN-VSP02	KSP/VEGF	Solid tumours	Phase I, completed
TKM-PLK1	PLK-1	GI-NET/ACC	Phase II, ongoing
DCR-MYC	MYC	HCC	Phase II, ongoing
siRNA-EphA2	EphA2	Solid tumours	Phase I, ongoing

Table 1.2. Clinical trials of siRNAs systemically administered.

M2 subunit of ribonucleases reductase (RRM2), protein kinase 3 (PKN3), kinesin spindle protein (KSP), polo-like kinase-1 (PLK-1), gastrointestinal neuroendocrine tumours (GI-NET), adrenocortical carcinoma (ACC), hepatocellular carcinoma (HCC), ephrin type-A receptor 2 (EphA2).

SiRNAs and miRNAs have similar physico-chemical properties and for *in vivo* administration encounter similar limitations due to the scarce stability and poor bioavailability of RNA; therefore, similar strategies can be employed in principle to improve their *in vivo* efficacy.

1.3.3. Delivery of RNA-interfering molecules

In the last two decades, RNA-based therapies have been explored widely for clinical translation; RNAi-based therapies, able to interfere with the expression of genes, are endowed with potential to expand availability of anti-tumour agents and improve the efficacy of current therapies when used in combination. In principle, the use of siRNA and miRNA to inhibit the aberrant expression of oncogenes should provide the advantage of enhanced specificity compared to chemotherapeutics. However, even though these RNA-based therapies may have promising application in cancer treatment, there are some limitations that complicate their clinical application. For example, RNA molecules lack stability (half-life lower than 10 minutes), have poor bioavailability, may accumulate in off-target sites and activate immunoresponses [Juliano R.L., 2016].

The use of chemical modifications improved the stability of RNA therapeutics, reduced undesired off-target effects and maximised on-target pharmacological activities. Modifications of the sugar as well as the introduction of phosphorothioate linkages, changes of nucleosides with introduction of 5'-methylcytidine nucleotide have been made among others [Juliano R.L., 2016]. These structural modifications partially overcome RNase degradation and the activation of immune system response, improving the potency and pharmacological properties of RNAi drugs [Khvorova A. and Watts J.K., 2017]. Even so, the delivery of RNA molecules through the various biological barriers remains the main problem hindering the widespread development of RNA therapeutics. The negative charge

and the high molecular weight of RNA-based therapeutics are the main reasons why these molecules have no ability to cross cellular membranes [Dowdy S.F., 2017]. Moreover, molecules smaller than 10 nm in diameter would be susceptible to rapid renal clearance due to the glomerular pore size, which is approximately 8 nm [van de Water F.M. et al., 2006].

In order to overcome these obstacles, sophisticated delivery technologies for nucleic acids are required. For RNA delivery, different strategies have been developed including physical, chemical, and viral approaches. The physical methods include needle injection, gene gun, electroporation, and hydrodynamic delivery [Mellot A.J. et al., 2013]. The chemical approaches include the use of nanoparticles, for instance, lipid-based material, cationic polymers, or peptide-based carriers [Zhang S. et al., 2007]. Finally, the most efficient delivery approach is based on transduction by using viral vectors that infect cells. Unfortunately, this system presents high immunogenicity and safety issues due to the risk for viral recombination [Schott J.W. et al., 2016; Kaczmarek J.C. et al., 2017].

1.4. Nanoparticles-based tools for RNAi delivery

In this thesis, we investigated the use of two delivery platforms both developed in Dr. Tasciotti's laboratory at the Houston Methodist Research Institute (HMRI): 1) hybrid nanogel particles (HNPs), comprising a pH-responsive cross-linked hydrogel shell around a silica core [Khaled S.Z. et al., 2016]; 2) leukosomes, that are liposome-like nanoparticles formulated using membrane proteins extracted from purified circulating leukocytes and synthetic biocompatible phospholipids [Molinaro R. et al., 2016].

Nanoparticles are particles between 1 and 1000 nm size with different physico-chemical properties that have been widely exploited for the delivery of various payloads. Several therapeutic nanoparticle platforms, including liposomes, polymeric- and albumin-based nanoparticles have been FDA approved for cancer treatment. Various systems are currently

under clinical and preclinical investigation for the nanodelivery of chemotherapeutic agents, small molecules, short nucleic acids, immunotherapeutics for cancer treatment and other therapeutic applications. The FDA-approved nanoparticles are primarily liposomal formulations of chemotherapeutics (*i.e.*, Doxil/Doxorubicin, Daunoxome/Daunorubicin, Marqibo/Vincristine sulphate, Onivyde/Irinotecan) and the albumin bound paclitaxel Abraxane. No RNAi-based nanotherapy has been approved for cancer treatment yet, but many types of nanoparticles are under investigation for nucleic acid delivery in preclinical and clinical studies [Bobo D. et al., 2016; Zhang P. et al., 2018]. The use of delivery systems provides the opportunity to enhance *in vivo* targeting properties, pharmacokinetics, half-life and bioavailability of nucleic acid therapeutics [Tatiparti K. et al., 2017].

A major challenge in nanoparticle delivery is to favour the transport of therapeutics across biological barriers while excluding foreign material out and allowing only selected molecules to cross. The nanoparticles have to overcome different hindrances at both the systemic and cellular level:

1) Immune surveillance by the mononuclear phagocytic system. After administration, plasma proteins rapidly bind to nanoparticles in a process called opsonisation and phagocytic cells recognise and sequester them.

2) Non-specific accumulation at undesired sites, such as liver, spleen and kidneys, contributing to side effects at healthy organs.

3) Crossing of the biological barriers while preserving their cargo. Nanoparticles have to interact with vessel walls and extravasate to disease site. This phenomenon is facilitated by the enhanced permeability and retention effect typical of tumours, but it is limitated by the interstitial fluid pressure caused by poor lymphatic drainage, as well as extensive fibrosis and a dense extracellular matrix.

4) Penetration of target cell membranes escaping the endosomal compartment. Commonly, nanoparticles undergo active uptake and are internalised in endocytic vesicles that eventually fuse with lysosomes, causing the degradation of the payload. Finally, tumour cells can neutralise the effects of drug-delivering nanoparticles by activating multi drug resistance mechanisms, such as the expression of drug efflux pumps to reduce the sensitivity to treatments (Figure 1.9) [Blanco E. et al., 2015].

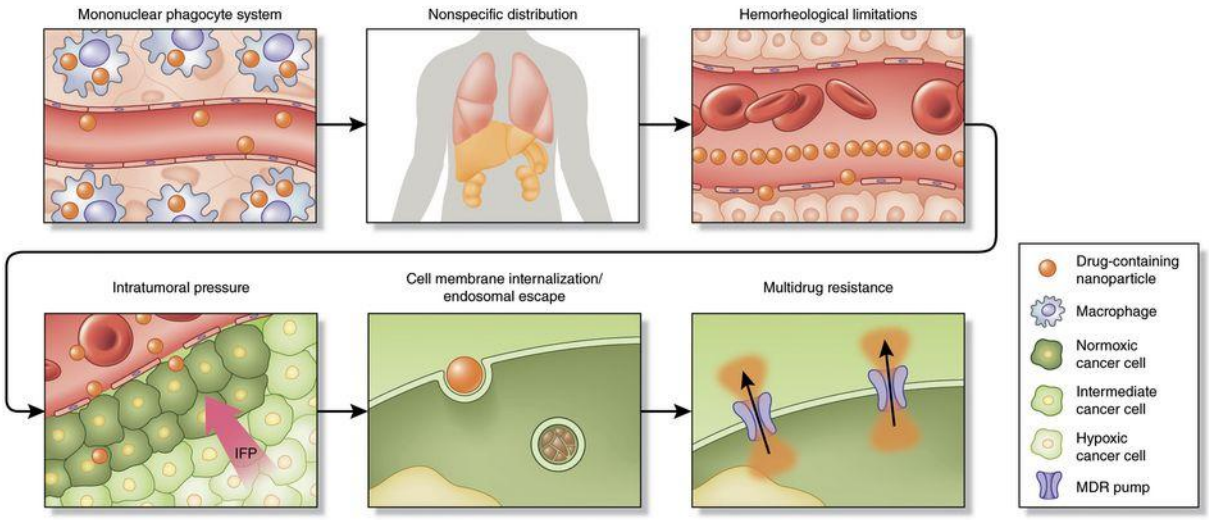

Figure 1.10. Biological barriers.

In the blood circulation, nanoparticles undergo opsonisation and subsequent degradation by immune cells. They can also be accumulated in excretory organs, such as the spleen, kidney and liver, contributing to non-specific distribution of nanotherapeutics to non-specific targets. To reach their target tissue, nanoparticles must exit the blood vessels and extravasate in tumours. Next, they have to cross cell membrane and avoid endosomal entrapment. IFP, interstitial fluid pressure. [Blanco E. et al., 2015]

The delivery of nucleic acids using nanocarriers can be achieved by passive or active targeting. The former one relies on the enhanced permeability and retention effect, *i.e.*, the prolonged circulation of nanoparticles combined with the leaky vasculature that leads to an accumulation in the tumour site, in a non-selective way. The main weakness of this system is the off-target delivery to undesired tissues, potentially leading to toxicity and adverse side effects [Ngoune R. et al., 2016]. Conversely, an active transport can be mediated by the specific ligand-receptors interaction between nanoparticle's surface and the target tissue. This relies on functionalisation of nanoparticles with specific ligands (*e.g.*,

transferrin, folic acid). The active delivery minimises the non-specific off-target effects typical of passive targeting [Alavi M. and Hamidi M., 2019]. Among frequently used nanocarriers there are liposomes and polymers, whose properties can effectively be examined using *in vitro* and *in vivo* cellular models.

Liposomes are spherical lipid-based nanovesicles usually composed of neutral or charged lipids, which are amphiphilic molecules containing a polar head group connected by a linker to a hydrophobic tail. When liposomes are prepared to deliver nucleic acids, the positive charge is necessary for the electrostatic interaction with their anionic phosphate groups [Wasungu L. and Hoekstra D., 2006]. Cell lines can be transfected with liposomal nanoparticles to achieve high transfection efficiency. The subsequent release of nucleic acids can occur mainly in two different ways: 1) fusion of liposomal and cellular membranes through the interaction between the cationic headgroups of liposomes and the anionic glycoproteins and/or proteoglycans of the cellular membrane or 2) the liposome can undergo receptor-mediated endocytosis. In the latter case, following cell uptake, liposomes are embedded into the endosomes, where the anionic lipids diffuse from the endosomal membrane to the cationic liposomes, thus buffering and destabilising the endosomal membrane itself. This so-called “flip-flop” mechanism results in the displacement of the nucleic acid which is released to the cytosol [Xu Y. and Szoka F.C. Jr., 1996]. The main advantages of liposomes are their biocompatibility, biodegradability and low toxicity, due to the presence of naturally occurring materials. On the other hand, due to their positive charge, they may lead to non-specific interactions with serum proteins and cause cytotoxicity and haemolysis [Wasungu L. and Hoekstra D., 2006], as well as immune system triggering through the activation of toll-like receptors [Molinaro R. et al., 2013].

Cationic polymers represent a valid alternative to liposomes with relatively high transfection efficiency, easy preparation procedures, good biodegradability, low toxicity

and high stability [Wagner E., 2014]. These polymers electrostatically bind to the anionic phosphate groups along the backbone of the nucleic acids. These interactions enable the packing of the nucleic acids in nanoparticles called polyplexes [Aied A. et al., 2013]. The use of polymers provides protection from enzymatic degradation and prevents disaggregation in the presence of serum proteins. The polyplexes enter the cell mainly by endocytosis; this mechanism and the ability to escape the endosomal compartment depend on polymer composition, size and surface potential [Buyens K. et al., 2010; Molinaro R. et al., 2013].

Among the most commonly used polymer, polyethylenimine (PEI) presents good transfection capacity, but has low biocompatibility. PEI is a cationic polymer with high number of amines that provides the polymer with high charge density, conferring unique features such as strong nucleic acid condensation with protection from enzymatic degradation, and buffer capacity through the "proton sponge effect", which allows endosome disruption and escape of nanoparticles from the endo-lysosomal entrapment [Godbey W.T. et al., 2001]. PEI exists in two forms, *i.e.*, linear and branched, and this feature affects complexation with the nucleic acids and transfection efficiency. Branched PEI presents a higher number of primary amines, allowing the formation of more stable complexes essential for the delivery of siRNA [Kwok A. and Hart S.L., 2011]. Transfection efficiency also depends on PEI molecular weight, with higher molecular weight enhancing transfection efficiency, but also significantly increasing cytotoxicity due to high charge density and lack of degradable linkages [Goyal R. et al., 2014]. A proper balance between molecular weight and branched/linear form is needed for successful RNA delivery. In order to overcome PEI cytotoxicity, a proposed strategy is to conjugate PEI with other molecules (*i.e.*, cholesterol, polyethylene glycol) [Cavallaro G. et al., 2017] or other nanoparticles [Buchman Y.K. et al., 2013; Ewe A. et al., 2017].

1.4.1. Hybrid nanogel particles

Hydrogels are hydrophilic polymeric networks with 3D configuration with high liquid absorbing capacity. Hydrogels are similar to living tissues, by virtue of their high water content, their soft and rubbery consistency, and low interfacial tension with biological fluids [Ratner B.D. and Hoffman A.S., 1976]. For drug delivery, they are required to be biodegradable and biocompatible. As they can swell in an aqueous environment, the most common mechanism of payload release from hydrogels is passive diffusion, which can be further regulated by adjusting the polymer composition. Other mechanisms of release are: 1) diffusion-controlled, 2) swelling-controlled, or 3) chemically-controlled. In this way, the drug is released in a specific predetermined temporal and/or spatial manner within the body. Moreover, the release form hydrogel-based delivery systems can be time-controlled or stimuli-induced, such as under specific physiopathological conditions (*i.e.*, temperature, pH, etc.) [Hamidi M. et al., 2008]. The use of hydrogel nanoparticles is limited by their low structural integrity and poor mechanical stability. The mechanical properties of hydrogels can be improved by increasing the amount of crosslinking, although this can affect the responsiveness and biocompatibility [Yang J. et al., 2013; Buwalda S.J. et al., 2014]. Hybrid systems can be used to overcome the limitations of hydrogels. As a matter of fact, a rigid inorganic core can stabilise the hydrogel without losing its environmental responsiveness and biocompatibility [Yang J. et al., 2013].

The nanoparticles used in this thesis (HNPs) have a silica core encased within a pH-responsive hydrogel composed by poly(diethylaminoethyl methacrylate) (PDEAEM) crosslinked with polyethylene glycol methacrylate (PEGMA) and triethylene glycol dimethacrylate (TEGDMA) linkers [Khaled S.Z. et al., 2016] (Figure 1.10).

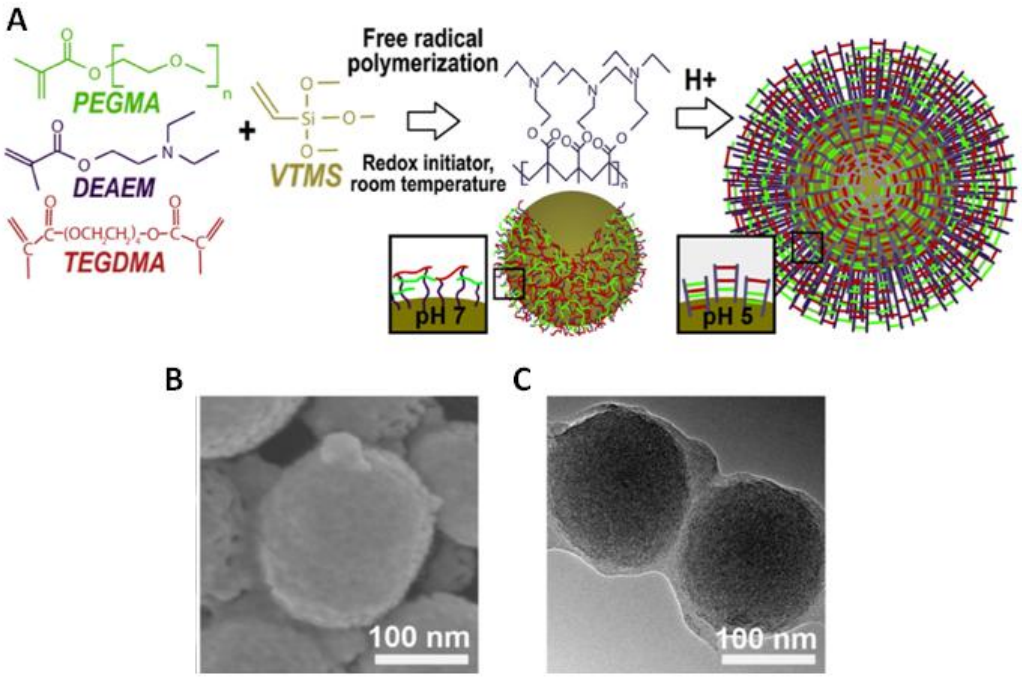

Figure 1.11. HNP.

(A) Schematic representation of a HNP. (B) Scanning electron microscope (SEM) image of HNPs, (C) transmission electron microscopy (TEM) image of HNPs [Khaled S.Z. et al., 2016].

HNPs demonstrated the ability to buffer the acid microenvironment through the protonation of the tertiary amines exposed on the particle surface, thereby acquiring a positive surface charge and increasing their size. This mechanism, known as "proton sponge effect", endorses the nanoparticles with the ability to escape endosomal compartment [Khaled S.Z. et al., 2016].

In a previous study, siRNA loaded onto HNPs was efficiently released in an acidic pH environment, escaping endosomal sequestration. These nanoparticles were shown to significantly decrease the expression of CXCR4 in a human breast cancer cell line both *in vitro* and *in vivo*; moreover, they accumulated preferentially at the tumour site after intravenous injection [Khaled S.Z. et al., 2016]. Based on the afore-mentioned properties of HNPs and combining them with the physiopathological features of STS models, we decided to investigate the delivery of siRNAs to the tumour tissue using HNPs. We

hypothesised that the enhanced angiogenesis and subsequent leaking vasculature of STSs would trigger the accumulation of HNPs to the tumour.

1.4.2. Leukosomes

Leukosomes, which are liposome-like nanovesicles enriched in leukocyte membrane proteins, were developed in Dr. Tasciotti's laboratory and firstly described by Molinaro [Molinaro R. et al., 2016]. These nanoparticles, prepared using membrane proteins extracted from purified circulating leukocytes and synthetic biocompatible phospholipids, were formulated to target and treat local inflammation [Molinaro R. et al., 2016]. The leukosome surface contains several membrane-associated proteins of leukocytes: among them, integrins (*e.g.*, LFA-1, Mac-1, VLA-4), which facilitate particles binding to inflamed endothelium, while self-tolerance biomarkers (*e.g.*, CD47, CD45 and MHCI) allow prolonged circulation and biocompatibility (Figure 1.11) [Molinaro R. et al., 2016].

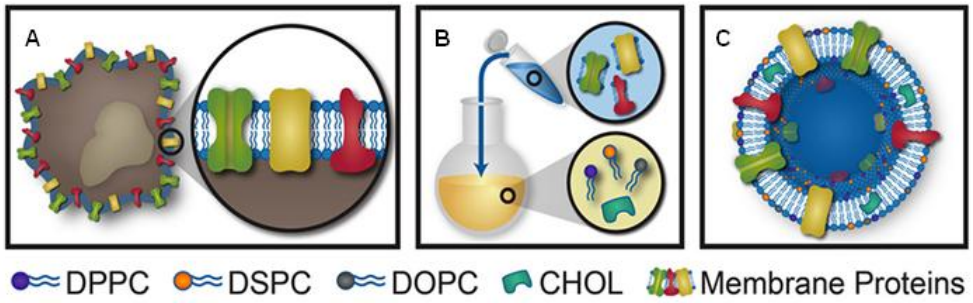

Figure 1.12. Graphic representation of leukosome.

(A) Leukocyte-derived membrane proteins. (B) Phospholipids and protein mixture. (C) Leukosome phospholipid bilayer with integrated proteins. Dipalmitoylphosphatidylcholine (DPPC), 1,2-Distearoyl-sn-glycero-3-phosphocholine (DSPC), 1,2-dioleoyl-sn-glycero-3-phosphocholine (DOPC), Cholesterol (CHOL) [Molinaro R. et al., 2016].

Owing to their size and molecular composition, leukosomes can be considered similar to exosomes, which are also nanosized membrane vesicles composed by a bilayer of phospholipids with proteins [Arrighetti N. et al., 2018]. Exosomes are natural carriers of a wide variety of biological molecules, such as lipids, proteins, DNA, mRNA, non-coding

RNA and various metabolites [Valadi H. et al., 2007]. In addition, leukosomes can be manufactured using a microfluidic-based platform, named NanoAssemblr, which allows a standardisable, batch-to-batch consistent, scalable, and high-throughput assembly method (Figure 1.12) [Molinaro R. et al., 2018]. This approach represents a universal, versatile and scalable tool for the manufacturing of lipid-based nanoparticles.

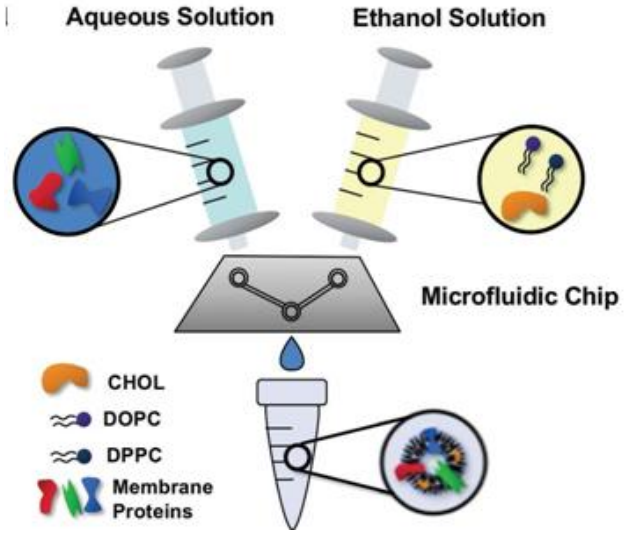

Figure 1.13. Schematic representation of the assembly of leukosomes using NanoAssemblr.

The NanoAssemblr platform allows the simultaneous synthesis of liposome-like nanoaprticles and the incorporation of a nucleic acid within them. An aqueous phase containing nucleic acid and membrane proteins is injected with an organic phase containing lipids in a microfluidic chip. By controlling the flow rate ratio between the two phases, the total flow rate of the two streams, and the temperature, it is possible to tune the size and shape of nanoparticles [Molinaro R. et al., 2018].

Based on the afore-mentioned properties of leukosomes, we decided to investigate the delivery of siRNAs to the sarcoma tissue using leukosomes. We hypothesised that the pro-inflammatory function of heparanase, facilitating leukocyte recruitment, can be exploited for targeting the inflamed tumour microenvironment and efficiently deliver the cargo to STSs.

2.SCOPE OF THE THESIS

Treatment of recurrent and metastatic STS remains a challenge. Despite a few recently approved molecular targeted and histology-driven therapies, survival rates are still largely unsatisfactory and prognosis is poor for most patients, underscoring the need for new therapeutic strategies.

Advances in understanding the pathogenesis of sarcomas have evidenced a crucial role for the tumour microenvironment. As in other solid tumours, the complex interactions between tumour cells and components of the microenvironment are essential for sarcoma growth and dissemination, and influence the response to therapies. Accumulating evidence indicates that the heparanase/HSPG system plays a crucial role at the interface between tumour and stromal components, and highlights the implication of heparanase in critical processes of tumour biology (*e.g.*, inflammation, growth, angiogenesis, metastasis, drug resistance).

Several lines of evidence support heparanase as a suitable target for cancer treatment; first of all, its expression is increased in all cancer types examined and several studies have correlated heparanase overexpression with reduced survival. There is only one enzimatically active form of heparanase in humans that is expressed at very low levels in healthy tissues. Moreover, preclinical studies of heparanase overexpression or knockdown demonstrated the relevant role of heparanase in tumour progression. Finally, preclinical and early clinical data with HS mimetics confirmed the feasibility and safety of targeting heparanase for treatment of cancer patients.

Understanding the effects of specific heparanase inhibition in various tumour contexts is important to optimise the use of inhibitors alone and in rational combinations. By neutralising mRNA molecules, RNAi allows specific and efficient gene silencing and, combined with nanodelivery systems, represents a promising approach potentially transferable to the therapeutic setting.

On the basis of these considerations, the ultimate goal of this study was to assess *in vitro* and *in vivo* effects of heparanase RNAi approaches, with potential therapeutic application, in different sarcoma models.

Specific aims of the thesis work were to:

1) Identify small RNAi molecules (*i.e.*, miRNA or siRNA) down-regulating heparanase expression and examine *in vitro* their functional effects in sarcoma cell lines characterised by high expression of heparanase.
2) a. Optimise a nanoparticle-based system to deliver heparanase RNAi molecules *in vitro*.

   b. Assess distribution and therapeutic efficacy of nanoparticle-delivered anti-heparanase RNAi in *in vivo* sarcoma preclinical models.

3.MATERIALS AND METHODS

3.1. Cell lines and culture conditions

The human RT cell line A204 was obtained from American Type Culture Collection. Previously listed as a rhabdomyosarcoma cell line, in 2002 it was found to harbour a mutation in the SMARCB1 (hSNF5/INI1) gene, causing the loss of the encoded protein, consistent with classification as a RT [Betz B.L. et al., 2002]. The human SS cell line CME-1 was obtained from a monophasic tumour containing the SS18-SSX2 translocation and established by immortalisation with SV40 [Renwick P.J. et al., 1995]. This cell line was already available in our Institute [Mancuso T. et al., 2000]. The human non small cell lung cancer cell line A549, the human breast cancer cell line MDA-MB-231 and the human umbilical vein endothelial cells (HUVEC) were obtained from American Type Culture Collection. All tumour cell lines were authenticated by short tandem repeat analysis using the AmpFLSTR Identifiler PCR Amplification Kit (Applied Biosystems, Thermo Fisher Scientific, Waltham, MA, USA). For A204 cell line, microsatellite information is available online, while for CME-1 cell line the identity was confirmed by comparing the microsatellite profile with the analysis performed when the cells were received. Cell line identities were further confirmed by western blot analysis detecting expression of the SS18-SSX2 fusion protein and the loss of SMARCB1 in CME-1 and A204 cells, respectively. Cells were kept in culture for no more than 20 passages and thawed from an authenticated frozen stock. A204, CME-1 and A549 cell lines were grown in RPMI-1640 medium (Lonza, Basel, Switzerland) supplemented with 10% fetal bovine serum (FBS) (Gibco, Thermo Fisher Scientific). MDA-MB-231 cell line was grown in DMEM-F12 medium (Lonza) supplemented with 5% FBS. HUVEC cell line was grown in EBM-2 medium (Lonza) supplemented with EGM-2 SingleQuots (Lonza). Cells were grown as monolayer, at 37 °C in a 5 % CO_2 atmosphere and routinely checked for mycoplasma contamination (MycoAlert Mycoplasma Detection Kit, Lonza). Previous characterisation of the cell lines performed in our laboratory showed that A204 and CME-1

cells grow as intramuscular tumour xenografts in SCID mice. Microscopic metastatic foci have been observed in the lungs of tumour bearing mice (Figure 3.1).

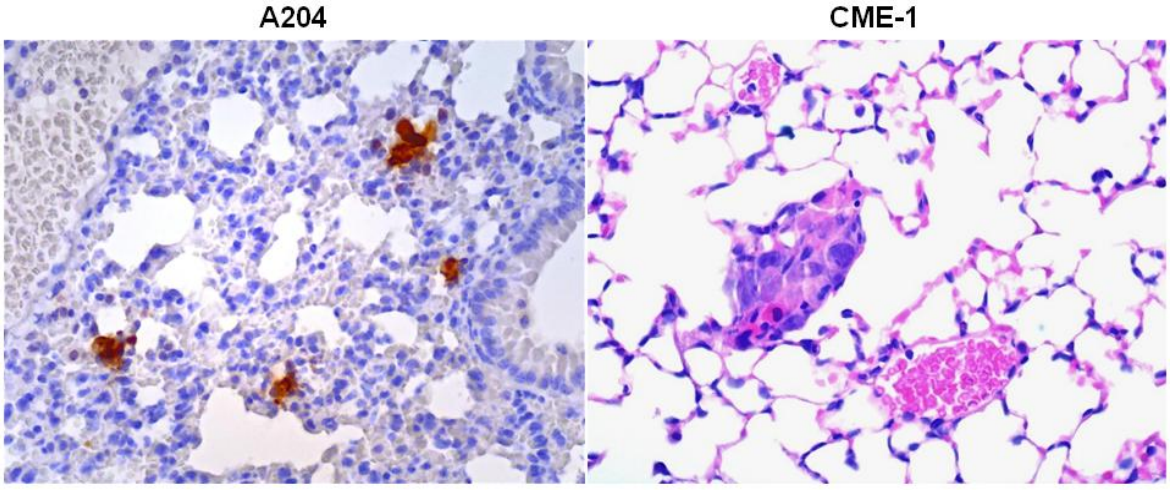

Figure 3. 1. Representative images of metastatic deposits in lungs from mice harbouring orthotopic A204 or CME-1 tumours.

The lungs lobes were formalin fixed and paraffin embedded. For A204, sections were subjected to immunohistochemistry with anti-Vimentin (of human origin) [unpublished]. For CME-1, sections were stained with hematoxylin and eosin [Cassinelli G. et al., 2018].

3.2. Cell transfection and transient gene silencing

For transfection, A204 and CME-1 cells were plated into 6-well plates at a density of 2.5 x 10^4 cells/cm^2 and 3 x 10^4 cells/cm^2, respectively. Transfection efficiency was preliminary evaluated using BLOCK-iT™ Alexa Fluor Red Fluorescent Control (Ambion). Twenty four h later, cells were transfected in RPMI-1640 medium without FBS, using Lipofectamine RNAiMAX (Thermo Fisher Scientific) as transfection reagent with various concentrations of selected miRNA (has-miR-1258 ID: MC13267, mirVana™, Ambion, Thermo Fisher Scientific, or ID: mi0006392, MiRIDAN, Dharmacon, Lafayette, CO, USA), siRNA (HPSE Silencer Select Validate siRNA, s21304/siR04, s21305/siR05 and s21306/siR06 Ambion) or negative control (mirVana™ miRNA mimic Negative Control #1, and Silencer Select Negative Control #2, Ambion). Cells were incubated with the transfection mix for 5 h and then the transfection medium was replaced with complete medium. Cells were harvested at different time points after transfection for further

analyses. The levels of miRNA upon transfection were checked by qRT-PCR. When required, transfected cells were reseeded for cell growth curves, colony formation assays, migration and invasion assays.

3.3. MiR-1258 and heparanase gene expression analysis

3.3.1. RNA isolation

RNA was isolated using miRNeasy Mini Kit (Qiagen, Hilden, Germany) following manufacturer's instructions. The miRNeasy Mini Kit enables purification of total RNA with efficient enrichment of miRNA and small RNAs. Absorbance at 260 nm (A260) and 280 nm (A280) was detected using a NanoDrop 2000c (NanoDrop, Thermo Fisher Scientific) spectrophotometer. A260 was used to calculate RNA concentration. A260/A280 was used as a first means of assessing RNA purity. After quantifying RNA samples, they were stored at -80 °C.

3.3.2. Quantitative reverse transcriptase polymerase chain reaction

Quantitative RT-PCR was applied to quantify miRNAs and transcripts levels. RNA was first reverse transcribed to cDNA; then cDNA was amplified. Reverse transcription was performed using 2 different kits: miScript II RT Kit (Qiagen), for total RNA including miRNAs, or High Capacity cDNA Reverse Transcription Kit (Applied Biosystems) for mRNA. The reaction was carried out using 1 μg RNA in the presence of RNase inhibitors, in a Biometra thermocycler (Biometra GmbH, Göttingen, Germany) following the manufacturer's instruction. Two negative controls where included to check for possible reagent contaminations (one sample without reverse transcriptase and one without RNA).

Amplification of the synthesised cDNA was performed using PrimeTime qPCR assays: HPSE Hs.PT.58.15529804 and GAPDH Hs.PT.39a.22214836 (Integrated DNA Technologies, IDT, Coralville, Iowa), based on the TaqMan technology (Applied

Biosystems). Amplification of miRNA was performed using miScript Primer assays: Hs_miR-1258_1 MS00014315 and Hs_SNORD48_1 MS00007511 (Qiagen) using SYBR Green-based real-time PCR. Technical triplicate reactions were carried out on MicroAmp Optical 96-Well reaction plates (Applied Biosystems). For genes, each reaction volume (10 μL) contained 2.5 μL cDNA, 5 μL master mix (TaqMan Universal PCR Master Mix, Applied Biosystems) and 0.5 μL of the specific assay; for miRNAs, each reaction volume (25 μL) contained 2.5 μL of reverse transcribed miRNA, 12.5 μL master mix (QuantiTect SYBR Green PCR, Qiagen), 2.5 μL miScript Universal Primer (Qiagen), 2.5 μL of specific assay and 5 μL nuclease-free water. Amplification reactions were performed using a 7900HT Fast Real-Time PCR System (Applied Biosystems) equipped with Sequence Detection Systems 2.4 software (Applied Biosystems). Data analysis was performed by the use of RQ manager software (Applied Biosystems).

Relative levels of heparanase and miR-1258 were determined through the relative quantification (RQ) method using the comparative cycle threshold (Ct) (ΔΔCt) assay configuration. Briefly, for each reaction a value of Ct was identified.

ΔCt, ΔΔCt and RQ were then calculated as follow:

$$\Delta Ct = Ct_{(\text{target gene/miRNA})} - Ct_{(\text{reference gene/miRNA})}.$$

$$\Delta\Delta Ct = \Delta Ct_{(\text{target sample})} - \Delta Ct_{(\text{reference sample})}$$

$$RQ = 2^{-\Delta\Delta CT}$$

GAPDH and SNORD48 were used as reference gene or miRNA, respectively. For each time point, cells transfected with negative control were chosen as reference samples.

3.4. Protein expression analysis

3.4.1. Protein extraction and quantification

Protein lysates were prepared using a lysis buffer derived from the Laemmli buffer [Laemmli U.K., 1970] composed of 0.125 M Tris HCl pH 6.8 (Trizma hydrochloride, Sigma-Aldrich, Merck, Burlington, MA, USA), 5% sodium dodecyl sulfate (SDS, Lonza) and protease/phosphatase inhibitors (25 mM sodium fluoride, 10 μg/mL pepstatin A, 1 mM phenylmethylsulfonyl fluoride, 10 μg/mL trypsin inhibitor, 12.5 μg/mL leupeptin, 30 μg/mL aprotinin, 1 mM sodium orthovanadate and 1 mM sodium molibdate), all purchased from Sigma-Aldrich.

At the appropriate time, A204 and CME-1 cells were harvested after washing twice with ice-cold 'v-PBS' (phosphate-buffered saline, PBS, Lonza, containing 100 μM sodium orthovanadate), to inhibit the action of phosphatases. The lysis buffer was added to wells and cell detachment from plastic was completed on ice by using a cell scraper (Corning Inc, Corning, NY, USA). Lysed cells were collected in tubes that were then boiled for 5 min and sonicated for 30 s with immersion probe at 10% amplitude, 400W/20kHz (Branson 450 Digital Sonifier, Emerson Electric Co, Ferguson, MO, USA).

An aliquot of cell lysates was kept for quantification of protein concentration that was performed through the bicinchoninic acid (BCA) assay method (Pierce, Thermo Fisher Scientific) using a 562 nm-reading-spectrophotomer (Uvikon 930, NorthStar Scientific, Leeds, UK). This method is based on a colorimetric reaction produced by the interaction between BCA and cuprous ions, which in turn are generated by the reduction of cupric ions by proteins. Briefly, a standard curve was prepared using a series of dilutions of known concentration of bovine serum albumin (BSA) and assayed alongside the unknown proteins. Protein concentrations were calculated by comparing OD readings with those obtained from the standard curve. Lysates were frozen and stored at -80 °C.

3.4.2. Nucleus/cytoplasm fractionation

Fractionated protein lysates were prepared using a Nuclear Extraction Kit (Cayman Chemicals, Ann Arbor, MI, USA) following manufacturer's instruction. Briefly, cell lysis was obtained using a hypotonic buffer, followed by a spin recovery of cytoplasmic lysates. Next, pelleted nuclei were lysed in a 'nuclear extraction buffer'. Samples were stored at -80 °C. To test the efficiency of fractionation, HDAC1 and α-tubulin as nuclear and cytoplasmic protein markers were used in membrane immunodecoration.

3.4.3. Gel electrophoresis and western blotting

After total cell lysis or nucleus/cytoplasm separation, 20 µg samples were fractionated by SDS-polyacrylamide gel electrophoresis. Gradient NuPAGE gels (4-12%) were employed following the manufacturer's procedures (Applied Biosystems). After gel fractionation, proteins were transferred on Hybond ECL nitrocellulose membranes (GE Healthcare, Chicago, IL, USA) using a wet transfer apparatus. The transfer was performed overnight (O/N) at constant 37 V, using a transfer buffer (10% Tris-glycine pH 8.3 and 20% methanol). Transfer efficacy was evaluated by Ponceau S staining (Sigma-Aldrich).

Membranes were first washed with 'Tris-buffered saline (TBS)-Tween' (TBS containing 0.1% Tween-20, Sigma-Aldrich), then incubated with a 'blocking buffer' (TBS-Tween containing 5% (w/v) dried skimmed milk (Merck)). Membranes were then incubated on rotation, O/N at 4°C, with primary antibodies (Table 3.1) dissolved in blocking buffer. After rinsing 3 times with TBS-Tween, membranes were incubated for 1 h with peroxidase-conjugated mouse or rabbit IgG secondary antibodies (NA9310 and NA9340, GE Healthcare) dissolved in blocking buffer. After washing 3 times with TBS-Tween and once with TBS, the binding of secondary antibodies to membranes was detected on autoradiography film by chemiluminescence (ECL, GE Healthcare). Briefly, oxidation of luminol, a chemiluminescent substrate, is catalysed by horseradish peroxidase. This

reaction forms excited intermediates that release photons which are captured by the X-ray film when they decay to a lower energy level. This reaction occurs in presence of enhancers that amplify the light intensity by about 1000 folds.

All western blot analyses were repeated at least 3 times using independent biological samples. Band quantification was performed taking advantage of the ImageJ software [Abramoff M.D. et al., 2004], following the specific protocol for 1D gel quantification available on ImageJ website (http://rsb.info.nih.gov/ij/docs/menus/analyze.html#gels).

I tested 5 anti-heparanase antibodies: HPA-1 (H-80): sc-25825, HPA-1 (E-10): sc-515935 [Santa Cruz Biotechnology, Dallas, TX, USA], anti-heparanase 1: ab42817 [Abcam, Cambridge, UK], anti-heparanase 1:MBS178331 [MyBioSource, San Diego, CA, USA] and HPA-1 733 [obtained from Professor Vlodavsky I.]. For this thesis, HPA-1 (H-80): sc-25825 was selected as the best option.

Antibody	Dilution	Catalog. No.	Company
Heparanase	1:500	sc-25825	Santa Cruz
HDAC1	1:1000	sc-10809	Santa Cruz
α-tubulin	1:1000	T5168	Sigma-Aldrich
Actin	1:3000	A2066	Sigma-Aldrich

Table 3.1. List of the employed antibodies and their dilutions.

3.4.4. Antibody Arrays

Antibody Arrays were used to investigate the relative levels of multiple angiogenic factors in sarcoma cells, (Human Angiogenesis Array Kit, ARY007, R&D Systems, Minneapolis, MI, USA) following the manufacturer's procedures. Briefly, A204 and CME-1 cells were lysed in 1% NP-40 lysis buffer and centrifuged at 14.000 g for 15 min. The supernatant was recovered and the BCA assay method was used to quantify the protein concentration.

One mg of proteins was applied to each array.

3.4.5. Enzyme-linked immunosorbent assays

Heparanase concentration in cell culture conditioned media of transfected cells was determined by solid phase sandwich enzyme-linked immunosorbent assays (ELISA) (CSB-E09899H, Cusabio Technology LLC, Houston, TX, USA). To obtain conditioned medium, 48 h after cell transfection, the supernatant was removed and replaced with RPMI-1640 without FBS. Twenty-four h later, the conditioned medium was collected and stored at -80 °C until use. To obtain cell lysates, A204 and CME-1 cells were detached with a scraper in PBS containing phosphatase and protease inhibitors (Halt™ Protease Inhibitor Cocktail (100X) 78430, Halt™ Phosphatase Inhibitor Cocktail (100X) 78428, Thermo Fisher Scientific), and stored O/N at -80 °C. After 2 freeze-thaw cycles, cells were centrifuged at 5000 x g at 4 °C for 5 min. The supernatant was collected and assayed immediately. Samples from each experiment were tested in duplicate, according to the manufacturer's instructions. The coloured product generated by the enzyme activity was detected by a microplate reader set at 450 nm (iMark, Bio-Rad, Hercules, CA, USA).

3.4.6. Immunofluorescence staining

A204 and CME-1 cells were seeded at appropriate density in 6-well plates containing 3 coverslips. After 24 h, cells were transfected with anti-heparanase siRNA or negative control. Forty-eight h later cells were rinsed in PBS and fixed in 3.7% formaldehyde dissolved in PBS for 15 min. After washing with PBS, cells were permeabilised with 1% bovine serum albumin (BSA, Sigma-Aldrich) in PBS (PBA) + 0.1% Triton X-100 (Honeywell Fluka, Morris Plains, NJ, USA), for 5 min. After washing with PBA, cells were incubated with PBA for 1 h. Wells were then incubated at room temperature with a heparanase antibody at 8 µg/mL for 3 h. After 2 washes with PBA, cells were incubated

with an AlexaFluor 488-conjugated goat anti-rabbit antibody (Life Technologies, Thermo Fisher Scientific) at 4 µg/mL for 1 h. After washing with PBA, wells were incubated with 2 µg/mL Hoechst 33342 (Sigma-Aldrich) for 1 min, to counterstain nuclei. Coverslips were then removed from wells and mounted on glass slides with ProLong Antifade Mountants (Thermo Fischer Scientific) and let dry O/N. Fluorescence imaging was performed using a fluorescence microscope equipped with a digital camera.

3.5. Functional studies *in vitro*

3.5.1. Cell growth curves

Cells were seeded in 12-well plates (A204 8 x 10^3 cells/cm^2; CME-1 7 x 10^3 cells/cm^2) and, after 24 h, transfected with anti-heparanase siRNA or negative control. Cells were counted daily, after harvesting with trypsin-EDTA (Gibco), with an automated cell counter (Beckman Coulter, Brea, CA, USA). All cell growth experiments were performed at least 3 times.

3.5.2. Soft agar colony assay

A 5% agarose (low gelling temperature, Sigma-Aldrich) in Millipore water (Merck) was prepared and autoclaved at 120 °C for 30 min. For CME-1 cells, 1.5 mL base of 0.5% agarose was prepared by diluting the melt 5% agarose in pre-warmed medium at 37 °C, allowed to solidify in Petri dishes (9.6 cm^2) for 1 h. A cell suspension in medium was added to agarose to obtain final 0.33% agarose which was poured on the 0.5% agarose layer and allowed to solidify at room temperature for 1 h. Since A204 cells tended to invade across the base, growing below as monolayer, the agarose concentrations were adjusted to 0.7% for the base and 0.46% for the cell containing upper layer. The plates were then incubated at 37 °C for 7-10 days. To highlight colonies, 0.5 mL of p-iodonitrotetrazolium (1 mg/mL in saline solution) vital dye was added to the plates. The next day, colonies were counted under a magnificator.

3.5.3. Cell migration assay

A wound healing assay was performed to assess migration of both cell lines by examining the cell ability to close gaps in a monolayer. A204 and CME-1 cells were seeded in 6-wells plates 4.2 x 10^4 cells/cm^2. Twenty four h later, cells were transfected with anti-heparanase siRNA or negative control. Following additional 24 h, wounds were induced by scratching

the cell monolayer with a sterile 200 µl pipette tip. Images were captured by phase-contrast microscopy immediately following wound induction (0 h), and at 16, 24, 48 and 72 h post-scratching. To quantify cellular migration across the width of the wound, the length of 40 individual lines throughout the wound were measured at each time point. Experiments were performed in triplicate.

3.5.4. Cell invasion assay

The invasion ability of cells was determined using the Transwell permeable support (8.0 µm Polycarbonate Membrane, 6.5 mm Insert, Costar, Corning). Membranes were coated with 60 µL of 208 µg/mL Matrigel (Corning). Forty-eight h after transfection, cells were seeded in duplicate onto the upper chamber in FBS-free RPMI-1640 medium (4-6 x 10^5 cells/mL in a volume of 300 µL). The lower chamber contained 1 mL medium with FBS. The chambers were incubated at 37 °C for 24 h allowing cells to invade Matrigel and pass through the microporous membrane. Then, cells adherent to filters on the lower chamber side were fixed with 100% ethanol for 30 min and stained with 0.4% sulforhodamine B (SRB, Sigma-Aldrich) in 1% acetic acid at room temperature for 20 min. Filters were then washed with 1% acetic acid and left to dry for 24 h. Finally, cells in 10 random fields per chamber were counted at the microscope. Experiments were performed in triplicate.

3.6. Synthesis and characterisation of nanoparticles for RNAi delivery

Nanoparticles have been synthesised and characterised in Dr. Tasciotti's laboratory, at the HMRI, by high qualified chemists. All the *in vitro* studies testing nanoparticles efficacy on A204 cells were performed at the HMRI in collaboration with Tasciotti's team.

3.6.1. Synthesis and characterisation of pH-responsive hybrid nanogel particles (HNP)

HNPs were fabricated and characterised by chemists from Dr. Tasciotti's laboratory, through a novel one-pot synthesis approach, as previously described [Khaled S.Z. et al., 2016]. In summary, this procedure is based on the free radical co-polymerisation of the cationic monomer 2-(diethylamino)ethyl methacrylate and the monomeric silica precursor vinyltrimethoxysilane in the presence of polyethylene glycol methacrylate, triethylene glycol dimethacrylatelinkers and Fluorescein-5-isothiocyanate (FITC) for the imaging purposes (Thermo Fisher Scientific). This procedure yielded the *in-situ* formation of a cross-linked PDEAEM hydrogel shell around the fluorescent silica core. To eliminate the surfactants and unreacted monomers, the particles were washed several times in repeated cycles of resuspension in acetone and water, and then centrifuged. The particles were then lyophilised and stored in a desiccator until use.

3.6.2. Synthesis and characterisation of Leukosomes

Leukosomes were already available in the laboratory of Dr. Tasciotti. They were fabricated and characterised by designated personnel, as previously described [Molinaro R. et al., 2016]. Leukosomes were prepared using the thin layer evaporation (TLE) method. Briefly, DPPC or the fluorescent equivalent, DSPC, DOPC, and CHOL (Avanti Polar Lipids Inc. Alabaster, AL, USA) were dissolved in a chloroform:methanol mixture (3:1 v/v) at 5:1:3:1 molar ratio, respectively, and the solvent was then evaporated through a rotary evaporator (BÜCHI Labortechnik AG, Switzerland) to form a thin film. Films were hydrated with membrane proteins from inflammatory cells (1:300 protein-to-lipid ratio) dispersed in PBS to assemble leukosomes by 3 cycles of heating at 45 °C and vortexing, 3 min each. Membrane proteins were obtained from T cells and macrophages of Balb/c mice. Briefly, Balb/c mice (4 weeks old) were used to isolate fresh infiltrating leukocytes after injecting

thioglycollate medium (2.5 mL) into the peritoneum, to induce inflammation. Four days later, animals were sacrificed and the peritoneum washed 3 times with cold PBS in order to collect the peritoneal lavage. Fluorescence activated cell sorting (FACS) was performed to purify T cells and macrophages, taking advantage of specific surface markers. A commercial kit (Qiagen) was used to isolate enriched membrane protein fractions. Finally, following to lipid suspension hydration with membrane proteins, the formulation was extruded 10 times through 200 nm pore-size cellulose acetate membranes at 45 °C in order to obtain unilamellar vesicles, which were then dialysed overnight through 1000 KDa membranes (Spectrum Laboratories, Inc. Rancho Dominguez, CA, USA) to eliminate raw material and unincorporated proteins. Final leukosome concentration was assessed by measuring the fluorescence of 1,2-dioleoyl-sn-glycero-3-phosphoethanolamine-N-(carboxyfluorescein) (ammonium salt) [Molinaro R. et al., 2016] and normalised to the one of control liposomes.

Leukosomes and liposomes were also synthesised using the above mentioned microfluidic approach [Kastner E. et al., 2014; Kastner E. et al., 2015] as described in Molinaro R. et al., 2018. By using this system it was possible to simultaneously synthesise leukosomes and incorporate the siRNA within the nanoparticles. Briefly, an aqueous phase containing siRNA and membrane proteins and an organic phase containing lipids were injected in a Y-shaped inlet channel, one for each arm of the Y (Figure 3.2). Then, by controlling the flow rate ratio between the aqueous and organic phases, the total flow rate of the two streams, and the temperature, the leukosomes were produced with the desired size of about 100 nm.

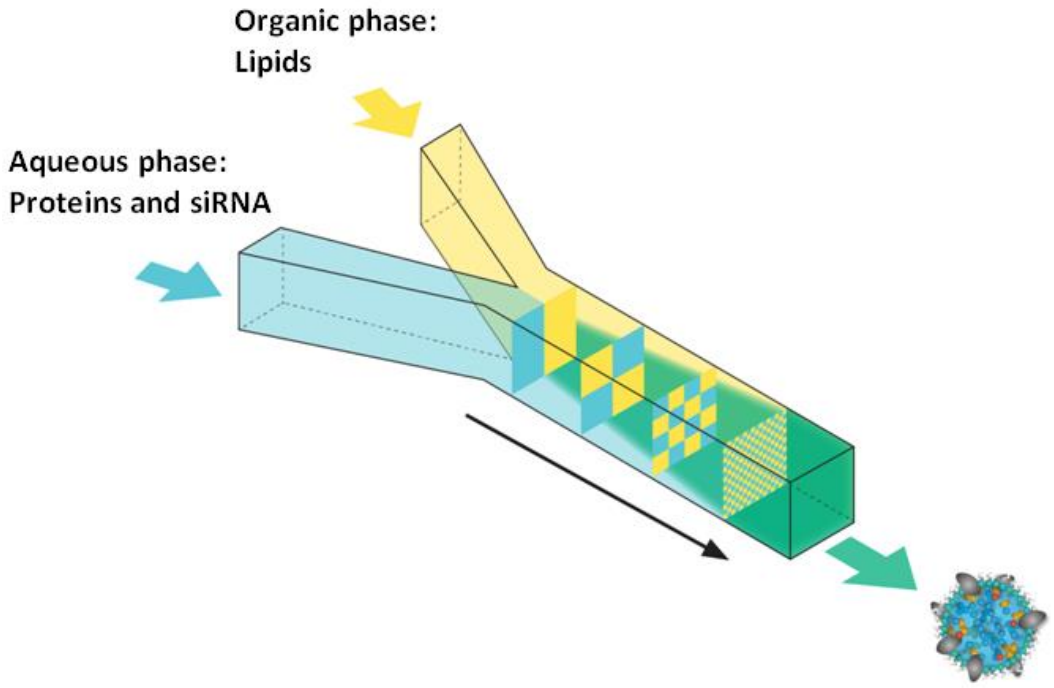

Figure 3.2 Schematic representation of leukosomes/liposomes synthesis with NanoAssemblr.

https://www.precisionnanosystems.com

Leukosomes were stored at 4 °C until use. For *in vivo* imaging, 1,2-dioleoyl-sn-glycero-3-phosphoethanolamine-N-(lissamine rhodamine B sulfonyl (Avanti Polar Lipids) was dissolved with the other lipids (0.1 v/v molar ratio) in chloroform before the hydration phase.

3.6.3. Dynamic Light Scattering

The hydrodynamic diameters (Dh), Zeta (ζ) Potential and polydispersity index (PDI) of HNPs, liposomes and leukosomes were characterised by dynamic light scattering (DLS) using a ZetaPALS Zeta Potential Analyzer with a Multi-Angle Particle Sizing Option installed (Brookhaven Instruments Corporation, Holtsville, NY, USA), operating with a 25 mW laser at a wavelength of 660 nm. Typically, 2.5 mL suspensions of the HNPs in phosphate buffer (PB) with physiological ionic strength (100 mM) at a concentration of 0.1 mg/mL were used for the characterisation at a temperature of 25 °C. Scattered light was detected at 90° to the incident beam. A 9 mM leukosome suspension was diluted in

bidistilled water at a final concentration of 100 µM and used for the characterisation at a temperature of 25 °C. Scattered light was detected at an angle of 15°. Seven measurements were performed with 20 runs each and the results averaged.

3.6.4. Fourier transform infrared analysis

Fourier transform infrared (FT-IR) spectra were obtained on a Nicolet 6700 spectrometer (Thermo Fisher Scientific) with a deuterated triglycine sulfate detector and potassium bromide (KBr) beam splitter. Typically, 64 scans were performed in the wave number range of 4000–600/cm, both forward and backward at 4 kHz, with a manual gain of one. Pellets of about 10 mg of HNPs and 200 mg KBr (spectroscopy grade) (Thermo Fisher Scientific) were pressed using a Carver laboratory press. Spectra were collected by transmitting IR light through the pellets.

3.6.5. Atomic force microscopy

Atomic force microscopy (AFM) images of HNPs were collected in the ScanAsyst mode on a Multimode (Bruker Corporation, Santa Barbara, CA, USA) microscope using single-beam silicon cantilever probes (Bruker MLCT at a resonance frequency of 10 kHz, a nominal tip curvature radius of 10 nm, and a force constant of 0.04 N/m). All measurements were subjected to first-order flattening. Particle size was calculated using the Nanoscope 6.13R1 software (Digital Instruments, Tonawanda, NY, USA). Mean values from 40 random particles in 3 independent experiments are reported. Quantitative AFM force mapping analysis was performed to evaluate the relative elasticity of particles in order to obtain a complete elastic property map of heterogeneous samples. HNPs were kept in acidic (phosphate/citrate buffer solution) or alkaline buffer (phosphate buffer/NaOH buffer solution) before AFM analysis. Young's modulus was calculated for six different samples corresponding to 512x512 force–separation curves obtained over a

10x10 μm area. Young's modulus represents the ability of a material to withstand changes in length when under lengthwise tension or compression. Young's modulus was calculated using the following equation

$$F - F_{\text{adh}} = 4/3E^* \sqrt{R(d - d_0)^3}$$

where F − Fadh is the force on the cantilever relative to the adhesion force, R is the tip end radius, d − d_0 is the deformation of the sample and E* is the reduced modulus [Maugis D., 2013].

3.6.6. Nanoparticles toxicity assay

A204 cells were seeded into a 96-well plate at 5 x 10^3 cells/cm^2 and treated for 72 h with increasing concentrations (0.01 - 10 ng particle/cell) of HNPs. Then, 3-(4,5-dimethylthiazol-2-yl)- 2,5-diphenyltetrazolium bromide (MTT, Sigma-Aldrich) was added to complete media at 5 mg/mL and plates were incubated for 4 h at 37 ° C. The water-soluble tetrazolium dye is reduced in the mitochondria of viable cells and purple formazan crystals are formed and then solubilised with dimethyl sulfoxide. Cell viability is measured through OD reading at 570 nm.

3.6.7. Scanning electron microscopy

For SEM imaging, A204 cells were seeded on Silicon wafers chips (5x5 mm) at a density of 5 x 10^3 cells per filter and treated with HNPs. After 15 min, A204 were fixed in 2.5% glutaraldehyde O/N (Sigma-Aldrich), then, dehydrated with increasing concentrations of ethanol, followed by incubation in a 50% alcohol-hexamethyldisilazane (Sigma-Aldrich) solution for 10 min, with a final incubation in pure hexamethyldisilazane for 5 min, to prepare for O/N drying in a desiccator. Specimens were mounted on SEM stubs (Ted Pella, Inc., Redding, CA, USA) using conductive adhesive tape (12 mm OD PELCO Tabs, Ted Pella, Inc.). Samples were sputter coated with a 10 nm layer of gold using a Plasma

Sciences CrC-150 Sputtering System (Torr International, Inc., New Windsor, NY, USA). SEM images were acquired under high vacuum, at 20.00 kV, spot size 5.0, using a FEI Quanta 400 FEG ESEM equipped with an ETD (SE) detector (Thermo Fisher Scientific).

3.6.8. Flow cytometry measurements

The entry of nanoparticles into A204 cells was measured by FACS. For these experiments, cells were seeded in 6-well plates (3 x 10^4 cells/cm^2) in 2 mL complete medium. After 24 h, cells were washed and incubated with 0.01 - 0.1 - 1 ng/cell of nanoparticles freshly re-suspended in sterile water, or with 100µM of Rhodamine-labeled leukosomes for 3 h. After incubation with nanoparticles, cells were washed and detached from the plates with trypsin. Finally, cells were fixed in ice-cold PBS with 2% paraformaldehyde. HNPs fluorescence was acquired using a BD FACS Forteza flow cytometer (BD Biosciences, Franklin Lakes, NJ, USA). At least, 10^4 events/sample were acquired and analysed with FlowJo software (FlowJo LLC, Ashland, OR, USA). For cell cycle analysis, cells were fixed in 70% ethanol 24 h after transfection, stained in PBS containing 10 µg/mL propidium iodide (PI; Sigma-Aldrich), and RNase A (66 U/mL; Sigma-Aldrich) for 18 h, and analysed by BD Accuri™ C6 Cytometer (BD Biosciences); 10^4 events were acquired and analysed with the C6 Analysis Software (BD Biosciences).

3.6.9. Migration assay

A204 cells were seeded at 2 x 10^5 cells/ml in complete medium in the upper chamber (8 µm pore size) of 24-well Transwell plates (Costar) and treated with 0.1 ng/cell of HNPs for 3 h. Cells were then washed three times with PBS and serum-free media was added into the upper chamber while complete media was added into the lower chambers. After 24 and 72 h of incubation at 37º C, cells were fixed with 100% ethanol for 30 min and stained with 0.4% SRB in 1% acetic acid at room temperature for 20 min. Filters were then

washed with 1% acetic acid and left to dry for 24 h. Finally, cells in 10 random fields per chamber were counted at the microscope. Experiments were performed in triplicate.

3.6.10. Transmission electron microscopy

For TEM, A204 cells were plated at $2x10^5$ cells per well in a 6-well plate. The cells were treated with 0.1 ng of HNPs per cell for 3 h, and then washed. At 3, 6, 12, 24, 48 and 72 h after treatment, the cells were fixed in a solution of 2% paraformaldehyde and 3% glutaraldehyde in PBS, pH 7.4 at room temperature for 1 h. After fixation, the samples were washed and treated with 0.1% cacodylate buffered tannic acid, oxidised with 1% buffered osmium tetroxide for 30 min, and stained with 1% uranyl acetate. The samples were dehydrated in increasing concentrations of ethanol, infiltrated and embedded in Poly-bed 812 medium. The samples were then polymerised in a 60 °C oven for 2 days. Ultrathin sections were cut in Leica Ultracut microtome (Leica), stained with uranyl acetate and lead citrate in a Leica EM Stainer, and examined in a JEM 1010 TEM (JOEL, USA, Inc., Peabody, MA, USA) at an accelerating voltage of 80 kV. Digital images were obtained using the AMT Imaging System (Advanced Microscopy Techniques, Danvers, MA, USA) by HMRI personnel.

3.6.11. Hybrid nanogel particle-siRNA loading and release

A fluorescent siRNA (siGLO RISC-Free Control siRNA labeled with Dy547, Dharmacon) was used to determine the pH-mediated loading and release kinetics of the HNP system. Polyplexes were formed by mixing 25 pmol of Dy547-labeled siRNA with the HNPs at an amino/phosphate (N/P) ratio of 40 in PB solutions at a pH of 6 or 7.4. In a typical procedure, a 100 μL aliquot of 300 μg HNPs was mixed with a 100 μL aliquot of 0.3325 μg (25 pmol) siRNA in PB solution. The mix was gently shaken at room temperature for 15 min. The resulting mixture was left at room temperature for another 15 min. The

solution was then spun down at 21,000 g for 5 min. The loading was evaluated by analysing the fluorescence intensity of the supernatant with a spectrofluorimeter. The same procedure was used to load the functional anti-heparanase siRNA. To investigate the pH-mediated release of siRNA, the siRNA-HNP complexes loaded at pH 7 were incubated in PB solution at pH 5, 6 or 7.4. The amount of siRNA released was monitored by evaluating Dy547 fluorescence intensity with a spectrofluorimeter. All the procedures were performed in a RNAse-free environment.

3.6.12. Leukosome/liposome-siRNA loading

Leukosomes were loaded with siRNA following two different protocols. The first one relies on the use of Exo-Fect (System Biosciences, Palo Alto, CA, USA), a novel nucleic acid transfection agent that enables the transfection of nucleic acids directly into isolated exosomes and exosome-like nanoparticles. Dy547-labeled siRNA or anti-heparanase siRNA were incubated with Exo-Fect and leukosomes following the manufacturer instructions. Briefly, Exo-Fect solution was combined with siRNA (15-100 pmol), leukosomes and sterile 1X PBS. The solution was then incubated at 37°C in a shaker for 10 min and then placed on ice. The reaction was stopped by adding ExoQuick-TC reagent to the suspension and the tubes were placed on ice for 30 min. Finally, the samples were centrifuged at 13,000 rpm for 3 min to eliminate the unencapsulated siRNA and the pellet resuspended in sterile PBS. Encapsulation of siRNA was evaluated by analysing the fluorescence intensity of the siRNA loaded into leukosomes, with a spectrofluorimeter. The siRNA-leukosomes were immediately used to transfect cells.

The second loading method was performed by exploiting the electrostatic interaction between the anionic phosphate groups of siRNA and the cationic nitrogen groups of choline, which constitutes the polar head of phospholipids. The siRNA was added directly into the lipid formulation during leukosomes assembly with NanoAssemblr as

aforementioned. A fluorescent siRNA (Dy547-labeled siRNA) was used to evaluate the loading of this class of molecules. Fifteen – 100 pmol siRNA were loaded into the leukosomes and, after ultracentrifugation, siRNA encapsulation was evaluated by analysing the fluorescence intensity of the loaded leukosomes, with a spectrofluorimeter. An aliquot of 0.798 μg (60 pmol) of anti-heparanase siRNA was used for loading into leukosomes used for functional studies. Encapsulation of anti-heparanase siRNA was evaluated using Quant-iT RiboGreen Assay (Thermo Fisher Scientific), a fluorescence-based assay. Fluorescence generated by the binding of RiboGreen to double-stranded siRNA was measured using FLx-800 microplate reader (BIO-TEK Instruments, Winooski, VT, USA). Encapsulation efficiency was defined as the percent of siRNA initially added that was encapsulated in nanoparticles. All the procedures were performed in an RNAse free environment.

3.6.13. Polyethylenimine/siRNA-nanoparticle complexes formation.

Polyethylenimine (PEI) F25 (25 kDa)/siRNA complexes were prepared as previously described [Werth S. et al., 2006]. Briefly, the PEI/siRNA mass ratio was 5:1 (corresponding to N/P ratio 38) in nuclease-free water. The mixed solution was vortexed and incubated for 30 min at room temperature. Then, the PEI/siRNA complexes were incubated with nanoparticles as follow: for silica nanoparticles, the desired amount of PEI/siRNA was added to particles in aqueous solution, vortexed and incubated for at least 1 h at room temperature; for liposomes and leukosomes equal volumes of PEI/siRNA complexes and nanoparticles were added at a PEI/lipid mass ratio of 5, vortexed and incubated for at least 1 h at room temperature.

3.6.14. SiRNA-nanoparticles trafficking

A204 cells (2×10^4) were seeded in 4-wells Nunc 177399 Lab-Tek Chamber Slide

(Thermo Fisher Scientific). The next day, cells were transfected with Dy547-labeled siRNA using the Lipofectamine RNAiMAX for 5 h, or treated with Dy547-labeled siRNA-loaded HNPs or leukosomes for 3 h. After transfection, cells were washed twice with PBS and stained with LysoTracker Red DND-99 and Hoechst 33342 or, for later time point analysis, fresh culture medium was added. Twenty-four h later, live cells were stained with Wheat Germ Agglutinin (WGA) Alexa Fluor 633 conjugate or LysoTracker Red DND-99 and Hoechst 33342 (Thermo Fisher Scientific) following the manufacturer's instruction. All experiments were performed in 3 replicates. The cells were observed and the images were acquired with a Nikon fluorescence microscope (Nikon Corporation, Tokyo, Japan) using a 60X magnification lens. Images were analysed by using "NIS elements" (Nikon) and "ImageJ" software. To evaluate fluorescence intensity, 3 different fields were acquired from each well.

3.6.15. Intravital microscopy

Intravital microscopy (IVM) was carried out as described in van de Ven A.L. et al., 2013. A total of 5 x10^6 of A204 cells, suspended in 100 µL of PBS, was injected intramuscularly into the right leg of male SCID mice. Calipers were used to measure tumour diameters. Tumour volume was calculated using the following formula: [Length x $(width)^2$]/2. On day 20, when the mean tumour volume reached 200 mm^3, the mice were randomly assigned to 2 groups (n = 3). Groups were treated *via* intravenous administration with either FITC-labeled 1 mg HNPs, loaded with Dy547-labeled siRNA, or 1 mg rhodamine labeled leukosomes. Mice were maintained anesthetised by inhalation of 2% isoflurane throughout the experiment. Under deep anaesthesia, tumours were exposed with surgical dissection of the skin while an intact blood supply was maintained. Immediately after injection, images were acquired over 3 h from 200 µm Z-stacks using an upright Nikon A1R laser scanning confocal microscope (Nikon) equipped with a resonance scanner, motorised and heated

stage. All settings, including laser power, gain, offset, and pinhole diameter were maintained constant throughout each acquisitions. All images were analysed with NIS-Elements AR 4.12.01 64-bit software (Nikon). The Z-stack with the highest fluorescent intensity was used for further analyses. The threshold was adjusted to eliminate autofluorescence and the same threshold was applied for all image analyses. The relative fluorescent intensity was measured using a region of interest constructed using 5 concentric circles in the selected Z-stacks.

3.6.16. Immunofluorescence of tumour sections

Explanted mice tumours were washed twice with PBS, embedded in a cryomold in Optimal Cutting Temperature (O.C.T., Tissue-Tek O.C.T. Compound, Sakura Finetek, Alphen aan den Rijn, The Netherlands), and instantly frozen at −80 °C. Ten µm-thick slides were obtained by cutting tumour blocks with a cryostat at −20 °C. The slides were stored at −20 °C. Immunofluorescence (IF) staining was performed once cryo-sections were obtained. Briefly, slides were thawed and fixed in 4% paraformaldehyde followed by blocking with 5% BSA (Sigma-Aldrich) in PBS. After washing, they were incubated O/N at 4 °C with an anti-CD31 antibody (BD Biosciences) at 2 µg/mL. After O/N incubation, sections were washed and a secondary antibody (4 µg/mL Alexa Fluor 488) was added at room temperature for 1 h. Sections were then counterstained with 2 µg/mL Hoechst 33342 for 1 min, mounted using ProLong Gold Antifade, and cover-slipped. Tumour sections were imaged using a Nikon A1 Confocal Imaging System.

3.6.17. Animal studies

Animal studies were performed in accordance with the guidelines of the Animal Welfare Act and the Guide for the Care and Use of Laboratory Animals based on approved protocols by HMRI Institutional Animal Care and Use Committee. Male SCID mice were

purchased from Charles River Laboratories and housed in specific pathogen-free conditions.

3.7. Statistical Analysis

All the numeric data are presented as mean values ± standard deviation from at least three independent experiments. Two-tailed Student's t test was chosen as statistical analysis and performed by Prism GraphPad software. P-values <0.05 were considered statistically significant.

4.RESULTS

4.1. MiR-1258 transfection

As first RNAi approach to silence heparanase in sarcoma cells, a miR-1258 mimic was used in transient transfection experiments. MiR-1258 is an intronic miRNA transcribed in the antisense orientation to the gene of the zinc finger protein 385B, isoform 1. It maps on human chromosome 2 (GRCh38.p12, 179860836 – 179860908 – www.genome.ucsc.edu). MiR-1258 was previously described to target the 3' UTR of the human heparanase gene (Figure 4.1). Its expression was found inversely correlated with that of heparanase in breast cancer clinical specimens and brain metastatic breast cancer, characterised by heparanase over-expression, non small cell lung cancer and gastric cancer cell lines and tissues [Tang D. et al., 2013; Zhang L. et al., 2011; Liu H. et al., 2012; Shi J. et al., 2017].

Heparanase is up-regulated in sarcomas and its expression has been found correlated with tumour progression and poor prognosis in Ewing's sarcoma and osteosarcoma [Shafat I. et al., 2007; Cassinelli G. et al., 2013; Kazarin O. et al., 2014; Kim H.S. et al., 2006]. Due to its pro-metastatic and pro-angiogenic functions, it is a promising target for sarcoma therapy. A204 and CME-1 cell lines represent optimal models for the study of heparanase inhibition, because they express high levels of heparanase and display a metastatic behaviour *in vivo*.

First of all, the transfection's efficiency of A204 and CME-1 sarcoma cells was evaluated by using a commercial fluorescent oligonucleotide (BLOCK-iT Alexa Fluor Red Fluorescent Control) and Lipofectamine RNAiMAX as transfection reagent. Both A204 and CME-1 cells showed high transfection efficiency as shown by the comparison of light microscopy and fluorescence images (Figure 4.2).

Figure 4.1. Predicted target sequence of miR-1258 in the 3'-UTR of human heparanase mRNA.

Alignment of miR-1258 with human heparanase 3'-UTR. Complementary sequence on heparanase mRNA is shown in red. The seed sequence on miR-1258 is underlined [Zhang L. et al., 2011].

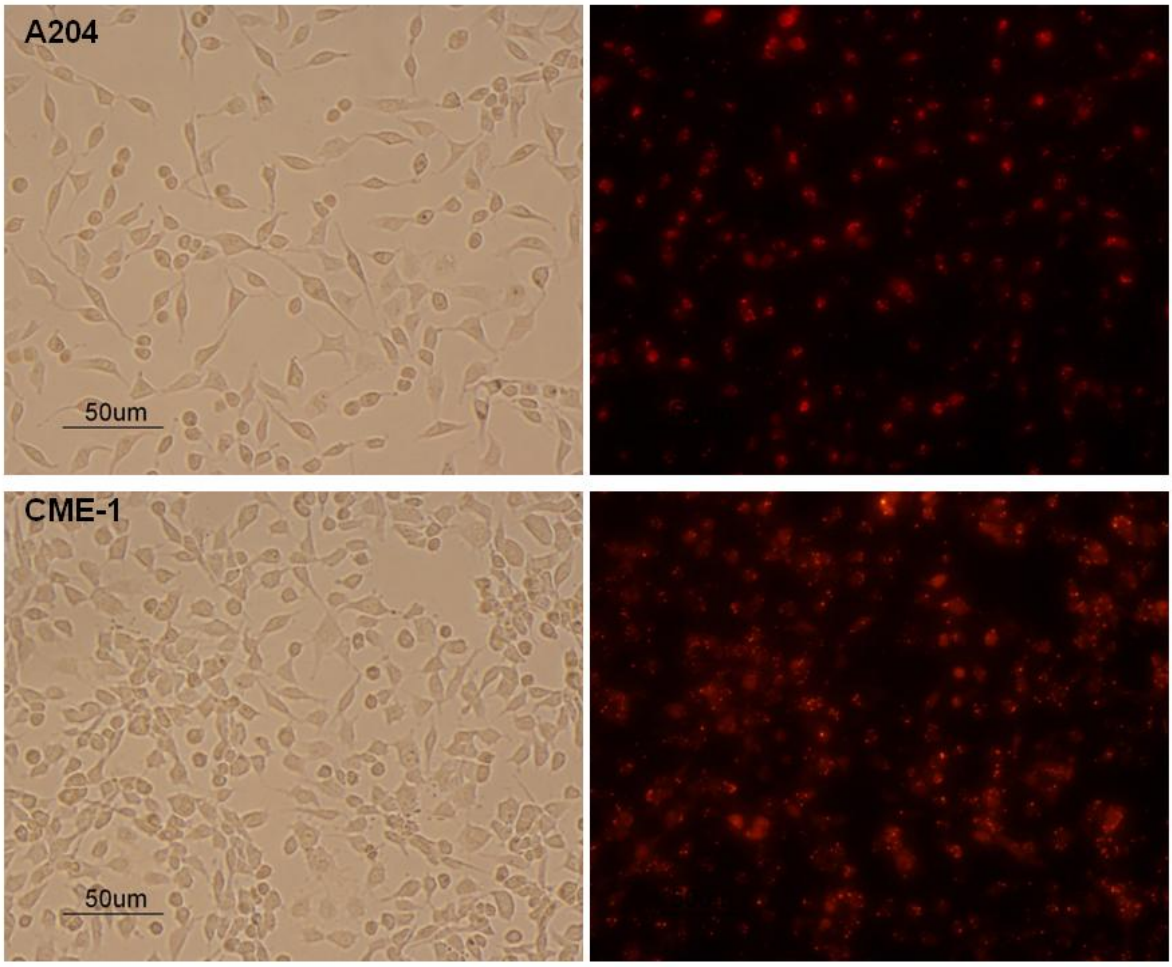

Figure 4.2. Transfection's efficiency of A204 and CME-1 cells.

Efficiency of transfection in the human sarcoma cell lines, A204 and CME-1, as detected by a fluorescent oligonucleotide using a fluorescence microscope 24 h after transfection.

The miR-1258 mimic or the negative control were then transiently transfected in the sarcoma cells to determine whether this miRNA functionally affected endogenous heparanase expression. Heparanase mRNA and protein levels were evaluated at different time points following transfection with miR-1258 mimic concentrations ranging from 5 to

50 nM. The qRT-PCR analysis showed high levels of miR-1258, which were maintained up to 14 days after transfection, in both cell lines (Figure 4.3, A). Heparanase mRNA levels were minimally affected by the miR-1258 mimic transfection (Figure 4.3, B). In fact, miR-1258 mimic induced, at the highest concentration of 50 nM, a mild down-regulation of heparanase in A204 cells, particularly at late time points; CME-1 cells presented fluctuant heparanase levels. Western blot analysis of A204 and CME-1 cell lysates prepared 48 h to 14 days after transfection with 50 nM miR-1258 mimic showed that heparanase protein expression was not decreased by exogenous miR-1258 over-expression (Figure 4.3, C).

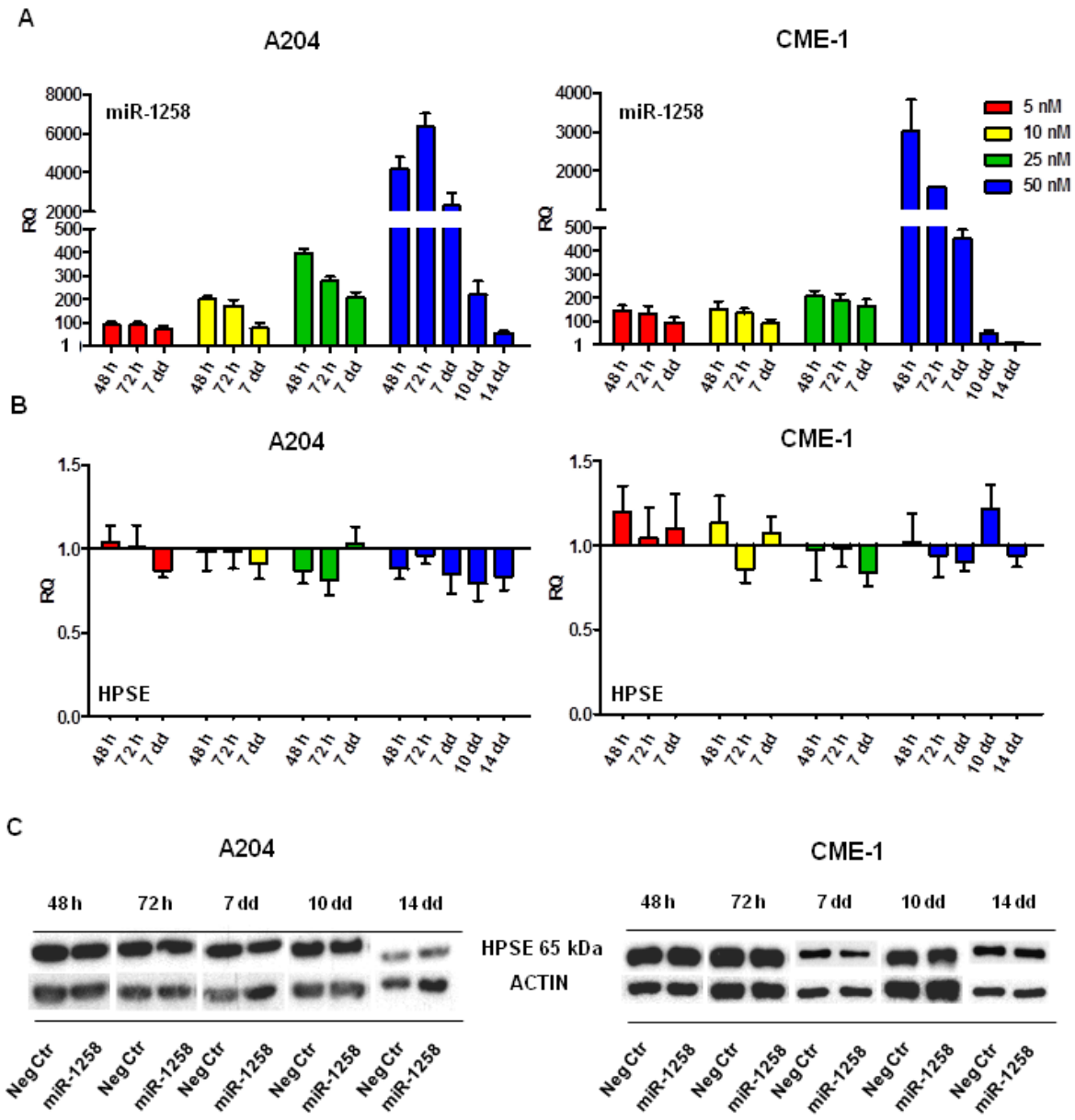

Figure 4.3. MiR-1258 mimic transfection in sarcoma cell lines.

Quantitative RT-PCR analysis of miR-1258 (A) and heparanase (B) in A204 and CME-1 cells. Expression levels are reported as Relative Quantification with respect to cells transfected with the negative control (RQ = 1). The columns represent the mean and standard deviation of 3 independent experiments. SNORD48 and GAPDH were used as housekeeping controls for miR-1258 and heparanase, respectively. Western blot analysis (C) of heparanase after transfection with 50 nM miR-1258 mimic or negative control. Actin was used as loading control. Relative Quantification, RQ; heparanase, HPSE; Negative control, Neg Ctr; miR-1258 mimic, miR-1258.

Further experiments, aimed at increasing the efficiency of heparanase silencing by miR-1258 mimic, were conducted using A204 cells, because these cells displayed a mild reduction of heparanase mRNA levels in the previous experiments. Thus, A204 cells were subjected to two consecutive transfections with 50 nM miR-1258 mimic or negative

control, in order to induce a consistent and durable decrease of heparanase levels. Cells were transfected again 72 h after the first transfection. After 7 and 10 days, cells were collected to assess miR-1258 and heparanase levels. As shown by the bar graphs, a strong increase of miR-1258 was detected applying two rounds of transfection. In contrast, a mild reduction was observed for heparanase mRNA levels (Figure 4.4, A).

Since lentiviral stable transfection of miR-1258 mimic was previously reported to induce heparanase silencing in brain metastatic breast cancer and non small cell lung cancer cells [Liu H. et al., 2012; Zhang L. et al., 2011], the miR-1258 mimic was also tested in cellular models similar to cells used in those studies to compare the efficacy of transient transfection. A549 non small cell lung cancer cells and MDA-MB-231 breast cancer cells were transfected with 50 nM miR-1258 mimic or negative control and qRT-PCR analysis was performed 72 h after transfection (Figure 4.4, B). In both cell lines, in spite of the rise of miR-1258 levels, heparanase mRNA expression was barely decreased. As a further control, a miR-1258 mimic produced by an alternative company and already tested by Zhang and collaborators [Zhang L. et al., 2011], was transfected in A204 cells and the effects were compared to those of a commercial anti-heparanase siRNA (siR06 - s21306, Thermo Fisher Scientific; Figure 4.5 and Table 4.1). Also the alternative miR-1258 mimic did not efficiently inhibit heparanase expression, whereas the siR06 reduced heparanase mRNA level more than 75% compared to cells transfected with negative control siRNA (Figure 4.4, C).

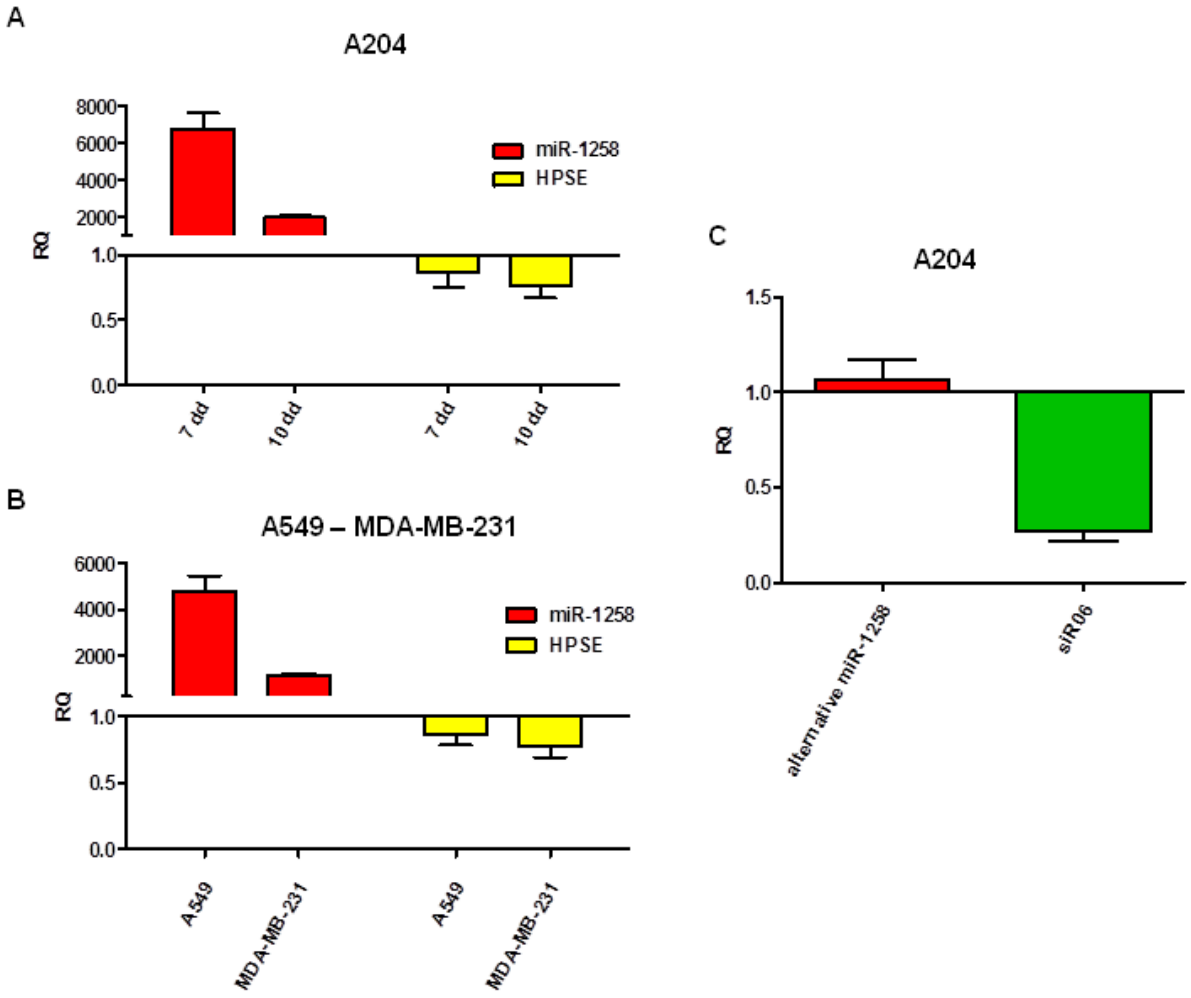

Figure 4.4. Attempts to increase miR-1258 mimic efficacy.

(A) Quantitative RT-PCR analysis of miR-1258 and heparanase in A204 cells. (B) MiR-1258 mimic transfection in A549 and MDA-MB-231 cells. (C) Heparanase levels in A204 after alternative miR-1258 mimic or siR06 transfection. Expression levels are reported as Relative Quantification with respect to cells transfected with the negative control (RQ = 1). The columns represent the mean and standard deviation obtained in 3 experiments. SNORD48 and GAPDH were used as housekeeping miRNA and gene for miR-1258 and heparanase, respectively. Relative Quantification, RQ; heparanase, HPSE.

siR04 (s21304)

Sense sequence: CCUGAUGUAUUGGACAUUUtt
Antisense sequence: AAAUGUCCAAUACAUCAGGgt

siR05 (s21305)

Sense sequence: CGUGCAAGGUUCAAAGAGAtt
Antisense sequence: UCUCUUUGAACCUUGCACGct

siR06 (s21306)

Sense sequence: CUCUAAAGAUGGUGGAUGAtt
Antisense sequence: UCAUCCACCAUCUUUAGAGtt

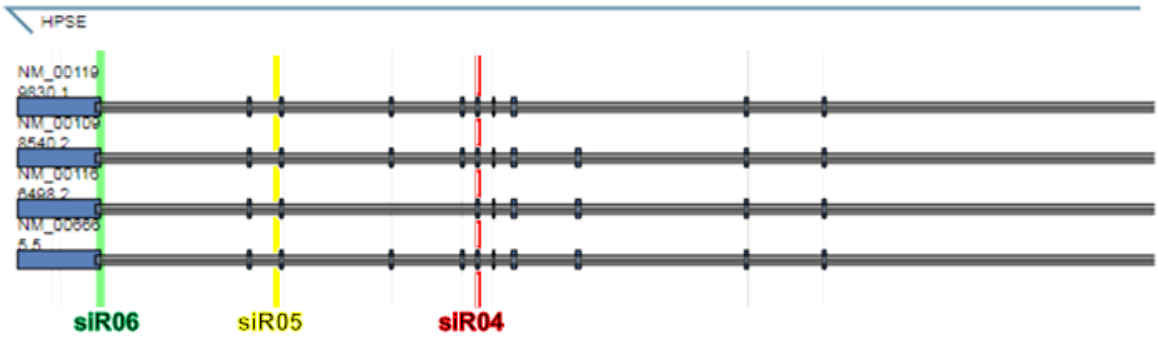

Figure 4.5. siR04, siR05 and siR06 sequences and binding sites on the four different transcript variants of heparanase.

The lines represent the heparanase transcript variants whose exons are represented as black boxes. Each siRNA is shown as a coloured line in correspondence with the binding exons.
Information available on www.thermofisher.com. Heparanase, HPSE.

siRNA Location	Clone ID	siR04 - Exon	siR05 - Exon	siR06 - Exon
NM_001199830.1	NP_001186759.1	6	9	11
NM_001098540.2	NP_001092010.1	7	10	12
NM_001166498.2	NP_001159970.1	8	9	11
NM_006665.5	NP_006656.2	8	11	13

Table 4.1. SiR04, siR05 and siR06 binding sites.

The table shows the targeted heparanase's exons for each siRNA in the fourth heparanase transcript variants.
Information available on www.thermofisher.com.

Taken together, these experiments indicated that transient transfection of miR-1258 mimic is not sufficient to inhibit heparanase expression in a stable and persistent way in the

examined models. For this reason, the following experiments were carried out using siRNA molecules to induce heparanase silencing, instead of miR-1258 mimic.

4.2. Anti-heparanase siRNA transfection

Preliminary experiments were performed to select an optimal siRNA concentration and specific siRNAs to be used in the next experiments. A204 and CME-1 cells were transfected with siR06 at 5, 25 and 50 nM. A 25 nM concentration was selected for further experiments because it was the lowest concentration able to silence heparanase for up to 7 days (Figure 4.6, A). Two additional anti-heparanase siRNAs (siR04, siR05) targeting different heparanase mRNA sites were tested (Figure 4.5 and Table 4.1). Heparanase expression was evaluated by qRT-PCR at 5 different time points up to 14 days after transfection (Figure 4.6, B) and by western blot analyses after 72 h (Figure 4.6, C). All the siRNAs tested were able to down-regulate heparanase mRNA expression up to 14 days, but with siR05 the silencing effect was progressively lost, particularly in CME-1 cells. Also western blot analysis showed a better reduction of heparanase protein level after siR04 and siR06 transfection. Thus, siR04 and siR06 were selected for further experiments, being the most effective at heparanase protein modulation.

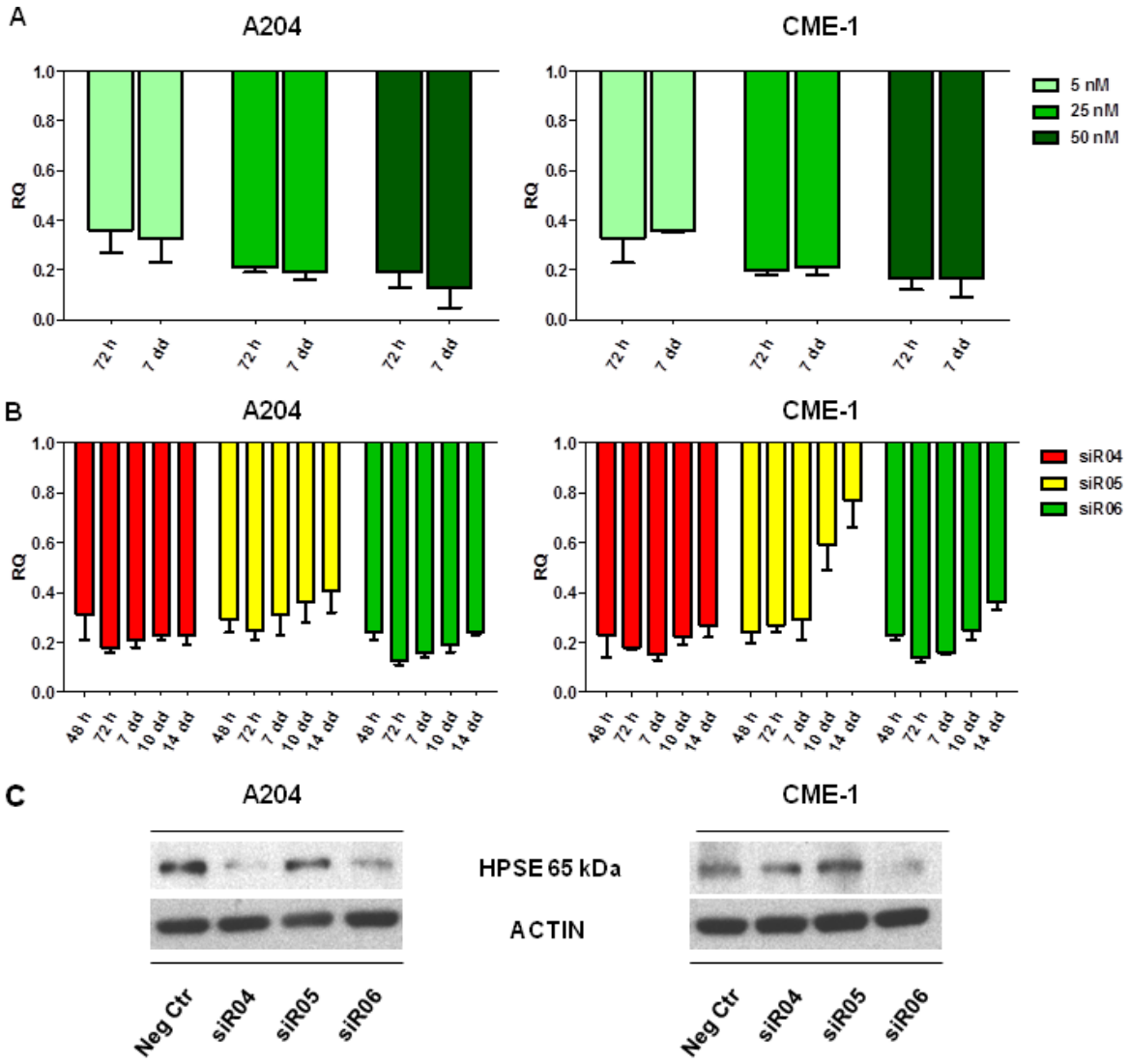

Figure 4.6. SiRNAs transfection in sarcoma cell lines.

(A) Quantitative RT-PCR analysis of heparanase in A204 and CME-1 cells transfected with different concentrations of siR06. (B) Quantitative RT-PCR analysis of heparanase in A204 and CME-1 cells transfected with 25 nM siR04, siR05 and siR06. Expression levels are reported as Relative Quantification with respect to cells transfected with the negative control (RQ = 1). The columns represent the mean and standard deviation of 3 experiments. SNORD48 and GAPDH were used as housekeeping miRNA and gene for miR-1258 and heparanase, respectively. (C) Western blot analysis of heparanase 72 h after transfection with 25 nM siRNAs or negative control. Actin was used as loading control. Relative Quantification, RQ; Negative control, Neg Ctr; heparanase, HPSE.

4.2.1. Effects of siRNA on extracellular heparanase

To evaluate the functional effects of heparanase silencing, the enzymatic activity of the endoglycosidase was assessed in conditioned media from siRNA-transfected cells. In fact, heparanase is known to exert its enzymatic activity in the extracellular environment, through cleavage of heparan sulfate, and it is therefore secreted by the cells. Moreover,

because of the peculiar trafficking following its synthesis, it is present in the extracellular space also as inactive form (Figure 1.6, from Introduction). The amount of heparanase in the conditioned media was first measured through ELISA, at 72 h after cell transfection with negative control, siR04 or siR06 (Figure 4.7, A). The level of heparanase was significantly reduced in the conditioned media after siRNAs transfection of both A204 and CME-1 cells, as compared to negative control transfection. Then, heparanase activity was quantified by an enzymatic assay in serum-free conditioned media of the transfected sarcoma cells. Heparanase enzymatic activity, expressed as ng of heparan sulfate released from a heparan sulfate-coated plate per minute, was significantly reduced in both cell lines transfected with the siRNAs compared to cells transfected with negative control (Figure 4.7, B).

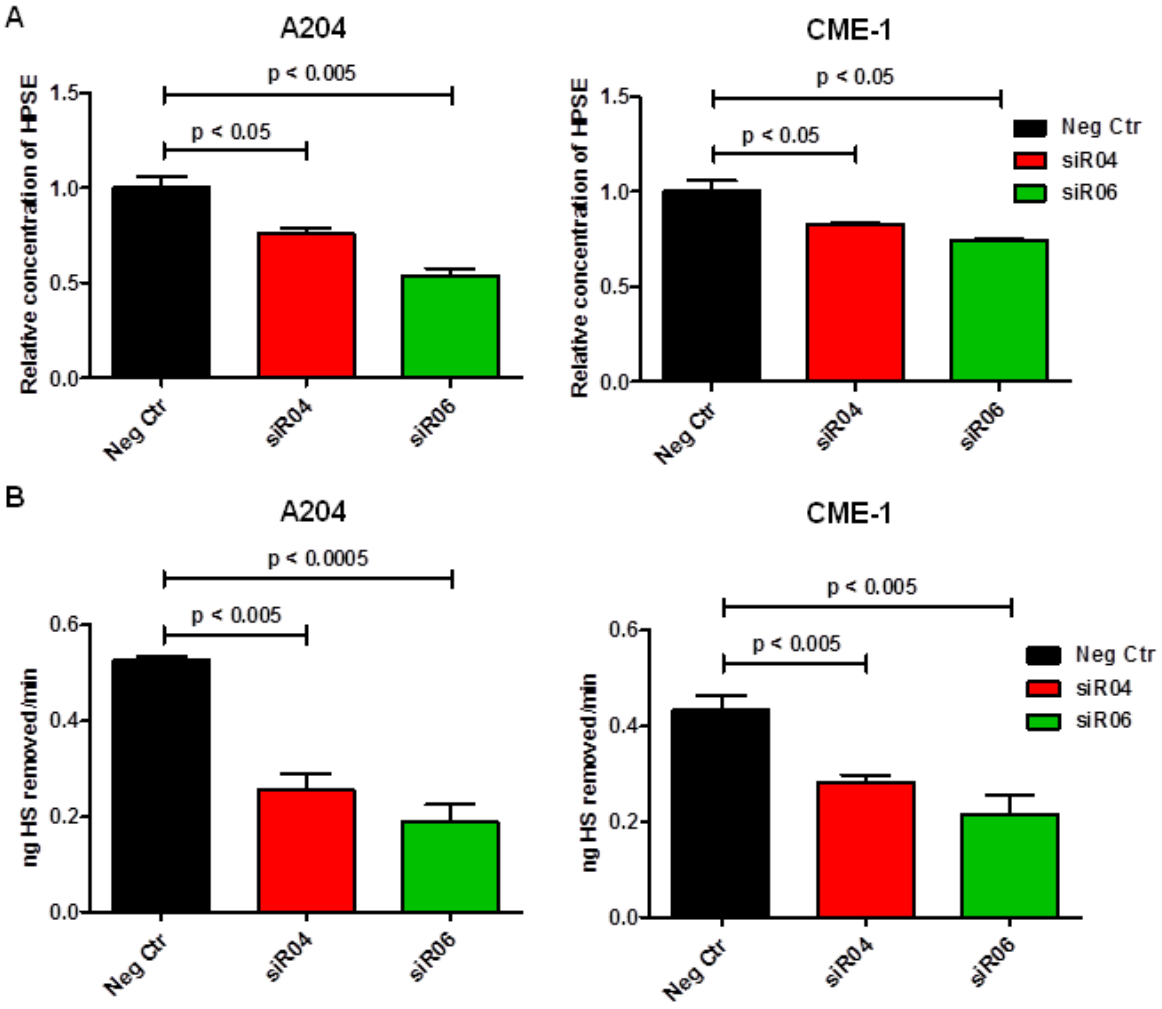

Figure 4.7. Down-regulation of heparanase in the extracellular environment.

(A) Heparanase concentration in conditioned media collected from human sarcoma cell lines 72 h after transfection with negative control, siR04 or siR06. (B) Heparanase enzymatic activity measured in conditioned media of A204 cells and CME-1 cells 72 h after transfection. The enzymatic activity is expressed as ng of heparan sulphate removed per minute. Data were normalised to the total amount of protein extracted from the cells. The results represent the mean ± standard deviation of 3 independent experiments performed in triplicate. Negative control, Neg Ctr; heparanase, HPSE; heparan sulphate, HS.

4.2.2. Effects of siRNA on cell motility

Since heparanase has been reported to exert pro-migrative and pro-invasive properties in several cancer cells, the effect of heparanase silencing on cell motility was examined in sarcoma cells. Confluent cells were transfected with either siRNAs or negative control and, after 5 h, the cells were subjected to wound healing. Pictures of the wound were taken at time 0 and 24 h, or 72 h, for CME-1 and A204 cells, respectively. Both siRNAs significantly inhibited the migration of A204 and CME-1 cells, as determined by the

measure of the migration distance. The migration distance of A204 negative control, siR04 and siR06 was 135 ± 4, 70 ± 2, and 60 ± 4 µm, respectively. The migration distance of CME-1 was 150 ± 3, 85 ± 2, and 55 ± 3 µm, respectively (Figure 4.8).

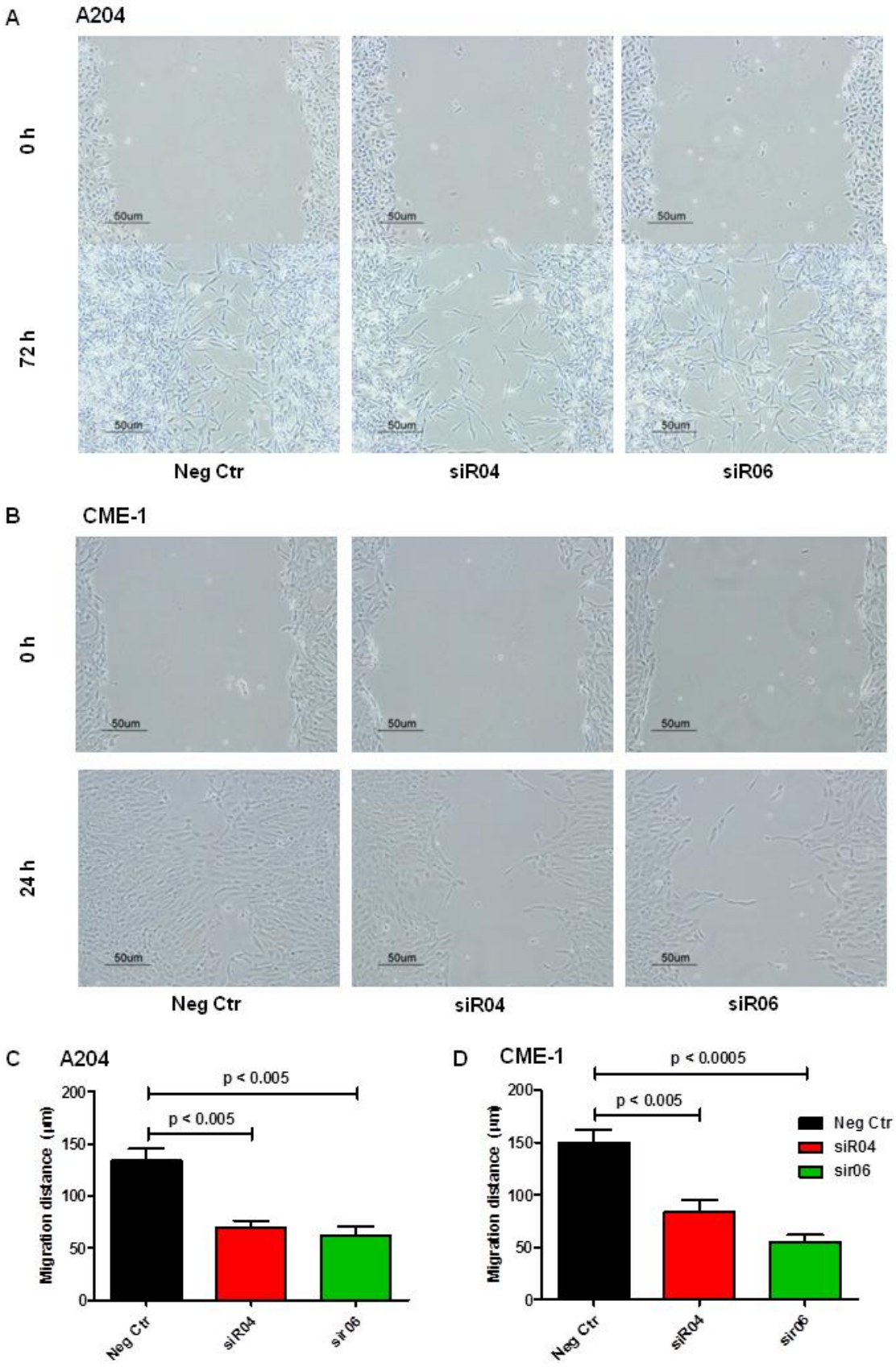

Figure 4.8. Effects of anti-heparanase siRNAs on migration in sarcoma cell lines.

Representative images of wound healing assay evaluated at 72 h for A204 (A) and at 24 h for CME-1 (B) cells aftyer scratch. Cells were treated with negative control, siR04 or siR06. The migration distance (in µm) is represented in bar charts (C and D). Graphs depict the mean and standard deviation of three independent experiments.

To assess the effect of heparanase silencing on the cell invasion capability, cells were seeded in transwells 48 h after transfection with negative control or siRNAs. Twenty-four h later, cells that invaded the lower chamber passing through Matrigel were counted. As shown in Figure 4.9, Matrigel invasion was significantly inhibited by the two siRNAs in both cell lines. These results indicated that the down-regulation of heparanase expression inhibited migration and invasion ability of the human sarcoma cells.

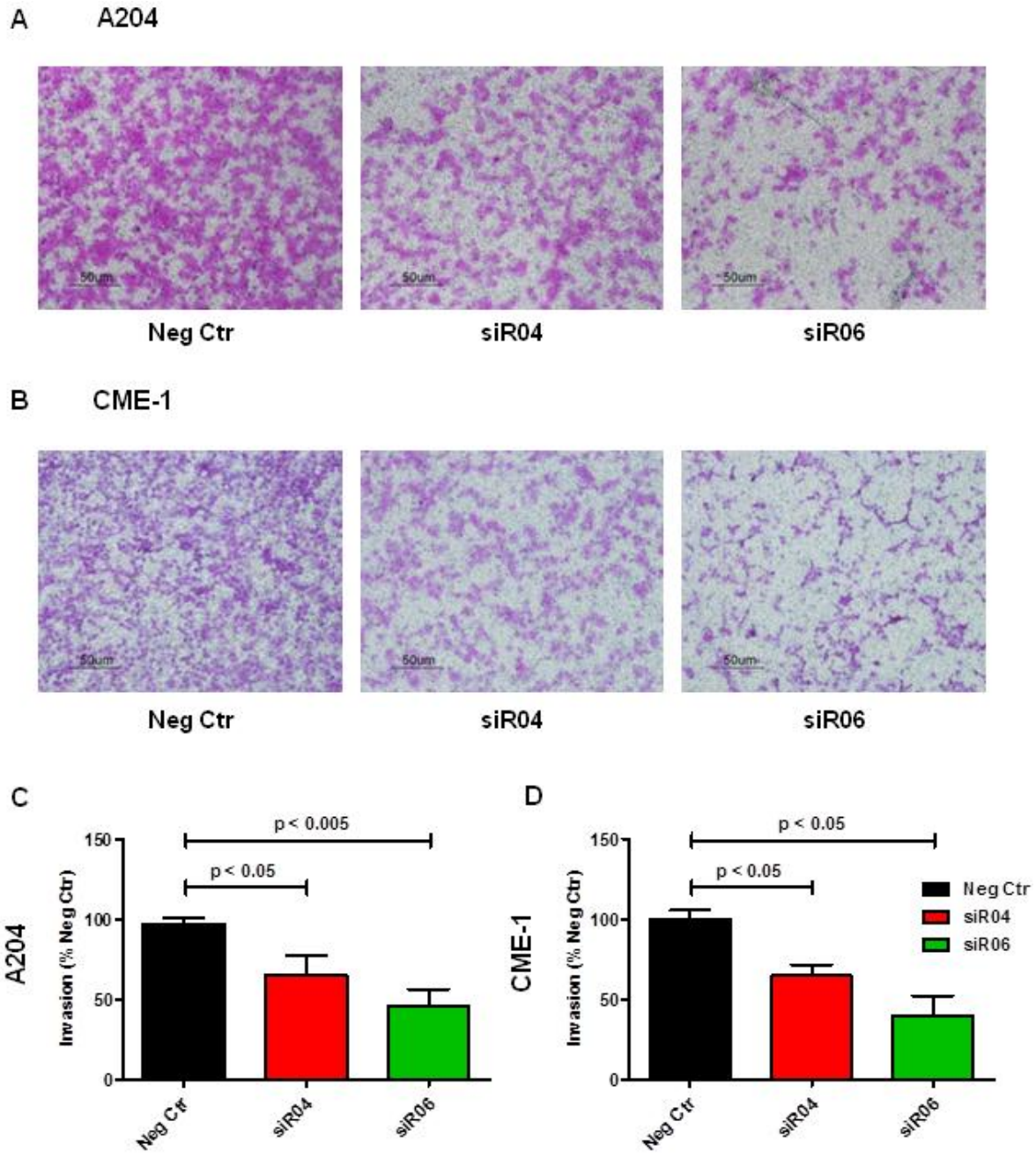

Figure 4.9. Effects of anti-heparanase siRNAs on invasion in sarcoma cell lines.

Representative images of transwell invasion assay of A204 (A) and CME-1 (B) cells treated with negative control, siR04 or siR06 at 72 h after transfection. Cells that invaded the Matrigel membrane of the Transwell were stained with SRB and counted under a microscope. In A204 cells the reduction of invasion was 31.8 % ± 6.6 or 52.2 % ± 6.7 for cells transfected with siR04 or siR06, respectively, compared to negative control. In CME-1 cells the reduction of invasion was 37.1 % ± 8.3 or 60.3 % ± 7.7 for cells transfected with siR04 or siR06, respectively, compared to negative control. The percentage of invading cells is represented in bar charts (C and D), graphs depict the mean and standard deviation of three independent experiments.

4.2.3. Effects of siRNA on cell proliferation and colony formation

To determine whether the observed effects of heparanase silencing were related to effects on cell growth and proliferation over the time frame of the migration and invasion experiments, cell proliferation assays were performed with transfected cells. After transfection with negative control or siRNAs, cells were counted over 6 consecutive days (Figure 4.10, A). These experiments showed that, actually, silencing of heparanase did not affect cell proliferation in adherent cells.

A204 and CME-1 cell ability to form colonies in soft agar was also tested to examine if silencing resulted in decreased anchorage independent growth which is evaluated in a long-term assay. SiR06 significantly reduced the colony number, especially in CME-1 cells; (Figure 4.10, B).

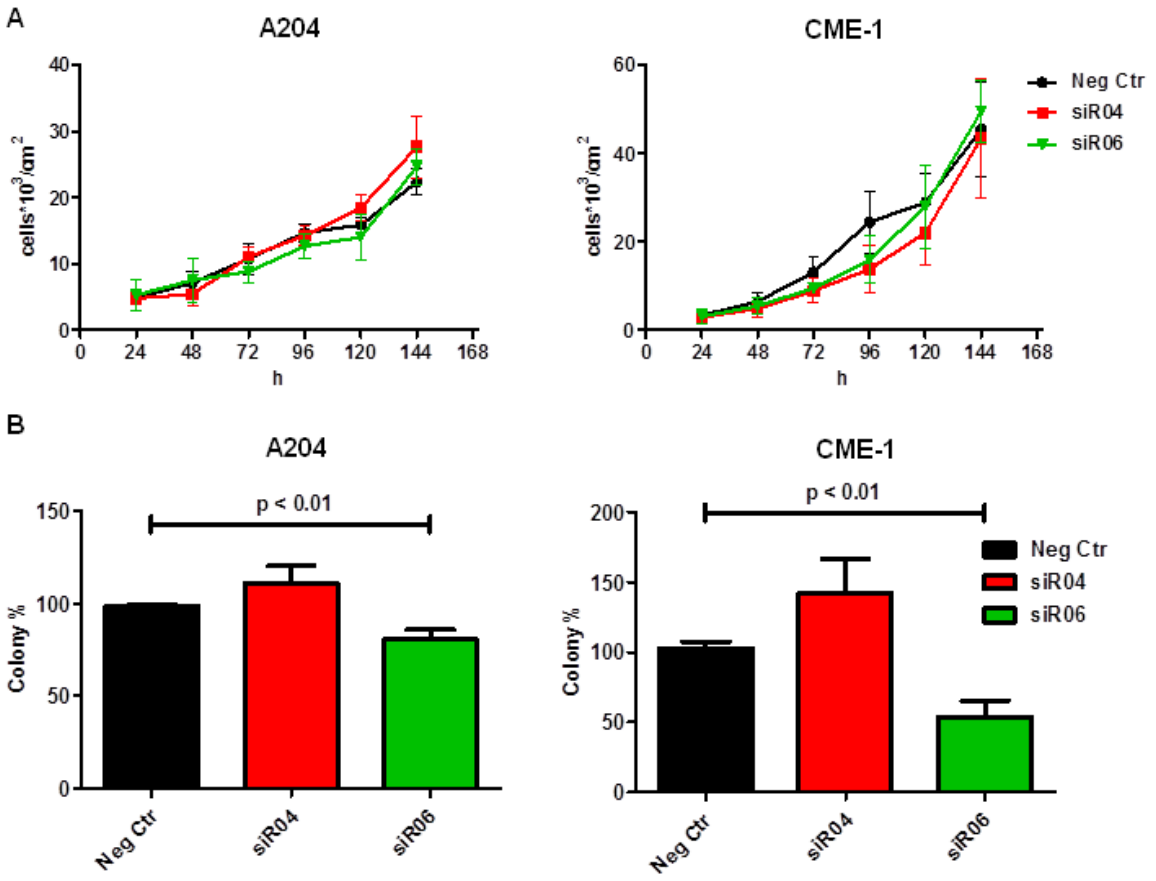

Figure 4.10. Heparanase siRNAs effect on cell proliferation and colony formation.

(A) Cell proliferation assay of cell transfected with negative control, siR04 or siR06. Cells were counted at the cell counter over 6 consecutive days. (B) Colony formation assay in soft agar of A204 and CME-1 transfected with negative control, siR04 or siR06.

4.2.4. Effects of siRNA on intracellular heparanase

On the basis of previous results, further experiments were carried out using only siR06, as it was the most efficient in heparanase silencing and simultaneously in counteracting tumour cells aggressiveness.

Heparanase is localised intracellularly in the cytoplasm, mostly in lysosomes, and into the nucleus, but also secreted in the extracellular space. To examine the effect of RNAi on heparanase protein levels in intracellular compartments, cell lysates from negative control- and siR06-transfected sarcoma cells were subjected to subfractionation. Cytoplasmic and nuclear fractions were then analysed by western blotting for heparanase expression.

Heparanase exists in different forms, in fact, it is translated as a pre-proenzyme and, after the cleavage of the signal peptide, a latent pro-heparanase is generated (65 kDa). This inactive enzyme undergoes further proteolytic cleavage, mediated by cathepsin L, and the active heparanase is obtained as a noncovalent heterodimer (8 kDa + 50kDa).

The pre-proheparanase form was highly sensitive to siRNA transfection and its reduction was evident in both cytoplasm and nucleus (red arrow in Figure 4.11). In contrast, latent heparanase level, sequestered into the nucleus, was not reduced by siRNA (blue arrow in Figure 4.11); also the level of cleaved form of the endoglycosidase was not affected by siRNAs transfection and it was mostly accumulated in the cytoplasm (green arrow in Figure 4.11). It is known from the literature that active heparanase is segregated in the lysosomes [Goldshmidt[b] O. et al., 2002; Zester A. et al., 2004]. This finding obtained by western blot analysis suggested that heparanase when localised into the nucleus and into the lysosomes is stable and has a longer half-life time compared to heparanase free in the cytoplasm; for this reason it might be resistant to siRNA effect.

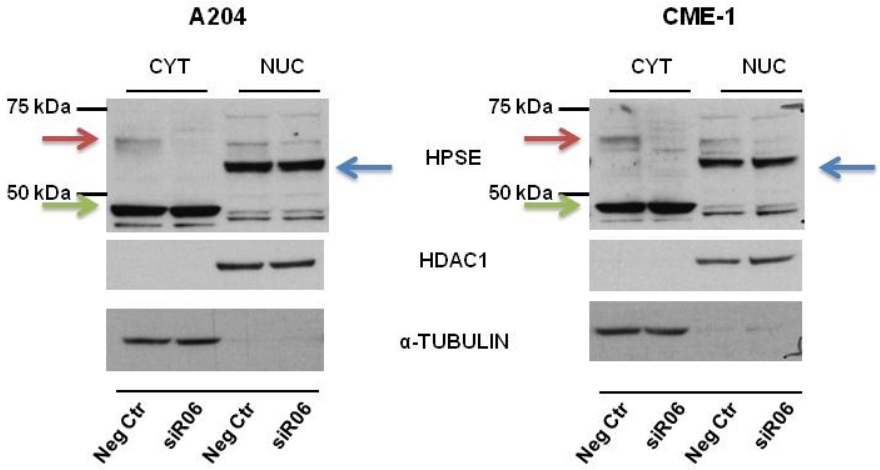

Figure 4.11. Western blot analysis of heparanase subcellular localisation.

Western blot analysis of subcellular localisation of heparanase in A204 and CME-1 cells transfected with negative control or siR06. Seventy-two h after transfection cells were lysated for nuclear/cytoplasm fractionation. HDAC1 and α-tubulin were used as loading control for nucleus and cytoplasm, respectively. Red arrows indicate the pre-proheparanase; blue arrows indicate the latent proheparanase; green arrows indicate the processed active heparanase. Heparanase, HPSE; Histone deacetylase 1, HDAC1; negative control, Neg Ctr.

The subcellular distribution of heparanase was also evaluated using IF microscopy in cells transfected with siR06 or the negative control. Heparanase was reduced in the cytoplasm of siR06 transfected cells, but not in the nucleus, confirming western blot results. It was also noticeable that heparanase accumulated in specific spots in the cytoplasm, likely corresponding to lysosomes, according to the study of Goldshmidt[b], O. et al. (Figure 4.12).

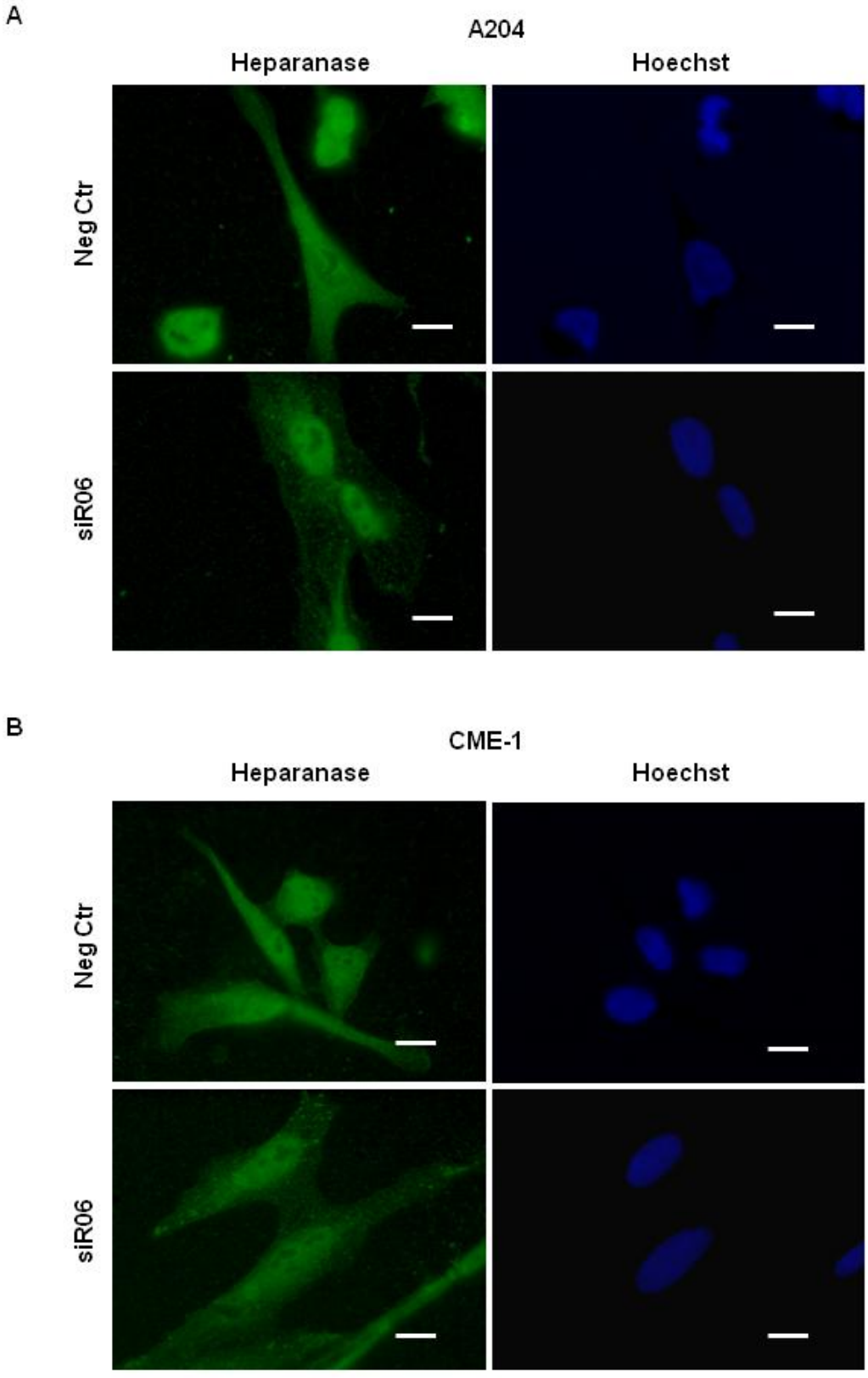

Figure 4.12. Immunofluorescence analysis of heparanase subcellular localisation.

Subcellular localisation of heparanase in A204 (A) and CME-1 (B) cells after transfection with negative control (Neg Ctr) and siR06. Seventy-two h after transfection cells were analysed by fluorescence microscopy. Bars represent 10 µm.

Overall, the observed effects of RNAi on intracellular and secreted heparanase indicated that pre-proheparanase was the most sensitive to the silencing, likely because it is the first one synthesised by the cells. After the synthesis, heparanase is commonly released in the extracellular space and this isoform was also affected by siRNA, as shown by ELISA. The latent proheparanase was found accumulated in the nuclei where it was protected and not affected by the silencing. Finally, heparanase processing occurs into the lysosomes [Zetser A. et al., 2004], where active endoglycosidase is sequestered and also in this compartment it was not sensitive to RNAi. It is conceivable that the segregation of heparanase in the nuclei or in the lysosomes increases the protein stability and consequently its half-life.

4.2.5. Effects of siRNA on angiogenic molecules

As mentioned above, heparanase plays an important role in tumour angiogenesis and invasion. Therefore, we examined the effect of heparanase silencing on angiogenesis-related factors profile by using an antibody array system. Protein lysates obtained from transfected A204 or CME-1 cells were tested using a Human Angiogenesis Array Kit. In both cell lines, the down-regulation of heparanase induced a decline in the expression levels of bioactive molecules known to play a significant pro-angiogenic and pro-invasion role. In particular, the levels of Tissue Factor/Coagulation Factor III (TF), Chemokine (C-X-C motif) ligand 16 (CXCL16) and CD26 were down-regulated in both A204 and CME-1 cells (Figure 4.13).

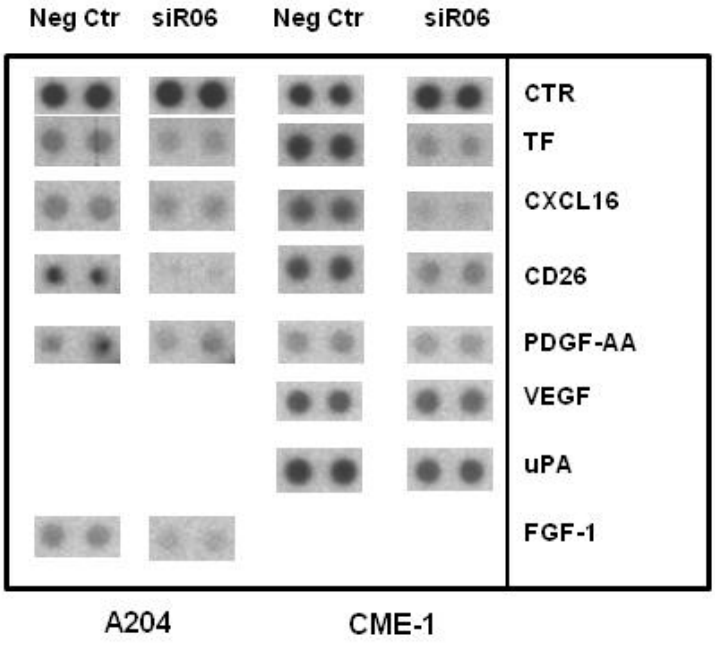

Figure 4.13. Effects of siRNAs anti heparanase on angiogenic molecules in sarcoma cells.

The levels of 55 angiogenesis related proteins were determined in A204 and CME-1 tumour cell lysates using a protein arrays after 72 h from the transfection. Every couple of filters probed with cell lysates treated with negative control or siR06 was taken from the same autoradiography film, as for each protein different exposure time was required. Negative control, Neg Ctr; uPA, Urokinase-type Plasminogen Activator.

4.3. Nanoparticles as tools for RNAi delivery

4.3.1. Design and characterisation of Hybrid Nanogel Particles

The first delivery platform tested consisted of HNPs, originally synthesised to deliver RNA molecules into tumour cells. The nanoparticles for this project were synthesised and characterised by specialised personnel following the protocols of Khaled, who described HNPs for the first time in a paper published in Biomaterials [Khaled S.Z. et al., 2016]. I participated in the characterisation of HNPs and *in vitro* tests.

These nanoparticles are characterised by a pH-responsive PDAEAM cross-linked hydrogel shell around a silica core (Figure 1.10). HNPs are known to be able to buffer and swell in acidic pH, thanks to the features of the hydrogel, however the properties of the HNPs need to be checked after each synthesis. Thus, DLS, ζ potential, and FTIR analyses were used to evaluate size and surface charge, and to confirm the presence of the polymer of HNPs. The

synthesised nanoparticles had homogeneous solvated Dh (119 nm ± 6) and positive charge (5.3 mV ± 0.8) as measured at pH 7.4 in aqueous buffer, with PDI 0.168, a value which revealed an ideal homogeneity. Indeed, PDI values lower than 0.2 identify ideal homogeneity properties for nanoparticles.

The vibrational modes and chemical signatures of HNPs, analysed through FTIR spectroscopy, showed the presence of a 10 nm PDAEAM shell around the silica core (data not shown).

The pH-responsiveness was evaluated. Specifically, the ability of HNPs to buffer pH was demonstrated by a titration study in which 0.1 M HCl was gradually added to the HNPs in solvent (PB) or to HNPs-free solvent. Under these conditions, HNPs were found to increase the amount of acidic solution needed to reduce the pH of the buffer (Figure 4.14, A).

To determine the ability of HNPs to change their size in response to pH variation, a suspension of 0.1 mg/mL HNPs was examined at different pH values using DLS. This analysis showed that the Dh of HNPs was inversely dependent on the environmental pH (Figure 4.14, B). The hydrogel buffering capability occurs through the protonation of the tertiary amines exposed on the nanoparticle surface, which results in swelling of the particles that became positively charged. In detail, the Dh of the HNPs increased from 117 ± 12 nm to 264 ± 9 nm as the environmental pH changed from 8 to 4. The ζ potential analysis showed that HNPs enhanced their positive charge as a consequence of shifting of the pH towards an acidic value, thereby confirming the protonation effect (Figure 4.14, C). Specifically, the particles charge increased from -9.1 ± 0.7 mV to 36.2 ± 2.5 mV as the environmental pH changed from 8 to 4. This phenomenon is known as “proton sponge effect” [Behr J.P., 1997] and it has been demonstrated to facilitate the escape of nanoparticles from endosomal vesicles [Pack D.W. et al., 2005].

The nanoparticles were further characterised by AFM to validate the size of the particles measured with DLS and to investigate the surface changes in response to pH variations. The analysis of HNPs diluted in acidic or alkaline buffer confirmed the ability of HNPs to swell in acidic environment. The diameter of the particles in an acidic environment was 63.8 nm ± 2.0, whereas in an alkaline environment was 48.8 nm ± 2.7. Viscoelastic properties of both acidic and alkaline HNPs were also investigated by calculating the Young's modulus as a measure of the stiffness of the particles. The elastic modulus for acidic nanoparticles demonstrated an increase in stiffness when compared to alkaline particles (831 ± 25 kPa vs. 643 ± 16 kPa) (Figure 4.14, D). Overall, these analyses demonstrated the ability of HNPs to swell and acquire a positive charge, while buffering the surrounding environment through the protonation of the tertiary amines exposed on the particle surface.

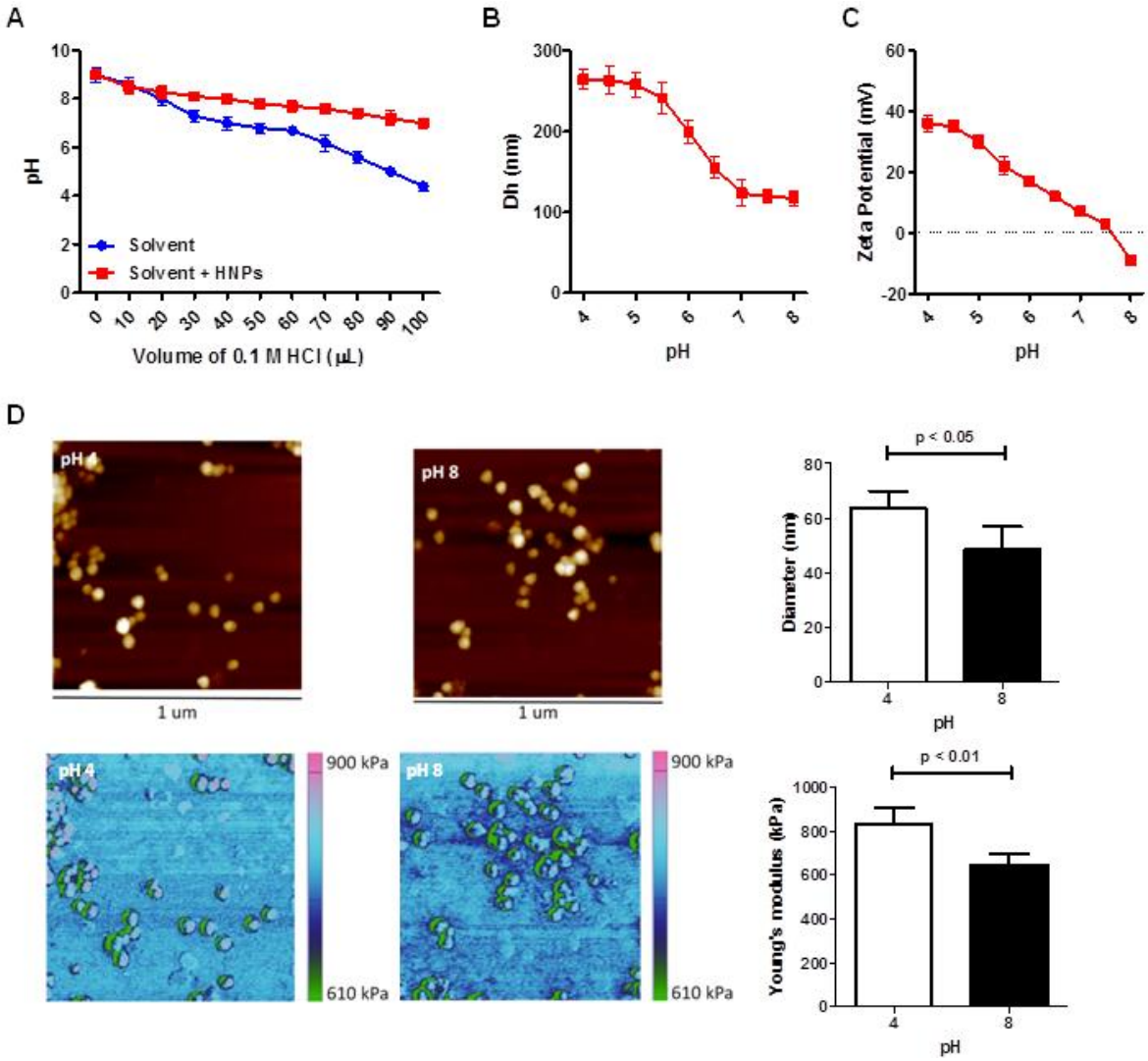

Figure 4.14. pH responsiveness of HNPs.

(A) The graph shows pH variation of phosphate buffer and phosphate buffer containing HNPs, after the gradual addition of 0.1 M HCl. (B) The line graph describes the size of the particles at different pH. (C) The line graph illustrates the surface charge of the system at different pH. (D) Representation of AFM topography maps and the corresponding Young's modulus maps of HNPs at pH 4 and 8. Variation of the size and the Young's modulus is represented in histograms on the right.

4.3.1.1. *In vitro* biological effects of HNPs

The human RT cell line A204 was used to evaluate the capability of HNPs to deliver siRNAs. First of all, the effects of the empty nanoparticles on cell viability were assessed. Cells were treated with HNPs at concentrations ranging from 0.01 to 10 ng/cell, and the cell viability was evaluated using the MTT assay after 72 h; it was observed that HNPs had a minimal effect on proliferation at concentrations ≤ 0.1 ng/cell (Figure 4.15, A).

The interaction of HNPs with the cell membrane and their internalisation were then examined. The surface interaction between particles and cell membrane was analysed by SEM after 15 min of treatment. HNPs displayed high affinity with the cell surface, resulting in membrane perturbations (Figure 4.15, B). The internalisation efficiency in A204 cells was evaluated by flow cytometry after cell exposure to fluorescent HNPs for 3 h. The percentages of cells with internalised nanoparticles were 44.9 ± 3.0, 93.3 ±0.85 and 42.0 ± 3.7 for cells treated with 0.01, 0.1 or 1 ng/cell, respectively (Figure 4.15, C). A concentration corresponding to 0.01 ng/cell was too low to achieve an optimal internalisation, whereas a concentration of 1 ng/cell was toxic and impaired viability. The intermediate concentration of 0.1 ng/cell was thereby used in further experiments.

The effect of nanoparticles internalisation on cell cycle was analysed using flow cytometry. Treatment with HNPs induced a strong reduction of the G2/M phase and an accumulation of cells in the S phase (Figure 4.15, D).

Furthermore, A204 cells displayed a significant slowing of migration capability 24 h after treatment with nanoparticles; this effect was reversible, because the cells fully resumed their ability to migrate 72 h after the nanoparticles uptake (Figure 4.15, E). These two effects might be linked with the intracellular accumulation of nanoparticles that interfere with the cytoskeleton functions, preventing cell division and motility.

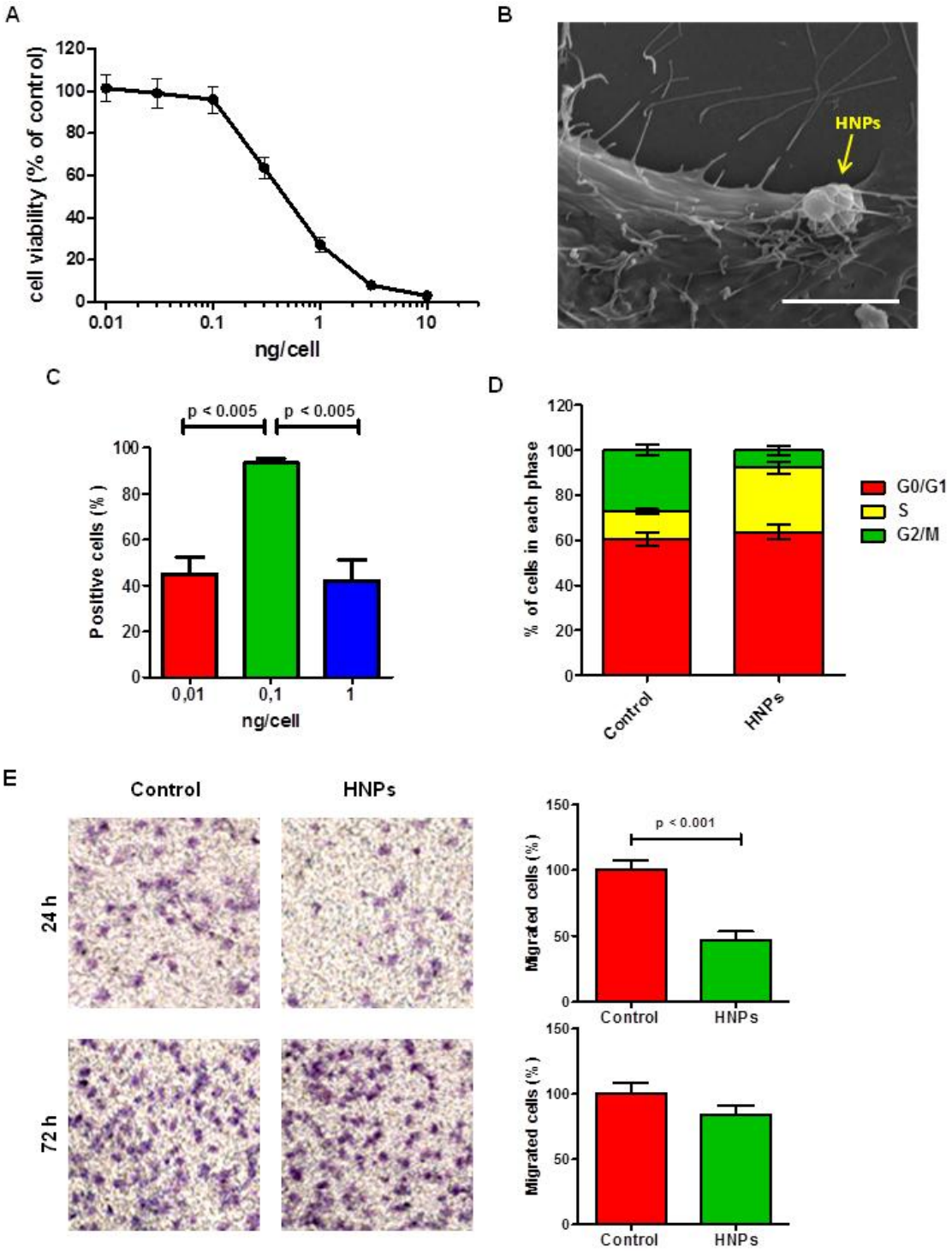

Figure 4.15. Biological effects of HNPs on A204 cells.

(A) Sensitivity of A204 cells to different concentrations of HNPs. The MTT assay was used to evaluate the cytotoxicity of HNPs on A204 cells exposed to increasing nanoparticles concentrations for 72 h. Untreated cells were used as control. The mean of at least three independent experiments is reported. (B) SEM analysis of A204 cells 15 min following particle treatment. Scale bars, 1 µm. (C) A204 cells where incubated with fluorescent nanoparticles for 3 h and then cells were harvested for flow cytometry. The percentage of cells with internalised fluorescent HNPs is represented in the graph. (D) Flow cytometric analysis of cell cycle profiles of A204 cells treated with HNPs. Cells were exposed to 0.1 ng/cell of nanoparticles for 3 h. After 24 h cells were harvested, stained with propidium iodide, and analysed for perturbations in the cell cycle. The columns depict the percentage of cells in each cell cycle phase. (E) A204 cells ability to migrate towards a chemotactic gradient (serum). Cells were seeded on 8 µm cell culture insert following 3 h particle exposure (0.1 ng/cell). Migrated cells were counted after 24 and 72 h.

To reach its mRNA target, a siRNA must be released into the cytoplasm; therefore it is essential that nanoparticles escape the endo-lysosomal compartment. The capacity of HNPs to escape from the endo-lysosomal compartment was evaluated by fluorescence microscopy. The endo-lysosomal vesicles were stained with LysoTracker, a red-fluorescent dye used for labeling and tracking acidic organelles in live cells. Fluorescent images were taken at different time points following treatment with FITC-labeled HNPs (0.1 ng/cell). HNPs displayed a partial colocalisation with LysoTracker after 3 h of exposure to nanoparticles, whereas they mainly colocalised with endo-lysosomal vesicles after 72 h (Figure 4.16, A). Given that around 50% (see Pearson's correlation value) of nanoparticles were colocalised with acidic vesicles at 3 h, the remaining fraction was assumed to be cytoplasmic. The increase of Pearson's correlation value at 72 h suggests the occurrence of re-internalisation of nanoparticles with time.

The endo-lysosomal escape phenomenon was further investigated in endothelial HUVEC cells and a paper on this subject is currently under review at the journal Small. TEM analysis showed that the endo-lysosomal compartment was re-organised after nanoparticles internalisation. In detail, HNPs were shown to be incorporated into vesicles at 3 h and then they damaged the vesicle membranes and broke out from the endo-lysosomes. At later time points, (*i.e.*, 24 and 72 h), TEM analysis showed the formation of multilamellar bodies around HNPs, likely an attempt to surround and sequester the particles (Figure 4.16, B).

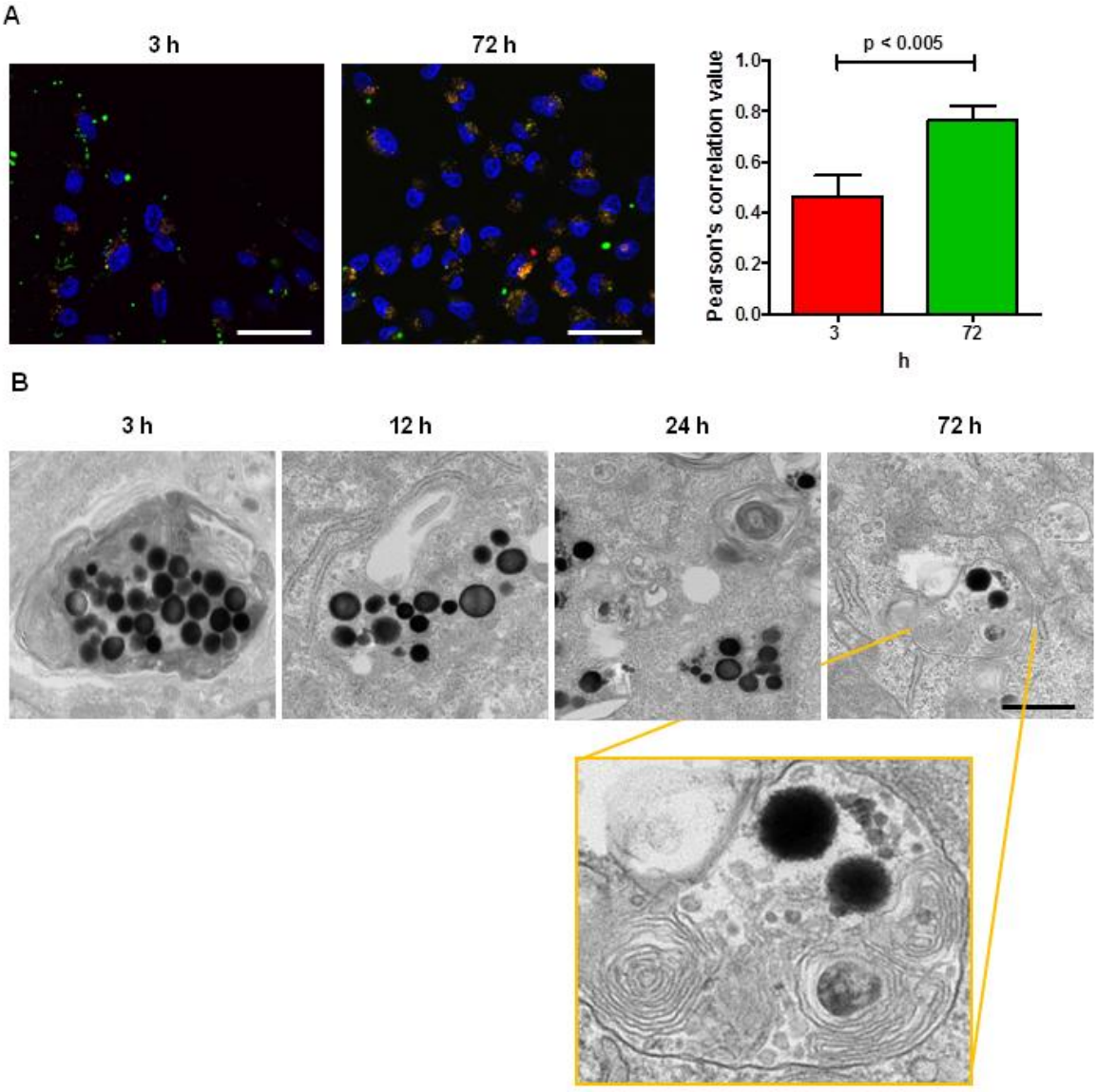

Figure 4.16. HNPs endo-lysosomal escape.

(A) Fluorescent microscope images showing the colocalisation of lysosomes and nanoparticles following a 3 h treatment. Lysosomes are stained red (LysoTracker Red DND-99), HNPs are green (FITC) and nuclei are blue (Hoechst). Scale bars, 50 μm. (B) TEM images of HNPs compartmentalisation in endo-lysosomal vesicles in HUVEC cells at 3, 12, 24 and 72 h. Scale bar: 1 μm.

4.3.1.2. *In vitro* HNP-delivery of siRNA

Since siRNAs have negative charges on the phosphate backbone and HNPs have positive charges on the hydrogel surface in acidic pH, loading of siRNA is expected to be mediated by the electrostatic interaction between the positive charge of the hydrogel and the negative charge of the nucleic acid. The loading efficiency of the siRNA molecules was assessed at diverse pH conditions by spectrofluorimeter detection. The maximum

measured loading efficiency was nearly 95% at pH 6 whereas decreased at other pH values, being 59.5% at pH 5 and 19% at pH 7 (Figure 4.17, A). Therefore, the subsequent experiments were carried out loading the siRNA on HNPs at pH 6.

For a siRNA to reach its target it is essential to have an efficient release from the carrier. A fluorescent siRNA release from HNPs was investigated in cell-free solutions at different pH representing physiologic (pH ~7), endosomal (pH ~6) or lysosomal (pH ~5) environments. After incubation, the cumulative siRNA released from the nanoparticle was measured over a period of 24 h. The release reached about 80% at pH 5, whereas the siRNA was mostly retained at pH 6 and 7 (Figure 4.17, B). Even if in acidic conditions the nanoparticles acquired a positive charge, the release of siRNA was higher at pH 5; it is conceivable that the shell, after swelling, had a broaden hydrogel net, allowing siRNA diffusion in the surrounding environment. In contrast, the siRNA was retained at higher pH even though siRNA had a lower electrostatic affinity for the hydrogel, probably because it was entrapped in the hydrogel structure that was tighter at pH 6 and 7, compared to pH 5 (represented in Figure 4.17, C).

To evaluate the capability of the HNPs to deliver siRNA into the cells, fluorescent microscopy analysis on A204 cells was performed 3 h after treatment with fluorescent siRNA-HNPs. This analysis showed that HNPs were able to deliver siRNA into the cells and about half of the nanoparticles still maintained the siRNA attached, as shown by the colocalisation of the red (Dy547-labeled siRNA) and the green (FITC-labeled HNPs) signals (Figure 4.17, D).

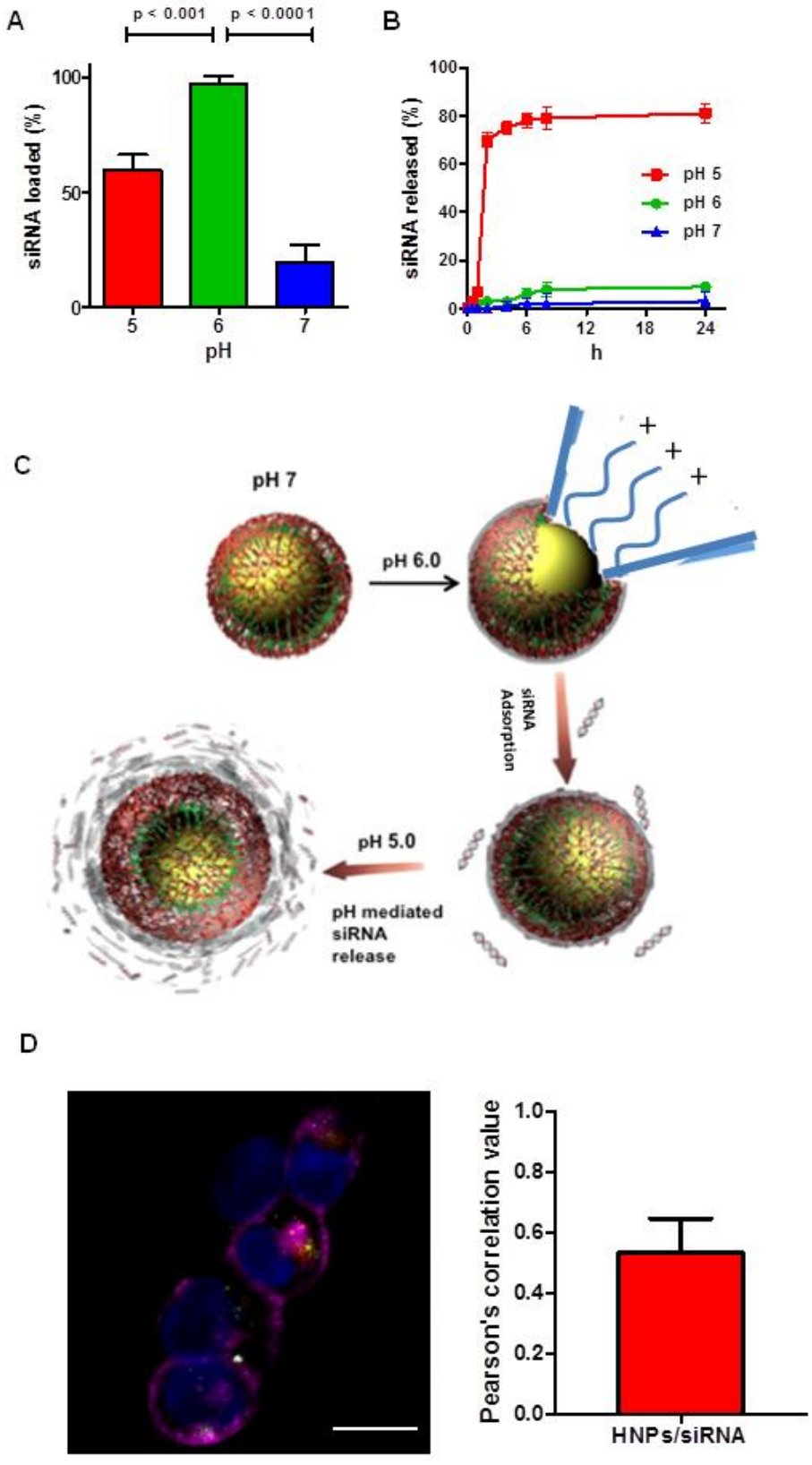

Figure 4.17. pH-driven siRNA/HNPs loading and release.

(A) The graph shows siRNA loading efficiency at different pH. The histograms depict the percentage of loaded siRNA. (B) The graph shows the percentage of siRNA released at different pH. (C) Graphic representation of siRNA loading and release on HNPs. (D) Fluorescent microscopy analysis of intracellular delivery of Dy547-labeled siRNA (red) mediated by FITC-labeled HNPs (green) into A204 cells (WGA staining, fuchsia). Nuclei are blue (Hoechst). Scale bar 20 μm. Histogram represents the Pearson's correlation value of the siRNA-HNPs colocalisation.

The ability of the HNPs to deliver active anti-heparanase siRNA was evaluated by treating the cells with siRNA-loaded HNPs compared to cells treated with scrambled siRNA-loaded HNPs or empty HNPs, as negative controls. The expression level of the heparanase gene was analysed 72 h after treatment, using qRT-PCR (Figure 4.18, A). Despite the promising HNPs characteristics and delivery, heparanase silencing was not achieved by siRNA delivered through nanoparticles.

In previous experiments it was demonstrated the ability of HNPs to load, release and efficiently deliver siRNAs into the cell cytoplasm, avoiding the endo-lysosomal compartment. Nevertheless, the system was not able to inhibit the expression of its target. One possibility is that the siRNA loaded onto the HNPs was not protected by the hydrogel from the environment and was released in an inactive form. Polyethylenimine (PEI) was then used to protect RNA during the loading on the silica core and the delivery to cells. PEI is a synthetic branched or linear polymer positively charged and able to buffer pH. The capability of PEI to protect siRNAs from degradation and to efficiently deliver siRNAs to the cell cytoplasm has already been described. [Jager M. et al., 2012]. The positive charges of PEI are responsible for the siRNA-PEI complex formation and favour cell internalisation. However, sometimes these complexes could lead to particles aggregation. *In vivo* administration of PEI causes toxicity due to the binding of free PEI with serum proteins and blood cells causing the formation of aggregates that interact with tissues or intracellular molecules inducing acute cell damage [Godbey W.T. et al., 2001]. To reduce PEI toxicity we conjugated the silica core with the siRNA-PEI complex, and tested these nanoparticles in A204 cells. Despite the ability of the sole PEI to deliver a functionally active siRNA, able to decrease heparanase mRNA, heparanase silencing was not achieved with PEI-silica nanoparticles as shown by qRT-PCR (Figure 4.18, B). Further studies have to be performed in order to optimise the transfection efficiency of the HNP/siRNA

complex *in vitro*. For this reason, we decided to test the biodistribution properties of those nanoparticles, but not their *in vivo* efficacy.

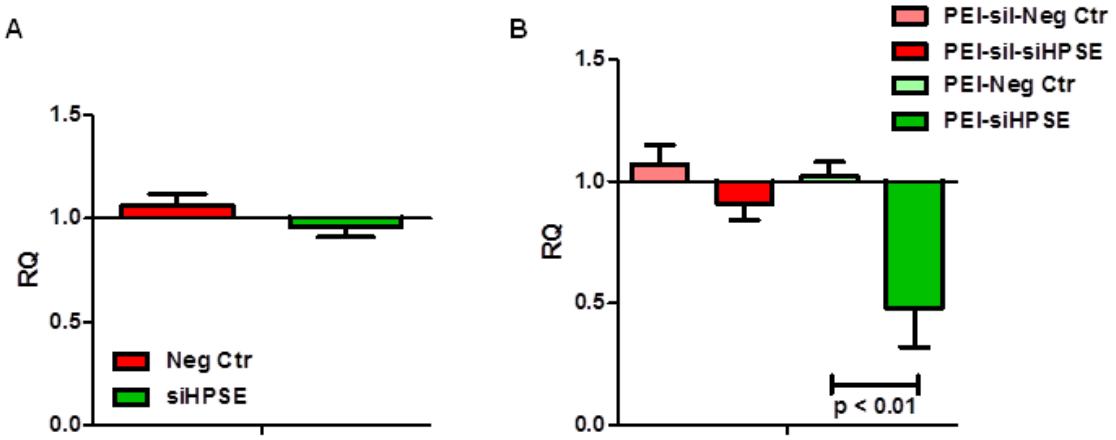

Figure 4.18. Heparanase levels after nanoparticle-delivered siRNA.

(A) Quantitative RT-PCR analysis of heparanase in A204 cells after transfection with negative control or anti-heparanase siRNA delivered with HNPs. (B) Quantitative RT-PCR analysis of heparanase in A204 cells after transfection with negative control or anti-heparanase siRNA delivered with PEI-silica or PEI alone. Expression levels are reported as Relative Quantification with respect to cells treated with empty nanoparticles (RQ = 1). The columns represent the mean and standard deviation of 3 experiments. GAPDH was used as housekeeping gene. HNPs loaded with negative control, Neg Ctr; HNPs loaded with anti-heparanase siRNA, siHPSE; Relative Quantification, RQ.

4.3.1.3. *In vivo* HNP-delivery of siRNA

In parallel experiments, we evaluated the ability of HNPs to target the tumour and associated vessels *in vivo*. In particular, evaluation of nanoparticle delivery was performed in RT xenografts established by intra muscular injection of A204 cells previously used for *in vitro* studies. Mice harbouring A204 tumours were treated with FITC-labeled HNPs loaded with Dy547-labeled siRNA and followed for 2 h using intravital microscopy, IVM. An accumulation of HNPs at the tumour vasculature was observed. Moreover, the fluorescence of siRNA and HNPs overlapped, indicating the nucleic acid delivery *in vivo* (Figure 4.19, A). Explanted tumours were used for further IF analyses, which confirmed the presence of HNPs at the tumour site and stroma (Figure 4.19, B).

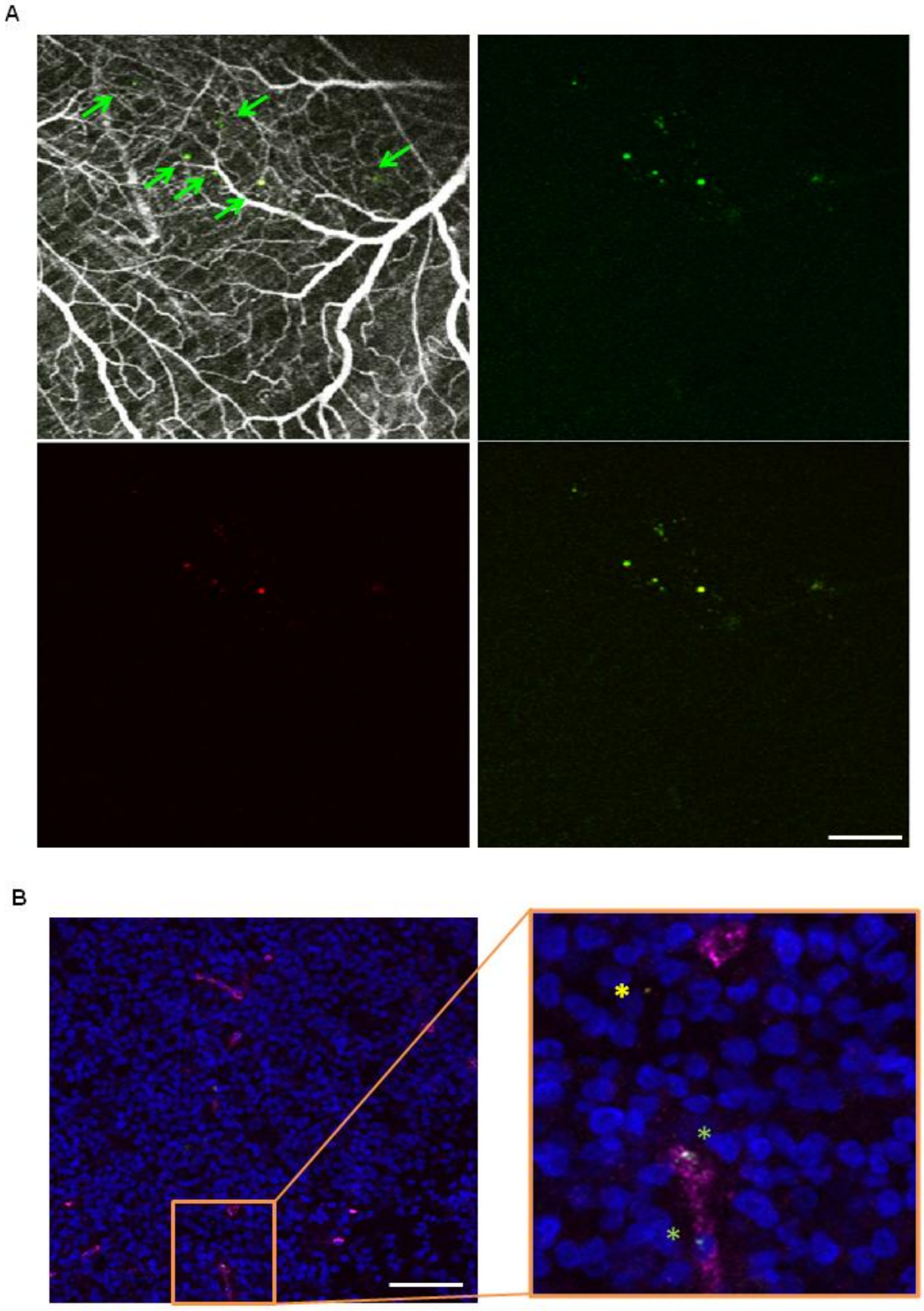

Figure 4.19. *In vivo* delivery of HNPs and siRNA.

A) Representative IVM images of A204 tumour vessels at 2 h after HNPs administration. Green arrows indicate HNPs accumulated at the tumour vasculature. HNPs are green, siRNA is red, and vessels are white. Scale bar: 25 μm. B) Representative IF images of A204 tumour sections depicting the distribution of HNPs (green asterisks) into the vessels (CD31 staining, fuchsia), and released into the stroma (yellow asterisk) at 2 h after nanoparticles administration. Scale bar: 100 μm.

4.3.2. Design and characterisation of leukosomes

HNP-based approach mainly deals with exploiting a) polymers for siRNA complexation and b) passive targeting for tumour accumulation. As mentioned above, we explored a second approach, based on biomimetic liposome-like nanoparticles, called leukosomes (Figure 1.16). This approach relies on the encapsulation of siRNA into the aqueous core of leukosomes and on the accumulation of the siRNA/leukosome complex to the tumour site through an active targeting approach.

Leukosomes were synthesised and characterised by specialised personnel. During my experience at the HMRI, I worked on the *in vitro* assays to test siRNA transfection efficiency. In a previous study, the leukosome synthesis method was shown to conserve the versatility and physico-chemical properties of liposomes, including the ability to load different compounds, while maintaining the structure of leukocyte membrane proteins, the ability to target inflammation and escape immune system clearance through the presence of proteins involved in adhesion (LFA-1, Mac-1, PSGL-1 and CD18), and self-tolerance (CD45 and CD47) [Molinaro R. et al., 2016]. Leukosomes synthesised for this thesis were 122 ± 3.91 nm and charged -13.8 ± 2.71 mV, as measured by DLS and ζ potential analyses, with a low PDI 0.148 a value which revealed an ideal homogeneity. Indeed, PDI values lower than 0.2 identify ideal homogeneity properties for nanoparticles.

4.3.2.1. *In vitro* biological effects of leukosomes

The human RT cell line A204 was used to evaluate the ability of leukosomes to deliver siRNA into the cell cytoplasm.

In preliminary experiments, the effect of empty leukosomes was assessed on cell viability. Cells were treated with these biomimetic nanoparticles at concentrations ranging from 0.5 to 100 μM and the cell viability was evaluated with MTT assay after 72 h. At all tested concentrations, leukosomes were non-toxic for the cells (Figure 4.20, A). Further

experiments were carried out using 10 μM leukosomes, a concentration already used in the laboratory for *in vitro* studies.

FACS analysis was applied to evaluate the internalisation of leukosomes and the effect on cell cycle. The internalisation efficiency of A204 cells was examined after cell exposure to rhodamine-labeled leukosomes (1-10 μM) for 3 h. The percentage of cells positive for rhodamine fluorescence was close to 80% for all the nanoparticle concentrations used (Figure 4.20, B). The treatment with leukosomes induced a mild effect on cell cycle with a slight increase of cells in S phase and decrease of those in G2/M phase (Figure 4.20, C).

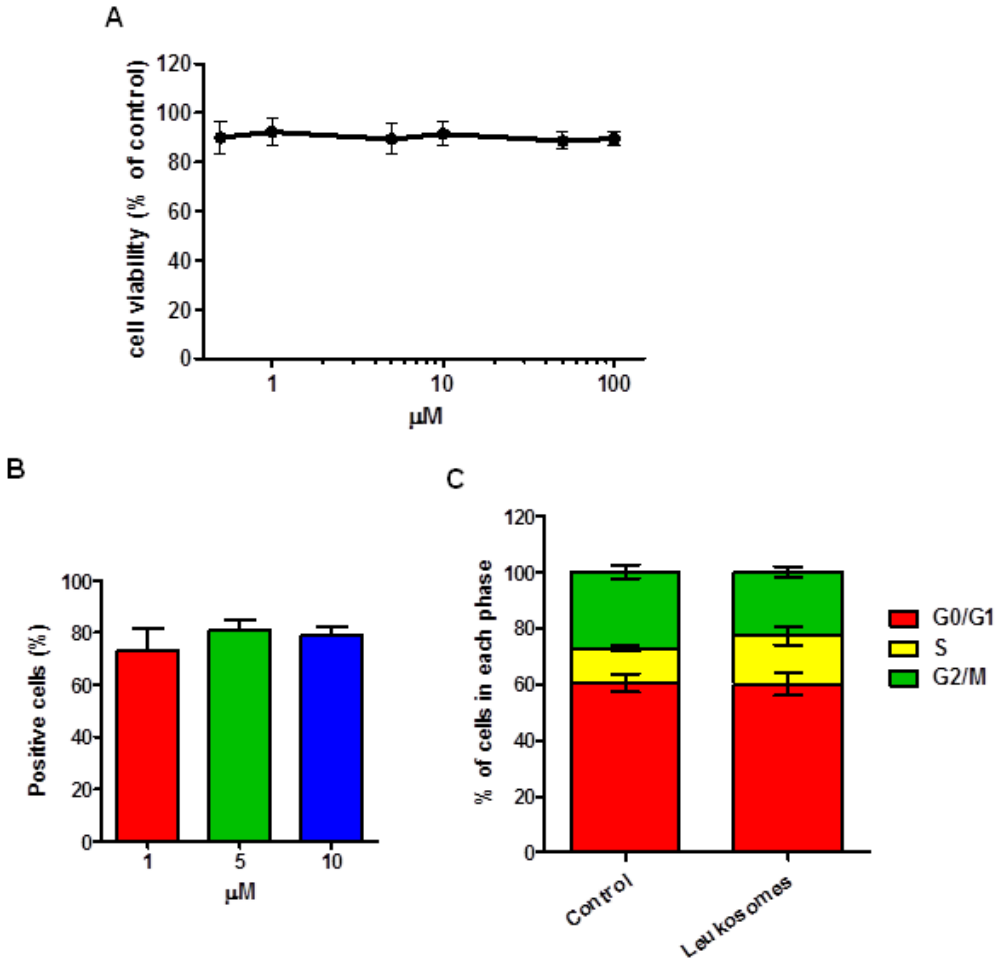

Figure 4.20. Biological effects of leukosomes on RT cells.

(A) The MTT assay was used to evaluate the cytotoxicity of leukosomes on A204 cells exposed for 72 h to increasing nanoparticles concentrations. The percent of viable cells was calculated by dividing absorbance at 550 nm of treated cells by that of untreated cells and multiplied *per* 100. The mean of at least 3 independent experiments is reported. (B) A204 cells were exposed to rhodamine-labeled leukosomes for 3 h and then subjected to flow cytometry. Cells were treated with 1, 5 or 10 µM leukosomes for 3 h. The percentage of cells that had internalised nanoparticles is represented in the graph. (C) Flow cytometric analysis of the cell cycle profiles of A204 cells treated with leukosomes. After 24 h cells were harvested, stained with propidium iodide and analysed for perturbations in the cell cycle. The columns depict the percentage of cells in each phase.

4.3.2.2. *In vitro* leukosome-delivery of siRNA

Another series of preliminary experiments was performed to assess siRNA loading into leukosomes and its fate after delivery to the cells. The siRNA was loaded into leukosomes using Exo-Fect, a reagent able to transfect exosome-like vesicles with nucleic acids [Torri A. et al., 2017]. A Dy547-labeled siRNA was incubated with Exo-Fect and leukosomes; then the loading efficiency of the siRNA was evaluated by analysing the fluorescence

intensity of the encapsulated siRNA with a spectrofluorimeter. Loading efficiency was around 85% with siRNA amount ranging from 15 to 100 pmol (Figure 4.21, A).

To possibly fulfil a therapeutic role, a siRNA has to be released into the cell cytoplasm, avoiding endo-lysosomal entrapment, a process depending on nanoparticle properties. Intracellular trafficking of siRNA-leukosomes was investigated by IF analysis, using Dy547-labeled siRNA, FITC-labeled leukosomes and LysoTracker to stain lysosomes. It was observed that most of the leukosomes rapidly fused with the cell plasma membrane, and the siRNA was subsequently released into the cytoplasm. Leukosome biology is similar to that of exosomes, and we hypothesised that they undergo the same mechanism of internalisation. It has been previously described that exosomes bind various cellular receptors of the recipient cell. After that, they may fuse with the cellular membrane or be endocytosed via phagocytosis, macropinocytosis or receptor-mediated endocytosis [McKelvey K.J. et al., 2015]. IF analysis demonstrated a similar behaviour for leukosomes. In fact, images taken at 3 and 24 h after treatment displayed an accumulation of green signal (FITC-labeled leukosomes) in correspondence of the cell membrane (Figure 4.21, B), and only a few particles were visible within the cells. This peculiar localisation was even more evident at 24 h. In addition, there was a negligible colocalisation of leukosomes with LysoTracker both at 3 and 24 h (Figure 4.21, C), indicating that leukosomes were able to avoid the endo-lysosomal compartment. The colocalisation between siRNA and leukosomes was low at 3 h and even lower at 24 h, suggesting that the siRNA was rapidly and mostly released, in a time dependent manner (Figure 4.21, D). Unexpectedly, the siRNA was partially colocalised with lysosomes, about 60% at 3 h and 40% at 24 h. To understand if this phenomenon was related to leukosome delivery, the fate of siRNA was evaluated after transfection with lipofectamine RNAiMAX. Also by this approach, a similar amount of siRNA was found colocalised with lysosomes (Figure 4.21, E and F). IF data were also used to calculate the amount of siRNA free in the cell cytoplasm. The

siRNA fraction colocalised with leukosomes or lysosomes was subtracted to total siRNA. The result indicated that the amount of siRNA available in the cytoplasm was slightly lower than 20% at 3 h and around 40% at 24 h (Figure 4.21, G).

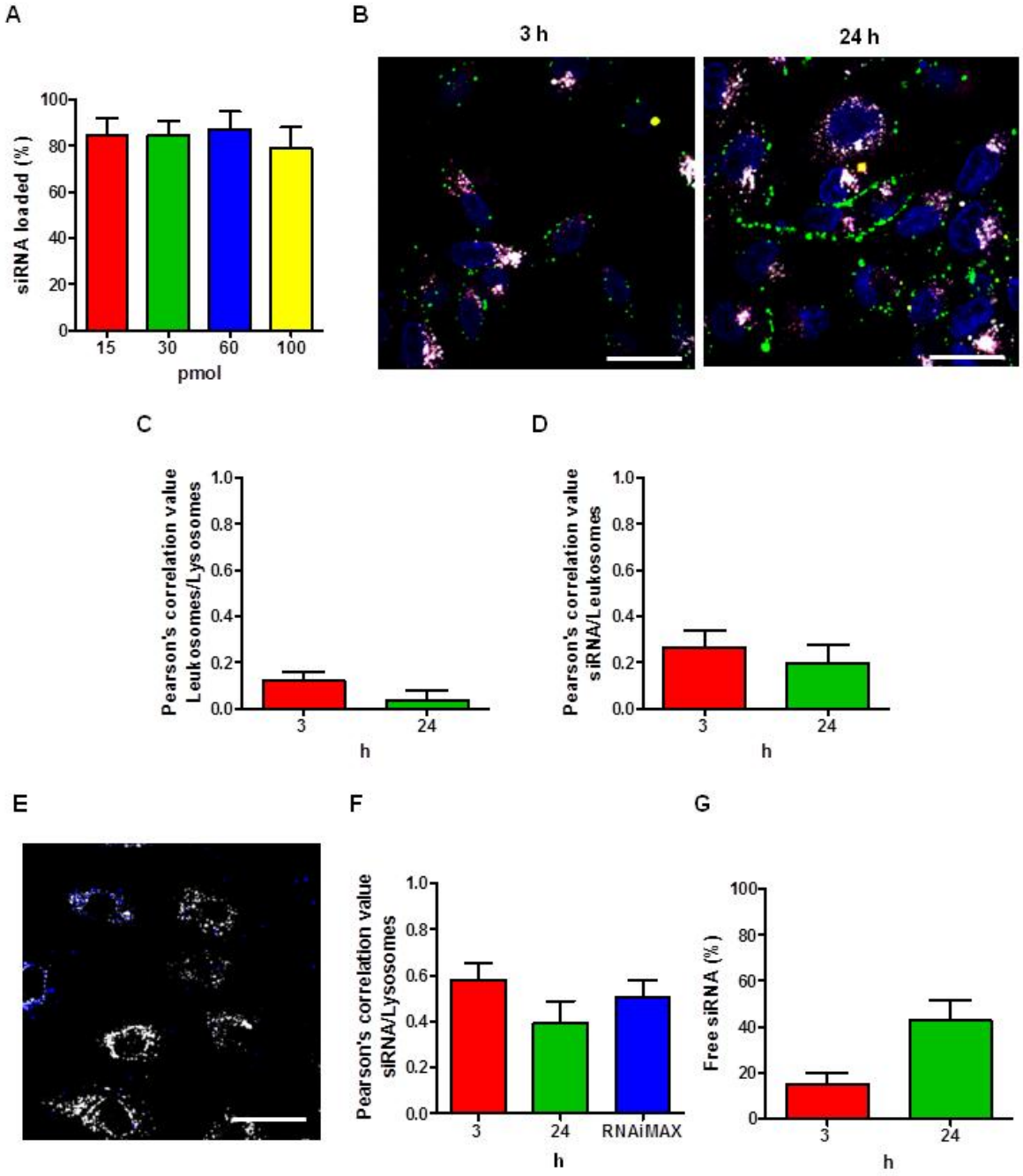

Figure 4.21. Leukosomes/siRNA trafficking.

(A) The graph shows siRNA loading efficiency with different starting concentrations. (B) Fluorescent microscope images showing siRNA-leukosomes trafficking in A204 cells after a 3 h exposure. Lysosomes are white, leukosomes are green, siRNA is red and nuclei are blue. Scale bars, 50 µm. (C) Histogram depicts the Pearson's correlation value regarding Leukosomes/lysosomes colocalisation. (D) Histogram depicts the Pearson's correlation value regarding leukosomes/siRNA colocalisation. (E) Fluorescent microscope image showing the siRNA and the lysosomes following transfection with lipofectamine RNAiMAX. Lysosomes are white, siRNA is blue. (F) Histogram depicts the Pearson's correlation value regarding siRNA/lysosomes colocalisation. (G) The graph shows the percentage of siRNA free in the cytoplasm.

After demonstrating the ability of leukosomes to load and deliver siRNA molecules into the cell cytoplasm, the efficacy of the anti-heparanase siR06, delivered through leukosomes, in targeting heparanase was investigated in A204 cells. Cells were treated with siR06-leukosomes, scramble siRNA-leukosomes, or empty leukosomes for 3 h. The expression level of heparanase mRNA was analysed using qRT-PCR 72 h after treatment (Figure 4.22, A, red bars). Heparanase silencing was not achieved by siRNA delivered through leukosomes.

The following experiments were performed in the attempt to understand and overcome the lack of efficacy of the leukosome-siRNA complex. As leukosomes were negatively charged, we supposed that the repulsion between the negative charges of siRNA and nanoparticles was responsible for an incorrect siRNA loading. To overcome this possible limitation, leukosome formulation was modified to make the nanoparticles positively charged. The specific amount of the different phospholipids was changed to favour the interaction between the anionic phosphate groups of siRNA and the cationic nitrogen groups of the phospholipids. The newly synthesised leukosomes were 109.8 ± 2.4 nm and charge 16.2 ± 3.28 mV as measured by DLS and ζ potential, with a PDI 0.151, In spite of this effort, heparanase silencing was not accomplished (Figure 4.22, A, green bars).

To better understand the reason why leukosomes were not able to deliver active siRNA, DLS analyses of siRNA-leukosomes and empty leukosomes were compared. It was noticed that siRNA-loaded leukosomes were larger than empty nanoparticles and were negatively charged (siRNA-leukosomes: 216 ± 24.4 nm, -39.1 ± 4.29 mV). These data indicated that the siRNA was not encapsulated into the leukosomes core when transfected with Exo-Fect, but it was deposited onto their surface.

To overcome this issue, we decided to fabricate leukosomes using the microfluidic-based platform (NanoAssemblr, Precision NanoSystem's Technology) just acquired and set up in the Houston laboratory. With this device, the manufacture of nanoparticles occurs under

extremely controlled conditions and the mixing ratio, flow rate and lipid composition can be adjusted.

For the synthesis, an ethanol solution containing the mixture of lipids and an aqueous solution containing siRNA and the leukocyte membrane proteins were injected into two separate channels of the NanoAssemblr and then the two solutions were mixed. During this process, the positive charges of the phospholipids interacted with the negative charges of the nucleic acid, allowing the encapsulation of siRNA into the leukosomes. This procedure led to the self-assembly of siRNA-leukosomes with a size of 127 ± 4.0 nm and a charge of 1.36 ± 0.88 mV as measured by DLS and ζ potential, with a PDI 0.121. Also with these new nanoparticles, heparanase silencing was not obtained (Figure 4.22, B, red bars). To exclude that the concurrent loading of siRNA and proteins into the NanoAssemblr might interfere with siRNA loading, siRNA-liposomes were fabricated with the same phospholipid formulation of leukosomes and tested in A204 cells. Even having eliminated proteins, siRNA-nanoparticles were not able to inhibit heparanase expression (Figure 4.22, B, green bars).

As in preliminary experiments the delivery and the trafficking of siRNA-leukosomes were quite satisfying, we hypothesised that the siRNA was degraded or inactivated in some phase of the procedure, thereby being unable to target heparanase mRNA.

In literature, PEI was conjugated with liposomes to reduce PEI toxicity and to achieve efficiently siRNA delivery [Ewe A. et al., 2017]. For this thesis, we conjugated both leukosomes and liposomes with siRNA-PEI complex, and tested these nanoparticles in A204 cells. Heparanase inhibition was obtained neither with PEI-liposomes nor with PEI-leukosomes (Figure 4.22, C).

Thus, despite the promising properties of leukosomes, in this thesis we demonstrated that the tested formulations of nanoparticles are not suitable for delivery of functional siRNA and that further optimisation of the encapsulation and release phases is required.

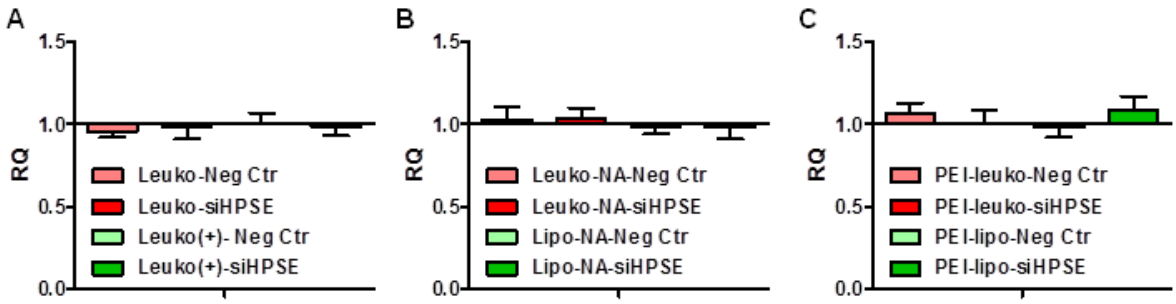

Figure 4.22. Heparanase mRNA levels after siRNA transfection with different nanoparticles.

(A) Quantitative RT-PCR analysis after siRNA delivery with leukosomes and positively charged leukosomes (+) assembled by TLE. (B) Quantitative RT-PCR analysis after siRNA delivery with leukosomes and liposomes assembled with NanoAssemblr. (C) Quantitative RT-PCR analysis after siRNA delivery with leukosomes and liposomes conjugated with PEI. Expression levels are reported as Relative Quantification with respect to cells transfected with empty nanoparticles (RQ = 1). The columns represent the mean and standard deviation of three independent experiments. GAPDH was used as housekeeping control. Leukosome, leuko; liposome, lipo; NanoAssemblr, NA; negative control, Neg Ctr,; anti-heparanase siRNA, siHPSE; Relative Quantification, RQ.

4.3.2.3. *In vivo* leukosome-delivery of siRNA

In parallel, the ability of leukosomes to target the tumour and associated vessels was evaluated in an *in vivo* model. *In vivo* experiments were performed in the metastatic RT xenograft established by intramuscular injection of A204 cells. Mice harbouring A204 tumours were treated with rhodamine-labeled empty leukosomes by intravenous administration and followed for 3 h using IVM. Leukosomes preferentially accumulated at the tumour site and were retained at least up to 3 h (Figure 4.23, A). It was also observed that leukosomes were able to target the lung metastasis, as assessed by confocal microscopy on a visible metastasis of explanted lungs, 3 h after leukosomes injection (Figure 4.23, B and C).

The capability of leukosomes to deliver siRNA *in vivo* was also evaluated. FITC-labeled leukosomes loaded with Dy547-labeled siRNA where intravenously injected in mice harbouring A204 orthotopic tumours and followed for 3 h with IVM. The siRNA was maintained within nanoparticles for all the duration of the experiment (Figure 4.23, D) and

a fraction of siRNA-leukosomes was also able to extravasate outside the vessels (Figure 4.23, E) as measured at the end of the experiment.

Interestingly, it was observed that there were no empty leukosomes at early time points (*i.e.*, from 0 to 30 min), and all the leukosomes were still carrying siRNA. After about 40 min, empty particles were visible at the IVM microscope, meaning that some leukosomes were releasing the siRNA while still circulating in the vessels.

The *in vivo* experiments demonstrated that leukosomes are able to target and accumulate at the tumour site; nonetheless a fraction of nanoparticles lost the cargo before extravasating from the vessels.

Taken together, these results support that leukosomes formulation and synthesis require further refinement to be suitable for nucleic acid delivery.

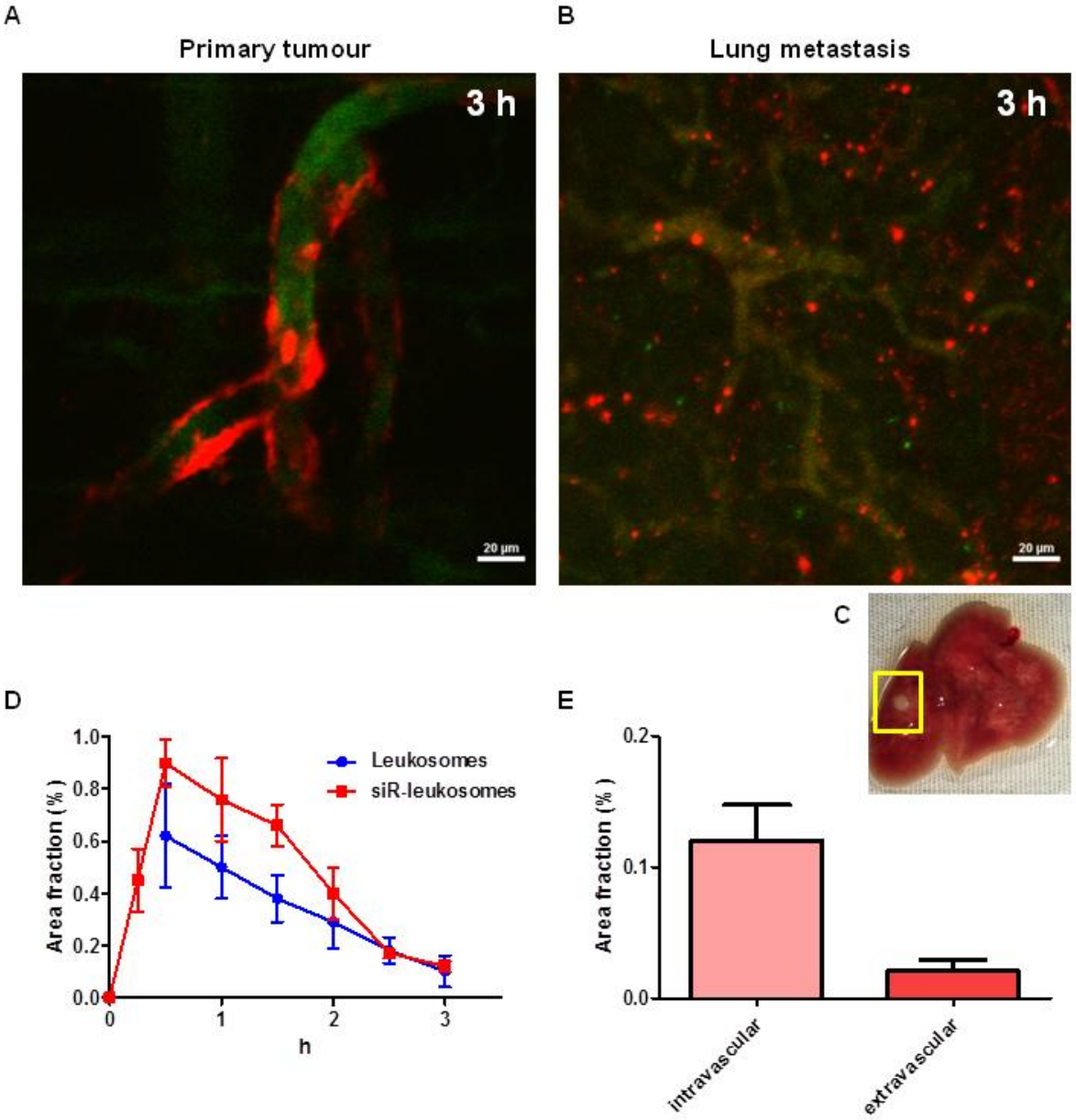

Figure 4.23. *In vivo* delivery of leukosomes and siRNA.

(A) Representative IVM image of A204 tumour vessels at 3 h after leukosomes administration. Leukosomes are red, vessels appear green for auto-fluorescence. Scale bar: 20 µm. (B) Representative IF image of lung metastasis 3 h after leukosomes administration. (C) Picture of lung metastasis used for B. (D) Plot of the first 3 h of leukosomes accumulation in A204 tumours. Error bars represent the standard deviation of measurements from at least 5 fields of views taken from 3 mice. E) Plot of leukosomes accumulation in lungs of A204 tumour bearing mice, 3 h after leukosomes administration. Error bars represent the standard deviation of measurements from at least 5 fields of views taken from 3 mice.

5.DISCUSSION

STSs are a heterogeneous group of over 50 histological subtypes of rare mesenchymal tumours, representing about 10% of tumours in paediatric age. Surgery, alone or in combination with chemotherapy and/or radiotherapy, is the best choice for local control whereas systemic treatment of advanced disease remains a challenge. In spite of the gold standard chemotherapy based on cytotoxic drugs, the prognosis for unresectable, recurrent or metastatic disease remains poor. Often, chemotherapy gives low response rates bringing acute and long term toxicity with it, which is particularly detrimental for children and adolescents. The high heterogeneity of sarcomas led to the current development of histology-driven, molecular targeted and immunomodulatory therapies also affecting the tumour stromal component [Noujaim J. et al., 2016]. The biomolecular complexity of sarcomas suggests that most of these tumours might not be dependent on a single targetable signaling pathway. Thus, innovative therapies should conceivably envision multi-targeted approaches and/or rational combination treatments, exploiting tumour dependence on its microenvironment as well. In this context, the heparanase/HSPG system plays a key role. In fact, the altered interplay between heparanase and its substrate HS in tumours disrupts the structural integrity of ECM and the homeostasis of several HS-binding bioactive molecules, and influences cell adhesion and motility [Vlodavsky I. and Friedmann Y., 2001; Sanderson R.D. et al., 2017]. Thus, heparanase has been extensively investigated as a master regulator of cancer progression and a potential therapeutic target, although the multiple mechanisms of its involvement in different tumour processes have not been completely clarified [Vlodavsky I. et al., 2016; Couchman J.R. et al., 2016; Sanderson R.D. et al., 2017; Lanzi C. et al., 2017].

In this thesis work, we investigated the possibility to specifically down-regulate heparanase by RNAi approaches based on nanoparticle delivery, potentially exploitable therapeutically in STS models. In fact, previous studies carried out in our laboratory suggested that the

heparanase/HSPG system represents a promising therapeutic target in these tumours [Cassinelli G. et al., 2013; Cassinelli[b] G. et al., 2016; Cassinelli G. et al., 2018].

The study was designed to inhibit heparanase expression in two human STS models, the rhabdoid tumour A204 and the synovial sarcoma CME-1, and to evaluate subsequent biochemical and biological effects. These cell lines were chosen because they both express high levels of heparanase and are well characterised by previous studies conducted in our laboratory [Cassinelli G. et al., 2013, Cassinelli[b] G. et al., 2016, Cassinelli G. et al., 2018]. Moreover, both cell lines grow orthotopically, spontaneously disseminating to the lungs in SCID mice [(Figure 3.1.) unpublished data and Cassinelli G. et al., 2018], thereby providing the opportunity to investigate the effects of heparanase inhibition on tumour growth and distant dissemination. The RNAi approach, distinct from other heparanase targeting strategies under investigation, such as small molecules and antibodies, would in principle be able to reduce expression of intracellular and extracellular heparanase, as well as its enzymatic and non-enzymatic functions. Moreover, heparanase gene silencing, being a selective approach, in contrast with HS mimetics would allow gene function and biological effects to be linked.

As a first approach, we evaluated the use of miR-1258 as an RNAi tool to down-regulate heparanase in the STS models. In fact, miR-1258 was previously found to correlate inversely with heparanase expression in clinical specimens of breast cancer and non small cell lung cancer [Tang D. et al., 2013; Liu H. et al., 2012]. In lung cancer, expression levels of miR-1258 and heparanase were significantly correlated to TNM staging and lymph node metastasis [Liu H. et al., 2012]. In breast cancer cell lines, miR-1258 levels correlated negatively with heparanase expression and enzymatic activity, as well as with the cell metastatic properties [Zhang L. et al., 2011]. Accordingly, in functional assays, lentiviral transfection of miR-1258 decreased heparanase expression and the *in vitro* invasive ability of brain metastatic breast cancer and lung cancer cells [Zhang L. et al.,

2011; Liu H. et al., 2012]. In addition, stable expression of miR-1258 in brain metastatic breast cancer cells inhibited *in vivo* experimental metastasis [Zhang L. et al., 2011].

Despite several attempts in treating A204 and CME-1 cells with miR-1258 by transient transfection, we observed only a mild reduction of heparanase mRNA, which did not affect the protein levels. These findings suggested that miR-1258 is not relevant in the control of heparanase expression in our sarcoma models.

As an alternative strategy to silence heparanase, we used commercially available siRNAs (siR04, siR05 and siR06). By this approach, heparanase was highly inhibited at mRNA level, and a partial down-regulation of the intracellular protein was also achieved, especially with siR04 and siR06. Moreover, these two anti-heparanase siRNAs were able to reduce extracellular secreted heparanase, as assessed by specific ELISA and enzymatic assays.

The down-regulation effect of anti-heparanase siRNA on extracellular enzymatically active heparanase was in agreement with the observed inhibition of wound healing and Matrigel invasion capacity of both sarcoma cell lines. Vlodavsky and his group, in fact, demonstrated that heparanase secreted and retained at the cell surface is mainly responsible for the protein pro-invasive effect *in vitro* and is a major determinant in the control of tumour angiogenesis and metastasis [Goldshmidt[a] O. et al., 2002]. Thereby, these findings suggest that heparanase RNAi may represent an exploitable strategy to counteract sarcoma progression. In line with our results, it has been recently reported that the invasive ability of A204 and CME-1 cells was reduced using small molecule heparanase inhibitors [Madia V.N. et al., 2018; Messore A. et al., 2018]. In addition, Cassinelli and collaborators showed a decrease of cell invasive ability and soft agar colony formation using other heparanase inhibitors, *i.e.*, the HS mimetics SST0001 and supersulfated low molecular weight heparin [Cassinelli G. et al., 2013; Cassinelli[b] G. et al., 2016; Cassinelli G. et al., 2018] in various sarcoma models, including CME-1. Interestingly, these effects were more marked than

those observed in the present study. This might be related to the double action of HS mimetics that inhibit heparanase and compete for HS-binding molecules. Thus, they can inhibit cell signaling also by blocking ligand-induced HS-dependent activation of cell surface receptors [Cassinelli[a] G. et al., 2016] (Figure 5.1).

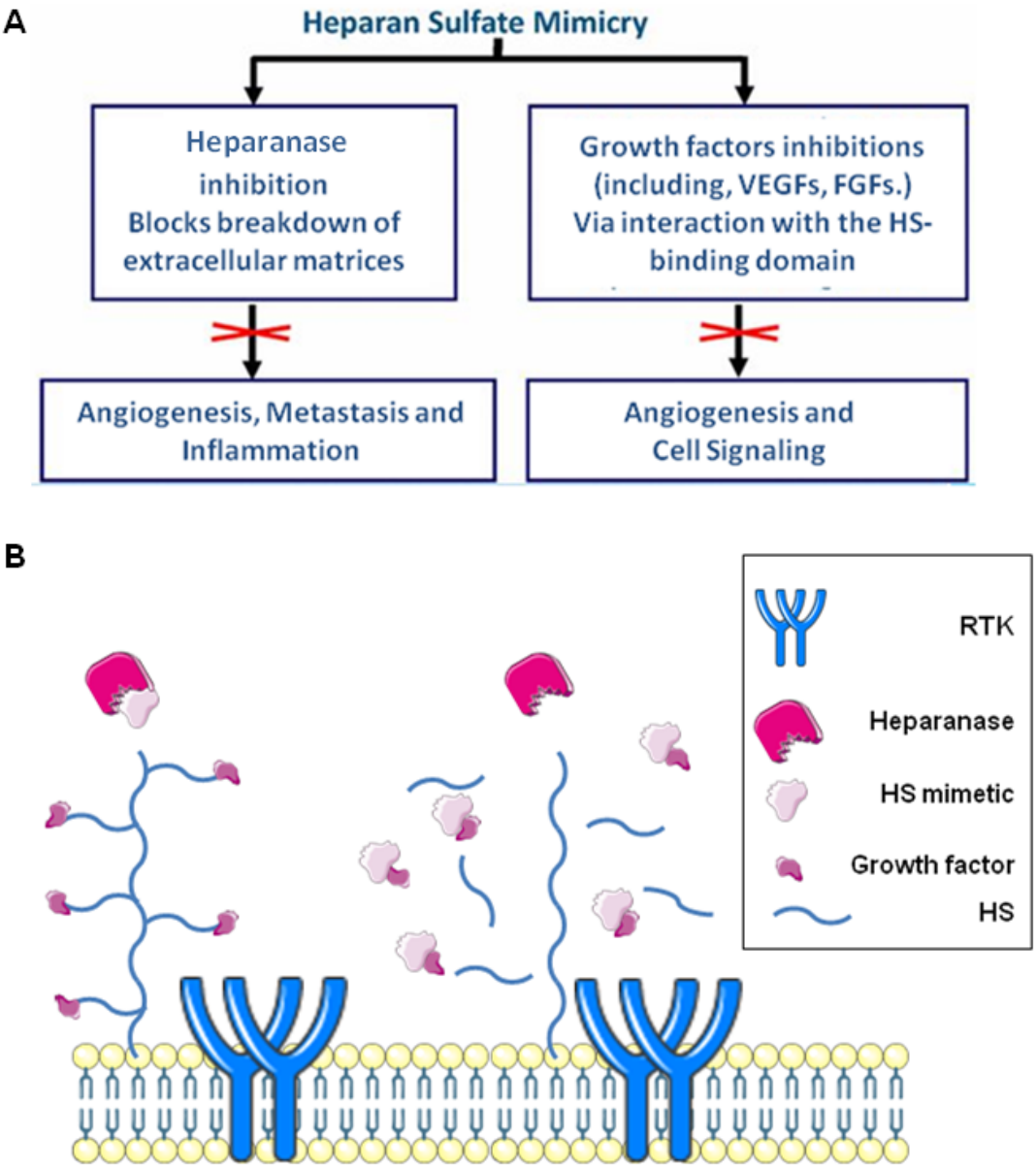

Figure 5.1. HS mimetics mechanism of action.

(A) Double action of HS mimetics, which inhibit heparanase and prevent the binding of bioactive molecule to HSPG. (B) HS mimetics block the activation of signaling pathways mediated by RTKs and heparanase released HS binding molecules.

It has been shown that intracellular heparanase is localised in the cytoplasm, mostly in lysosomes, and in the nucleus, where it exerts a multiplicity of functions [Goldshmidt[b] O. et al., 2002; Zester A. et al., 2004; Shubert S.Y. et al., 2004; Nobuhisa T. et al., 2007]. Thus, we analysed the intracellular heparanase in subcellular fractions to investigate whether it was differently modulated by RNAi in specific cellular compartments. By western blotting and IF staining, the two mature forms of heparanase were found to segregate differently, with the latent 65 kDa heparanase localised mostly in the nucleus and the 50 kDa active form in the cytoplasm, the latter concentrated in spots likely corresponding to lysosomes. Heparanase in these two cellular compartments was not substantially affected by gene silencing, whereas, as expected, the primary transcript product, pre-proheparanase, was reduced by the siRNA. It was previously demonstrated that heparanase accumulates in a stable form within the lysosomes, where the acidic microenvironment provides suitable conditions for storage and optimal enzymatic activity [Goldshmidt[b] O. et al., 2002]. It was also previously reported that, according to our findings, both the latent and the active heparanase forms are present in the nucleus, where the enzyme has been proposed to influence gene expression [Schubert S.Y. et al., 2004; Purushothaman A et al., 2011]. Our data indicate that heparanase is also present in the nucleus in a stable form resistant to siRNA-mediated silencing.

Heparanase role in the tumour aggressive phenotype has been ascribed in part to its expression enhancing effect on genes that participate in angiogenesis and cell motility, *e.g.*, VEGF, MMP-9, uPA/uPAR, TF, FGF-1 and -2 [Purushothaman A. et al., 2008; Cohen-Kaplan V. et al., 2008; Nadir Y. et al., 2006; Madia V.N. et al., 2018; Messore A. et al., 2018]. Heparanase can influence gene expression through indirect and direct mechanisms. An enzyme-independent signaling function has been described to activate protein kinases (*e.g.*, Akt, Src) ultimately inducing the transcription of genes [Fux L. et al., 2009]. Nuclear heparanase enzyme activity has been implicated in the loss of syndecan-1 which activates

HAT activity and expression of genes, such as VEGF and MMP-9, promoting aggressive tumour behaviour [Purushothaman A. et al., 2011]. In the present study, siR06-mediated heparanase silencing was found to reduce expression of angiogenesis-related proteins such as TF, CXCL16 and CD26 in A204 and CME-1 cells, and of FGF-1 in A204 cells. Only mild inhibition of other factors previously described as regulated by heparanase such as VEGF, uPA and PDGF-AA was detected by protein array, suggesting that they could be regulated by the nuclear heparanase fraction which was not affected by gene silencing. In fact, the HS mimetic heparanase inhibitor SST0001 was previously shown to down-regulate these molecules in A204 cells [Cassinelli G. et al., 2013].

Overall, these experiments demonstrated that heparanase silencing by siRNAs down-regulates the secreted protein and inhibits invasiveness of sarcoma cells. Prolonged exposure to RNAi is likely to be needed to achieve the down-regulation of heparanase stored in lysosomes and nuclei.

The second aim of this thesis was the optimisation of a delivery system for small nucleic acids (*i.e.*, miRNA and siRNA) to target heparanase in STS cells. There is a great interest in the delivery of nucleic acids for therapeutic purposes, with the development of innovative approaches designed to reach the tumour site. The *in vivo* delivery of RNAi molecules has shown many challenges, because nucleic acids have poor stability (half-life lower than 10 min), off-target effects, and inefficient cellular entry when administered systemically [Juliano R.L., 2016]. In this context, nanotechnology offers a potent tool for the development of drug delivery systems with the ability to carry and protect such payloads. In fact, nanoparticles have been shown to enhance *in vivo* targeting properties, pharmacokinetics, half-life and bioavailability of therapeutic nucleic acids [Tatiparti K. et al., 2017]. In addition, the high versatility of nanoparticle formulations can in principle permit the co-encapsulation of different therapeutics and the transferability of this technology to various diseases.

Here, we used different nanodelivery platforms which, in principle, should be endowed with high versatility allowing, after a successful set up, the use of miRNA or siRNA to specific targets in different tumour types.

The first nanoparticles examined in this study, HNPs, consisted of hybrid nanogel particles with a silica core covered with a polymeric shell responsive to pH shift, able to buffer and swell in acidic pH [Khaled S.Z. et al., 2016]. The hydrogel shell, due to its high hydrophilicity and elastic consistency, resembles living tissues and allows the release of the payload in a controlled manner. In fact, under specific physiopathological conditions (*i.e.*, pH) the hydrogel swells and the payload is released mainly by diffusion [Ratner B.D. and Hoffman A.S., 1976; Hamidi M. et al., 2008]. However, the use of the sole hydrogel is limited by poor stability. For this reason, hybrid nanoparticles, consisting of a hydrogel shell (PDEAEM/PEGMA/TEGDMA) conjugated with a solid core (*i.e.*, silica), were used to enhance the stability without affecting the biocompatibility and environmental responsiveness of the polymer [Yang J. et al., 2013].

The increase in size and the acquisition of a positive charge by HNPs under acidic conditions is known as “proton sponge effect”. We exploited this feature to load a siRNA. In fact, at acidic pH the structure of the HNP hydrogel was looser, allowing the incorporation of siRNA, and the positive charge acquired by the hydrogel determined the electrostatic binding with the siRNA. The pH-responsiveness also allowed endo-lysosomal escape. Indeed, the evaluation of *in vitro* effect of HNPs indicated that they were internalised in endosomes and accumulated in late endosomes and lysosomes, whose pH is gradually more acidic. The lowering of pH induced the swelling of HNPs that broke out from the endo-lysosomal membrane releasing their content into the cytoplasm.

After the characterisation of the physico-chemical properties of HNPs, it is key to examine *in vitro* biological effects. As expected, we observed that HNPs were devoid of toxic effects, *i.e.*, they did not impair the viability of A204 cells up to a precise concentration

(0.1 ng/cell). Cell treatment with this HNP concentration resulted in optimal internalisation, a phenomenon subsequent to interaction of the particles with the cell membrane, as supported by SEM images. In spite of the apparent lack of toxicity of HNPs at 0.1 ng/cell, a 3 h exposure to the nanoparticles with cell harvesting 24 h after treatment resulted in a marked cell cycle perturbation with increase of the S phase cell fraction and decrease of the G_2/M phase cells. This observation suggests that cells slow down proliferation upon treatment with HNPs. However, given that no effect on cell viability was observed upon 72 h exposure to 0.1 ng/cell HNPs, it is likely that the cell cycle perturbation is a transient and reversible effect. This interpretation is in line with the observed slowing down of the cell migration capability, an effect that was also reversible.

The subsequent *in vitro* evaluation of HNPs effects carried out by fluorescence microscopy tracking acidic organelles, showed a partial accumulation of HNPs in endo-lysosomal vesicles 3 h after treatment, implying that the remaining fraction of HNPs was in the cytoplasm. At a later time (*i.e.*, 72 h), HNPs were mainly localised in acidic vesicles as supported by Pearson's correlation values. These results imply that nanoparticle localisation in subcellular compartments is a dynamic process. In fact, a re-organisation of the vesicular compartment was also evidenced in endothelial cells, in which at 72 h after treatment HNPs were incorporated in vesicles presenting features of multilamellar bodies, as shown by TEM, suggesting that they will be extruded [Parodi A., Arrighetti N. et al., submitted]. In fact, multilamellar body formation has also been reported as the main source of exosomes, suggesting that cells constituted these vesicular formations around HNPs to extrude them within exosomes [Denzer K. et al., 2000]. It is conceivable that nanoparticles internalised in tumour cells undergo the same phenomenon; these findings support the hypothesis that the observed alteration of cell cycle and migration were due to the presence of nanoparticles free into the cytoplasm. Moreover, the restoration of physiological cell function may be a consequence of the sequestration of HNPs in multilamellar bodies.

To achieve efficient siRNA delivery, besides having proper subcellular localisation of nanoparticles, it is fundamental to obtain siRNA release. Although, under our *in vitro* experimental conditions, HNPs appeared to be able to release a fluorescent siRNA, functional studies with an anti-heparanase siRNA failed to achieve heparanase silencing. We hypothesised that the polymeric hydrogel shell of HNPs was not able to protect the siRNA functionality. Thus, we exploited a different polymer, polyethylenimine (PEI), already investigated for nucleic acid delivery [Kwok A. and Hart S.L., 2011; Buchman Y.K. et al., 2013]. We conjugated the PEI to the silica core with the aim to protect siRNAs from degradation. However, these modified nanoparticles also failed to deliver positive results in terms of heparanase silencing.

When tested *in vivo*, HNPs had a prolonged circulation time. Indeed, 2 h after administration, the nanoparticles were still detectable in the tumour by IVM. During this time, the siRNA was maintained attached to the nanoparticles throughout the experiment. The prolonged circulation time shown by these nanoparticles is advantageous for the accumulation of the therapeutics at the tumour site obtained through the enhanced permeability and retention effect.

Nevertheless, given the disappointing results obtained *in vitro* with HNPs, we decided not to pursue the HNPs and to evaluate a different platform based on biomimetic nanoparticles (*i.e.*, leukosomes) that was already under investigation at the HRMI.

Biomimetic nanoparticles are expected to substantially advance the current paradigm used for particle targeting and shielding relying on synthetic routes (*e.g.*, functionalisation with antibodies, peptides or hydrophilic polymers). Biomimetic nanoplatforms may allow the delivery and sustained release of a myriad of therapeutics to tumour tissues. The technology is based on the synergistic combination of nanotechnology and cancer cell biology.

Leukosomes are liposome-like nanoparticles obtained by the complexation of leukocyte membrane proteins, extracted from purified circulating leukocytes, and synthetic biocompatible phospholipids. Membrane proteins protect leukosomes from immune response recognition and favour the adhesion and margination to the endothelium [Molinaro R. et al., 2016]. In previous studies, leukosomes were shown to exhibit a predisposition to target inflamed endothelium and accumulate at tumour sites exhibiting intrinsic anti-inflammatory properties [Corbo C. et al., 2017; Martinez J.O. et al., 2018]. Besides, leukosomes have a structure and composition similar to those of exosomes, which are natural carriers of nucleic acids [Valadi H. et al., 2007]. Owing to their exosome-like structure, leukosomes undergo the same internalisation mechanisms, such as fusion with cell membrane, endocytosis or receptor mediated internalisation [McKelvey K.J. et al., 2015] (Figure 5.2). Based on these favourable features, we decided to test leukosomes for siRNA delivery. Leukosomes were first synthesised with the well-established TLE method and then loaded with the siRNA using the transfection reagent Exo-Fect. In this way, leukosomes by avoiding endo-lysosomal entrapment might release their cargo into the cell cytoplasm, where siRNAs accomplish their inhibitory function.

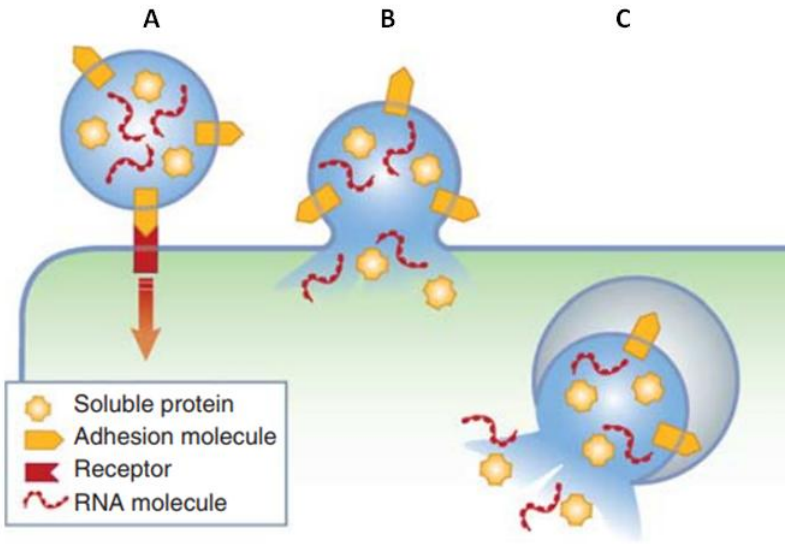

Figure 5.2. Exosome internalisation mechanisms.

(A) Ligand-receptor mediated; (B) fusion with cell membrane; (C) endocytosis [van Balkom B.W. et al., 2011].

In vitro evaluation of the biological effects of leukosomes indicated that, similarly to HNPs, they did not affect cell viability after long-term exposure (*i.e.*, 72 h) and that they are internalised efficiently producing a mild perturbation of the cell cycle. The analysis of the siRNA-leukosome trafficking in tumour cells showed that these biomimetic nanoparticles avoid the endo-lysosomal compartment and suggested that a fraction of siRNA was free in the cytoplasm, showing that indeed the small nucleic acid could be released and made available to interact with the target. Although this biomimetic platform was considered optimised for siRNA delivery, the results that we obtained in functional studies with an anti-heparanase siRNA indicated that the delivered siRNA was somehow inactivated. Interestingly, we observed a high colocalisation of fluorescent siRNA and lysosomes. To investigate whether siRNA sequestration was the reason for the lack of efficacy, we compared the fluorescent analysis of leukosome/siRNA with those of lipofectamine RNAiMAX/siRNA, the standard method for *in vitro* transfection. The comparison showed a similar amount of siRNA retained into lysosomes, so we excluded that this was the reason why heparanase expression was not inhibited with leukosomes transfection. Thus, we hypothesised that siRNA was compromised during the loading or delivery phases.

As the first synthesised leukosomes were negatively charged, and this could interfere with the loading of siRNA, in turn negatively charged, we developed a second type of leukosomes carrying a positive charge, ascribable to specific phospholipids. Further experimental effort supported the view that an incorrect encapsulation of the siRNA, deposited onto the leukosomes surface, instead of being encapsulated into them, was also the reason for our failure to silence heparanase with this alternative type of leukosome.

To overcome this issue, a new generation microfluidic approach, NanoAssemblr, was used for leukosome synthesis as it allows the encapsulation of siRNA during the synthesis phase, preventing the use of Exo-Fect. Since in this case, heparanase silencing was also not

obtained, we hypothesised that the leukocyte proteins within the leukosome membrane were somehow compromising the siRNA stability. To verify this hypothesis we also tested siRNA-liposomes without achieving heparanase silencing.

In additional experiments, we used PEI to protect siRNA during the loading of both leukosomes and liposomes, as previously shown in literature [Kwok A. and Hart S.L., 2011]. However, an appropriate formulation of these nanoparticles for delivery of functional siRNA was not obtained.

Finally, although *in vivo* testing in mice xenografted with A204 cells evidenced promising features of leukosomes, *i.e.*, ability to accumulate at primary tumour and metastatic sites, leukosomes appear to require further optimisation before being considered suitable for delivery of small nucleic acids.

Taken together, as far as nanoparticles are concerned, the results obtained during this thesis project support the view that, once the physico-chemical properties of nanoparticles are optimised, additional efforts will be needed before formulations useful for *in vitro* and, ultimately, *in vivo* delivery of RNAi molecules will be obtained. In this regard, besides the evaluation of the internalisation and subcellular distribution, it appears to be mandatory to address siRNA functionality maintenance.

6.CONCLUSIONS & FUTURE PERSPECTIVES

To identify a heparanase RNAi molecule effective in rhabdoid tumour and synovial sarcoma models, we tested a previously described heparanase miRNA, miR-1258, and commercially available validated siRNAs. Whereas miR-1258 did not produce a substantial reduction of heparanase expression by transient transfection in our sarcoma cell lines, the siRNAs effectively down-regulated expression and enzymatic activity of secreted heparanase. These effects were reflected in inhibition of sarcoma cell invasiveness and anchorage-independent growth, supporting the pro-metastatic role of secreted heparanase. In contrast, intracellular fractions, including lysosomal and nuclear heparanase, appeared to be resistant to transient siRNA silencing suggesting that their down-regulation likely requires a prolonged cell exposure to RNAi. This aspect needs further investigation.

The two delivery nanoplatforms tested in this thesis work, HNPs and biomimetic leukosomes, showed promising features in terms of *in vivo* targeting to the tumour and metastatic sites. However, their application for siRNA delivery still needs adjustments specifically addressing how to preserve the functionality of RNAi molecules.

After further optimisation, these innovative platforms may represent versatile tools available to hit various targets in different tumour types.

The results presented here may provide a starting point for future investigations.

The heparanase compartmentalisation evidenced in cell fractionation studies indicated a high stability of the protein in lysosomes and nuclei. This aspect should be deeply investigated in order to clarify the role of the enzyme in those compartments, specifically in relation to the suggested implication of heparanase in autophagy and gene transcription. Indeed, a better understanding of these functions is highly relevant in view of the therapeutic targeting of heparanase. The use of repeated transfections or stable silencing will be fundamental to enable the reduction of heparanase in all sub-cellular compartments.

Heparanase silencing reduced the expression of some angiogenesis-related factors as shown by protein array analysis. The validation of these effects using different techniques (i.e., real-time and western blotting) will be required to confirm their dependence on heparanase.

The heparanase/HSPG axis modulates a multiplicity of pathways in both tumour and microenvironment that have not been completely clarified. To elucidate the specific effects induced by this axis inhibition on downstream pathways in sarcoma, it may be useful to compare the effects achieved using different inhibitory approaches, for example siRNAs, small molecules or HS mimics. The identification of specific pathways altered by the heparanase/HSPG system will be useful for the rational design of new combinatorial treatments to counteract sarcoma progression.

7.REFERENCES

- Abramoff, M.D., Magalhães, P.J. & Ram, S.J. 2004, *Biophotonics international*, volume 11, issue 7, pp. 36 – 42.
- Aied, A., Greiser, U., Pandit, A. & Wang, W. 2013, "Polymer gene delivery: overcoming the obstacles", *Drug discovery today*, vol. 18, no. 21-22, pp. 1090-1098.
- Alavi, M. & Hamidi, M. 2019, "Passive and active targeting in cancer therapy by liposomes and lipid nanoparticles", *Drug metabolism and personalized therapy*.
- Alimova, I., Pierce, A., Danis, E., Donson, A., Birks, D.K., Griesinger, A., Foreman, N.K., Santi, M., Soucek, L., Venkataraman, S. & Vibhakar, R. 2018, "Inhibition of MYC attenuates tumor cell self-renewal and promotes senescence in SMARCB1-deficient Group 2 atypical teratoid rhabdoid tumors to suppress tumor growth in vivo", *International journal of cancer*.
- Almazan-Moga, A., Zarzosa, P., Molist, C., Velasco, P., Pyczek, J., Simon-Keller, K., Giralt, I., Vidal, I., Navarro, N., Segura, M.F., Soriano, A., Navarro, S., Tirado, O.M., Ferreres, J.C., Santamaria, A., Rota, R., Hahn, H., Sanchez de Toledo, J., Roma, J. & Gallego, S. 2017, "Ligand-dependent Hedgehog pathway activation in Rhabdomyosarcoma: the oncogenic role of the ligands", *British journal of cancer*, vol. 117, no. 9, pp. 1314-1325.
- Arrighetti, N., Corbo, C., Evangelopoulos, M., Pasto, A., Zuco, V. & Tasciotti, E. 2018, "Exosome-like nanovectors for drug delivery in cancer", *Current medicinal chemistry*.
- Arvatz, G., Shafat, I., Levy-Adam, F., Ilan, N. & Vlodavsky, I. 2011, "The heparanase system and tumor metastasis: is heparanase the seed and soil?", *Cancer metastasis reviews*, vol. 30, no. 2, pp. 253-268.
- Athale, U.H., Duckworth, J., Odame, I. & Barr, R. 2009, "Childhood atypical teratoid rhabdoid tumor of the central nervous system: a meta-analysis of observational studies", *Journal of pediatric hematology/oncology*, vol. 31, no. 9, pp. 651-663.
- Banito, A., Li, X., Laporte, A.N., Roe, J.S., Sanchez-Vega, F., Huang, C.H., Dancsok, A.R., Hatzi, K., Chen, C.C., Tschaharganeh, D.F., Chandwani, R., Tasdemir, N., Jones, K.B., Capecchi, M.R., Vakoc, C.R., Schultz, N., Ladanyi, M., Nielsen, T.O. & Lowe, S.W. 2018, "The SS18-SSX Oncoprotein Hijacks KDM2B-PRC1.1 to Drive Synovial Sarcoma", *Cancer cell*, vol. 34, no. 2, pp. 346-348.

- Barash, U., Cohen-Kaplan, V., Dowek, I., Sanderson, R.D., Ilan, N. & Vlodavsky, I. 2010, "Proteoglycans in health and disease: new concepts for heparanase function in tumor progression and metastasis", *The FEBS journal*, vol. 277, no. 19, pp. 3890-3903.
- Barham, W., Frump, A.L., Sherrill, T.P., Garcia, C.B., Saito-Diaz, K., VanSaun, M.N., Fingleton, B., Gleaves, L., Orton, D., Capecchi, M.R., Blackwell, T.S., Lee, E., Yull, F. & Eid, J.E. 2013, "Targeting the Wnt pathway in synovial sarcoma models", *Cancer discovery*, vol. 3, no. 11, pp. 1286-1301.
- Bartel, D.P. 2004, "MicroRNAs: genomics, biogenesis, mechanism, and function", *Cell*, vol. 116, no. 2, pp. 281-297.
- Beg, M.S., Brenner, A.J., Sachdev, J., Borad, M., Kang, Y.K., Stoudemire, J., Smith, S., Bader, A.G., Kim, S. & Hong, D.S. 2017, "Phase I study of MRX34, a liposomal miR-34a mimic, administered twice weekly in patients with advanced solid tumors", *Investigational new drugs*, vol. 35, no. 2, pp. 180-188.
- Begin, L.R. 2003, "Critical commentary to: Primary poorly differentiated monophasic synovial sarcoma of the lung", *Pathology, research and practice*, vol. 199, no. 12, pp. 835-836.
- Behr, J. 1997, "The proton sponge: A trick to enter cells the viruses did not exploit", *Chimia* 51: 34–36.
- Betz, B.L., Strobeck, M.W., Reisman, D.N., Knudsen, E.S. & Weissman, B.E. 2002, "Re-expression of hSNF5/INI1/BAF47 in pediatric tumor cells leads to G1 arrest associated with induction of p16ink4a and activation of RB", *Oncogene*, vol. 21, no. 34, pp. 5193-5203.
- Bhaskaran, M. & Mohan, M. 2014, "MicroRNAs: history, biogenesis, and their evolving role in animal development and disease", *Veterinary pathology*, vol. 51, no. 4, pp. 759-774.
- Biegel, J.A., Zhou, J.Y., Rorke, L.B., Stenstrom, C., Wainwright, L.M. & Fogelgren, B. 1999, "Germ-line and acquired mutations of INI1 in atypical teratoid and rhabdoid tumors", *Cancer research*, vol. 59, no. 1, pp. 74-79.
- Bishop, J.R., Schuksz, M. & Esko, J.D. 2007, "Heparan sulphate proteoglycans fine-tune mammalian physiology", *Nature*, vol. 446, no. 7139, pp. 1030-1037.

- Blanco, E., Shen, H. & Ferrari, M. 2015, "Principles of nanoparticle design for overcoming biological barriers to drug delivery", *Nature biotechnology*, vol. 33, no. 9, pp. 941-951.
- Blaney, S.M., Kocak, M., Gajjar, A., Chintagumpala, M., Merchant, T., Kieran, M., Pollack, I.F., Gururangan, S., Geyer, R., Phillips, P., McLendon, R.E., Packer, R., Goldman, S., Banerjee, A., Heideman, R., Boyett, J.M. & Kun, L. 2012, "Pilot study of systemic and intrathecal mafosfamide followed by conformal radiation for infants with intracranial central nervous system tumors: a pediatric brain tumor consortium study (PBTC-001)", *Journal of neuro-oncology*, vol. 109, no. 3, pp. 565-571.
- Bobo, D., Robinson, K.J., Islam, J., Thurecht, K.J. & Corrie, S.R. 2016, "Nanoparticle-Based Medicines: A Review of FDA-Approved Materials and Clinical Trials to Date", *Pharmaceutical research*, vol. 33, no. 10, pp. 2373-2387.
- Brett, D., Whitehouse, S., Antonson, P., Shipley, J., Cooper, C. & Goodwin, G. 1997, "The SYT protein involved in the t(X;18) synovial sarcoma translocation is a transcriptional activator localised in nuclear bodies", *Human molecular genetics*, vol. 6, no. 9, pp. 1559-1564.
- Brummelkamp, T.R., Bernards, R. & Agami, R. 2002, "A system for stable expression of short interfering RNAs in mammalian cells", *Science (New York, N.Y.)*, vol. 296, no. 5567, pp. 550-553.
- Buchman, Y.K., Lellouche, E., Zigdon, S., Bechor, M., Michaeli, S. & Lellouche, J.P. 2013, "Silica nanoparticles and polyethyleneimine (PEI)-mediated functionalization: a new method of PEI covalent attachment for siRNA delivery applications", *Bioconjugate chemistry*, vol. 24, no. 12, pp. 2076-2087.
- Bumcrot, D., Manoharan, M., Koteliansky, V. & Sah, D.W. 2006, "RNAi therapeutics: a potential new class of pharmaceutical drugs", *Nature chemical biology*, vol. 2, no. 12, pp. 711-719.
- Buwalda, S.J., Boere, K.W., Dijkstra, P.J., Feijen, J., Vermonden, T. & Hennink, W.E. 2014, "Hydrogels in a historical perspective: from simple networks to smart materials", *Journal of controlled release : official journal of the Controlled Release Society*, vol. 190, pp. 254-273.
- Buyens, K., Meyer, M., Wagner, E., Demeester, J., De Smedt, S.C. & Sanders, N.N. 2010, "Monitoring the disassembly of siRNA polyplexes in serum is crucial

for predicting their biological efficacy", *Journal of controlled release : official journal of the Controlled Release Society,* vol. 141, no. 1, pp. 38-41.

- Cairns, R.A., Harris, I.S. & Mak, T.W. 2011, "Regulation of cancer cell metabolism", *Nature reviews.Cancer,* vol. 11, no. 2, pp. 85-95.
- Calin, G.A. & Croce, C.M. 2006, "MicroRNA signatures in human cancers", *Nature reviews.Cancer,* vol. 6, no. 11, pp. 857-866.
- Carmody Soni, E.E., Schlottman, S., Erkizan, H.V., Uren, A. & Toretsky, J.A. 2014, "Loss of SS18-SSX1 inhibits viability and induces apoptosis in synovial sarcoma", *Clinical orthopaedics and related research,* vol. 472, no. 3, pp. 874-882.
- Carol, H., Boehm, I., Reynolds, C.P., Kang, M.H., Maris, J.M., Morton, C.L., Gorlick, R., Kolb, E.A., Keir, S.T., Wu, J., Wozniak, A.E., Yang, Y., Manfredi, M., Ecsedy, J., Wang, J., Neale, G., Houghton, P.J., Smith, M.A. & Lock, R.B. 2011, "Efficacy and pharmacokinetic/pharmacodynamic evaluation of the Aurora kinase A inhibitor MLN8237 against preclinical models of pediatric cancer", *Cancer chemotherapy and pharmacology,* vol. 68, no. 5, pp. 1291-1304.
- Cascales, P., Gomez-Caro, A.A., Ferri-Niguez, B., Roca, M.J., Torres, J. & Parrilla, P. 2006, "Poorly differentiated primary monophasic synovial sarcoma of the lung", *Asian cardiovascular & thoracic annals,* vol. 14, no. 6, pp. 511-513.
- Cassinelli, G., Lanzi, C., Tortoreto, M., Cominetti, D., Petrangolini, G., Favini, E., Zaffaroni, N., Pisano, C., Penco, S., Vlodavsky, I. & Zunino, F. 2013, "Antitumor efficacy of the heparanase inhibitor SST0001 alone and in combination with antiangiogenic agents in the treatment of human pediatric sarcoma models", *Biochemical pharmacology,* vol. 85, no. 10, pp. 1424-1432.
- Cassinelli[a], G., Zaffaroni, N. & Lanzi, C. 2016, "The heparanase/heparan sulfate proteoglycan axis: A potential new therapeutic target in sarcomas", *Cancer letters,* vol. 382, no. 2, pp. 245-254.
- Cassinelli[b], G., Favini, E., Dal Bo, L., Tortoreto, M., De Maglie, M., Dagrada, G., Pilotti, S., Zunino, F., Zaffaroni, N. & Lanzi, C. 2016, "Antitumor efficacy of the heparan sulfate mimic roneparstat (SST0001) against sarcoma models involves multi-target inhibition of receptor tyrosine kinases", *Oncotarget,* vol. 7, no. 30, pp. 47848-47863.

- Cassinelli, G., Dal Bo, L., Favini, E., Cominetti, D., Pozzi, S., Tortoreto, M., De Cesare, M., Lecis, D., Scanziani, E., Minoli, L., Naggi, A., Vlodavsky, I., Zaffaroni, N. & Lanzi, C. 2018, "Supersulfated low-molecular weight heparin synergizes with IGF1R/IR inhibitor to suppress synovial sarcoma growth and metastases", *Cancer letters,* vol. 415, pp. 187-197.
- Casu, B., Vlodavsky, I. & Sanderson, R.D. 2008, "Non-anticoagulant heparins and inhibition of cancer", *Pathophysiology of haemostasis and thrombosis,* vol. 36, no. 3-4, pp. 195-203.
- Cavallaro, G., Sardo, C., Craparo, E.F., Porsio, B. & Giammona, G. 2017, "Polymeric nanoparticles for siRNA delivery: Production and applications", *International journal of pharmaceutics,* vol. 525, no. 2, pp. 313-333.
- Chakraborty, C. & Das, S. 2016, "Profiling cell-free and circulating miRNA: a clinical diagnostic tool for different cancers", *Tumour biology : the journal of the International Society for Oncodevelopmental Biology and Medicine,* vol. 37, no. 5, pp. 5705-5714.
- Chakravadhanula, M., Hampton, C.N., Chodavadia, P., Ozols, V., Zhou, L., Catchpoole, D., Xu, J., Erdreich-Epstein, A. & Bhardwaj, R.D. 2015, "Wnt pathway in atypical teratoid rhabdoid tumors", *Neuro-oncology,* vol. 17, no. 4, pp. 526-535.
- Chen, G., Wang, D., Vikramadithyan, R., Yagyu, H., Saxena, U., Pillarisetti, S. & Goldberg, I.J. 2004, "Inflammatory cytokines and fatty acids regulate endothelial cell heparanase expression", *Biochemistry,* vol. 43, no. 17, pp. 4971-4977.
- Chen, Y., Zhao, H., Tan, Z., Zhang, C. & Fu, X. 2015, "Bottleneck limitations for microRNA-based therapeutics from bench to the bedside", *Die Pharmazie,* vol. 70, no. 3, pp. 147-154.
- Cheng, S.W., Davies, K.P., Yung, E., Beltran, R.J., Yu, J. & Kalpana, G.V. 1999, "c-MYC interacts with INI1/hSNF5 and requires the SWI/SNF complex for transactivation function", *Nature genetics,* vol. 22, no. 1, pp. 102-105.
- Chi, S.N., Zimmerman, M.A., Yao, X., Cohen, K.J., Burger, P., Biegel, J.A., Rorke-Adams, L.B., Fisher, M.J., Janss, A., Mazewski, C., Goldman, S., Manley, P.E., Bowers, D.C., Bendel, A., Rubin, J., Turner, C.D., Marcus, K.J., Goumnerova, L., Ullrich, N.J. & Kieran, M.W. 2009, "Intensive multimodality treatment for children with newly diagnosed CNS atypical teratoid rhabdoid

tumor", *Journal of clinical oncology : official journal of the American Society of Clinical Oncology,* vol. 27, no. 3, pp. 385-389.

- Chu, C.L., Long, A., Honan, C.M., Duffner, J., Avery, W., D'Alessandro, J., Kishimoto, T.K., Schultes, B.C. 2012, "M402, a novel heparan sulfate mimetic, inhibits pancreatic tumor growth and desmoplasia potentially via sonic hedgehog signaling in an orthotopic mouse model", *103rd Annual Meeting of the American Association for Cancer Research,* Abstract.
- Research: Philadelphia, PA, USA, 2012.Cohen-Kaplan, V., Naroditsky, I., Zetser, A., Ilan, N., Vlodavsky, I. & Doweck, I. 2008, "Heparanase induces VEGF C and facilitates tumor lymphangiogenesis", *International journal of cancer,* vol. 123, no. 11, pp. 2566-2573.
- Corbo, C., Cromer, W.E., Molinaro, R., Toledano Furman, N.E., Hartman, K.A., De Rosa, E., Boada, C., Wang, X., Zawieja, D.C., Agostini, M., Salvatore, F., Abraham, B.P. & Tasciotti, E. 2017, "Engineered biomimetic nanovesicles show intrinsic anti-inflammatory properties for the treatment of inflammatory bowel diseases", *Nanoscale,* vol. 9, no. 38, pp. 14581-14591.
- Cormier, J.N. & Pollock, R.E. 2004, "Soft tissue sarcomas", *CA: a cancer journal for clinicians,* vol. 54, no. 2, pp. 94-109.
- Couchman, J.R., Multhaupt, H. & Sanderson, R.D. 2016, "Recent Insights into Cell Surface Heparan Sulphate Proteoglycans and Cancer", *F1000Research,* vol. 5, pp. 10.12688/f1000research.8543.1. eCollection 2016.
- de Alava, E. 2007, "Molecular pathology in sarcomas", *Clinical & translational oncology : official publication of the Federation of Spanish Oncology Societies and of the National Cancer Institute of Mexico,* vol. 9, no. 3, pp. 130-144.
- de Bruijn, D.R., Allander, S.V., van Dijk, A.H., Willemse, M.P., Thijssen, J., van Groningen, J.J., Meltzer, P.S. & van Kessel, A.G. 2006, "The synovial-sarcoma-associated SS18-SSX2 fusion protein induces epigenetic gene (de)regulation", *Cancer research,* vol. 66, no. 19, pp. 9474-9482.
- Denzer, K., Kleijmeer, M.J., Heijnen, H.F., Stoorvogel, W. & Geuze, H.J. 2000, "Exosome: from internal vesicle of the multivesicular body to intercellular signaling device", *Journal of cell science,* vol. 113 Pt 19, pp. 3365-3374.

- Desar, I.M.E., Fleuren, E.D.G. & van der Graaf, W.T.A. 2018, "Systemic Treatment for Adults with Synovial Sarcoma", *Current treatment options in oncology*, vol. 19, no. 2, pp. 13-018-0525-1.
- Domanska, U.M., Kruizinga, R.C., Nagengast, W.B., Timmer-Bosscha, H., Huls, G., de Vries, E.G. & Walenkamp, A.M. 2013, "A review on CXCR4/CXCL12 axis in oncology: no place to hide", *European journal of cancer (Oxford, England : 1990)*, vol. 49, no. 1, pp. 219-230.
- Dong, W., Zhao, H., Zhang, C., Geng, P., Sarengaowa, Li, Q., Zhu, J., Li, G., Zhang, S., Ye, M. & Xiao, W. 2014, "Gene silencing of heparanase results in suppression of invasion and migration of hepatoma cells", *World journal of surgical oncology*, vol. 12, pp. 85-7819-12-85.
- Dowdy, S.F. 2017, "Overcoming cellular barriers for RNA therapeutics", *Nature biotechnology*, vol. 35, no. 3, pp. 222-229.
- Dreyfuss, J.L., Regatieri, C.V., Jarrouge, T.R., Cavalheiro, R.P., Sampaio, L.O. & Nader, H.B. 2009, "Heparan sulfate proteoglycans: structure, protein interactions and cell signaling", *Anais da Academia Brasileira de Ciencias*, vol. 81, no. 3, pp. 409-429.
- El Beaino, M., Araujo, D.M., Lazar, A.J. & Lin, P.P. 2017, "Synovial Sarcoma: Advances in Diagnosis and Treatment Identification of New Biologic Targets to Improve Multimodal Therapy", *Annals of surgical oncology*, vol. 24, no. 8, pp. 2145-2154.
- Ewe, A., Panchal, O., Pinnapireddy, S.R., Bakowsky, U., Przybylski, S., Temme, A. & Aigner, A. 2017, "Liposome-polyethylenimine complexes (DPPC-PEI lipopolyplexes) for therapeutic siRNA delivery in vivo", *Nanomedicine : nanotechnology, biology, and medicine*, vol. 13, no. 1, pp. 209-218.
- Fan, L., Wu, Q., Xing, X., Liu, Y. & Shao, Z. 2011, "Targeted silencing of heparanase gene by small interfering RNA inhibits invasiveness and metastasis of osteosarcoma cells", *Journal of Huazhong University of Science and Technology.Medical sciences = Hua zhong ke ji da xue xue bao.Yi xue Ying De wen ban = Huazhong keji daxue xuebao.Yixue Yingdewen ban*, vol. 31, no. 3, pp. 348-352.

- Fire, A., Xu, S., Montgomery, M.K., Kostas, S.A., Driver, S.E. & Mello, C.C. 1998, "Potent and specific genetic interference by double-stranded RNA in Caenorhabditis elegans", *Nature*, vol. 391, no. 6669, pp. 806-811.
- Fletcher, C.D, Bridge, J.A., Hogendoorn, P.C. & Mertens, F. 2013, "WHO Classification of Tumours of Soft Tissue and Bone", *IARC Press, Lyon*.
- Fouladi, M., Stewart, C.F., Blaney, S.M., Onar-Thomas, A., Schaiquevich, P., Packer, R.J., Gajjar, A., Kun, L.E., Boyett, J.M. & Gilbertson, R.J. 2010, "Phase I trial of lapatinib in children with refractory CNS malignancies: a Pediatric Brain Tumor Consortium study", *Journal of clinical oncology : official journal of the American Society of Clinical Oncology*, vol. 28, no. 27, pp. 4221-4227.
- Fux, L., Ilan, N., Sanderson, R.D. & Vlodavsky, I. 2009, "Heparanase: busy at the cell surface", *Trends in biochemical sciences*, vol. 34, no. 10, pp. 511-519.
- Gallagher, J.T. 2001, "Heparan sulfate: growth control with a restricted sequence menu", *The Journal of Clinical Investigation*, vol. 108, no. 3, pp. 357-61.
- Geller, J.I., Roth, J.J. & Biegel, J.A. 2015, "Biology and Treatment of Rhabdoid Tumor", *Critical reviews in oncogenesis*, vol. 20, no. 3-4, pp. 199-216.
- Geoerger, B., Bourdeaut, F., DuBois, S.G., Fischer, M., Geller, J.I., Gottardo, N.G., Marabelle, A., Pearson, A.D.J., Modak, S., Cash, T., Robinson, G.W., Motta, M., Matano, A., Bhansali, S.G., Dobson, J.R., Parasuraman, S. & Chi, S.N. 2017, "A Phase I Study of the CDK4/6 Inhibitor Ribociclib (LEE011) in Pediatric Patients with Malignant Rhabdoid Tumors, Neuroblastoma, and Other Solid Tumors", *Clinical cancer research : an official journal of the American Association for Cancer Research*, vol. 23, no. 10, pp. 2433-2441.
- Gilbert, N.F., Cannon, C.P., Lin, P.P. & Lewis, V.O. 2009, "Soft-tissue sarcoma", *The Journal of the American Academy of Orthopaedic Surgeons*, vol. 17, no. 1, pp. 40-47.
- Gilman, A.L., Jacobsen, C., Bunin, N., Levine, J., Goldman, F., Bendel, A., Joyce, M., Anderson, P., Rozans, M., Wall, D.A., Macdonald, T.J., Simon, S. & Kadota, R.P. 2011, "Phase I study of tandem high-dose chemotherapy with autologous peripheral blood stem cell rescue for children with recurrent brain tumors: a Pediatric Blood and MarrowTransplant Consortium study", *Pediatric blood & cancer*, vol. 57, no. 3, pp. 506-513.

- Gilat, D., Hershkoviz, R., Goldkorn, I., Cahalon, L., Korner, G., Vlodavsky, I. & Lider, O. 1995, "Molecular behavior adapts to context: heparanase functions as an extracellular matrix-degrading enzyme or as a T cell adhesion molecule, depending on the local pH", *The Journal of experimental medicine*, vol. 181, no. 5, pp. 1929-1934.
- Giraudet, A.L., Cassier, P.A., Iwao-Fukukawa, C., Garin, G., Badel, J.N., Kryza, D., Chabaud, S., Gilles-Afchain, L., Clapisson, G., Desuzinges, C., Sarrut, D., Halty, A., Italiano, A., Mori, M., Tsunoda, T., Katagiri, T., Nakamura, Y., Alberti, L., Cropet, C., Baconnier, S., Berge-Montamat, S., Perol, D. & Blay, J.Y. 2018, "A first-in-human study investigating biodistribution, safety and recommended dose of a new radiolabeled MAb targeting FZD10 in metastatic synovial sarcoma patients", *BMC cancer*, vol. 18, no. 1, pp. 646-018-4544-x.
- Godbey, W.T., Wu, K.K. & Mikos, A.G. 2001, "Poly(ethylenimine)-mediated gene delivery affects endothelial cell function and viability", *Biomaterials*, vol. 22, no. 5, pp. 471-480.
- Goldberg, R., Meirovitz, A., Hirshoren, N., Bulvik, R., Binder, A., Rubinstein, A.M. & Elkin, M. 2013, "Versatile role of heparanase in inflammation", *Matrix biology : journal of the International Society for Matrix Biology*, vol. 32, no. 5, pp. 234-240.
- Goldshmidt[a], O., Zcharia, E., Abramovitch, R., Metzger, S., Aingorn, H., Friedmann, Y., Schirrmacher, V., Mitrani, E. & Vlodavsky, I. 2002, "Cell surface expression and secretion of heparanase markedly promote tumor angiogenesis and metastasis", *Proceedings of the National Academy of Sciences of the United States of America*, vol. 99, no. 15, pp. 10031-10036.
- Goldshmidt[b], O., Nadav, L., Aingorn, H., Irit, C., Feinstein, N., Ilan, N., Zamir, E., Geiger, B., Vlodavsky, I. & Katz, B.Z. 2002, "Human heparanase is localized within lysosomes in a stable form", *Experimental cell research*, vol. 281, no. 1, pp. 50-62.
- Goyal, R., Bansal, R., Gandhi, R.P. & Gupta, K.C. 2014, "Copolymers of covalently crosslinked linear and branched polyethylenimines as efficient nucleic acid carriers", *Journal of biomedical nanotechnology*, vol. 10, no. 11, pp. 3269-3279.

- Haldar, M., Hancock, J.D., Coffin, C.M., Lessnick, S.L. & Capecchi, M.R. 2007, "A conditional mouse model of synovial sarcoma: insights into a myogenic origin", *Cancer cell*, vol. 11, no. 4, pp. 375-388.
- Haldar, M., Randall, R.L. & Capecchi, M.R. 2008, "Synovial sarcoma: from genetics to genetic-based animal modeling", *Clinical orthopaedics and related research*, vol. 466, no. 9, pp. 2156-2167.
- Hamidi, M., Azadi, A. & Rafiei, P. 2008, "Hydrogel nanoparticles in drug delivery", *Advanced Drug Delivery Reviews*, vol. 60, no. 15, pp. 1638-1649.
- Hammond, E., Brandt, R. & Dredge, K. 2012, "PG545, a heparan sulfate mimetic, reduces heparanase expression in vivo, blocks spontaneous metastases and enhances overall survival in the 4T1 breast carcinoma model", *PloS one*, vol. 7, no. 12, pp. e52175.
- Hashizume, R., Zhang, A., Mueller, S., Prados, M.D., Lulla, R.R., Goldman, S., Saratsis, A.M., Mazar, A.P., Stegh, A.H., Cheng, S.Y., Horbinski, C., Haas-Kogan, D.A., Sarkaria, J.N., Waldman, T. & James, C.D. 2016, "Inhibition of DNA damage repair by the CDK4/6 inhibitor palbociclib delays irradiated intracranial atypical teratoid rhabdoid tumor and glioblastoma xenograft regrowth", *Neuro-oncology*, vol. 18, no. 11, pp. 1519-1528.
- Hermano, E., Meirovitz, A., Meir, K., Nussbaum, G., Appelbaum, L., Peretz, T. & Elkin, M. 2014, "Macrophage polarization in pancreatic carcinoma: role of heparanase enzyme", *Journal of the National Cancer Institute*, vol. 106, no. 12, pp. 10.1093/jnci/dju332. Print 2014 Dec.
- Herzog, C.E. 2005, "Overview of sarcomas in the adolescent and young adult population", *Journal of pediatric hematology/oncology*, vol. 27, no. 4, pp. 215-218.
- Hook, M., Wasteson, A. & Oldberg, A. 1975, "A heparan sulfate-degrading endoglycosidase from rat liver tissue", *Biochemical and biophysical research communications*, vol. 67, no. 4, pp. 1422-1428.
- Hulett, M.D., Freeman, C., Hamdorf, B.J., Baker, R.T., Harris, M.J. & Parish, C.R. 1999, "Cloning of mammalian heparanase, an important enzyme in tumor invasion and metastasis", *Nature medicine*, vol. 5, no. 7, pp. 803-809.
- Hummel, T.R., Wagner, L., Ahern, C., Fouladi, M., Reid, J.M., McGovern, R.M., Ames, M.M., Gilbertson, R.J., Horton, T., Ingle, A.M., Weigel, B. & Blaney, S.M.

2013, "A pediatric phase 1 trial of vorinostat and temozolomide in relapsed or refractory primary brain or spinal cord tumors: a Children's Oncology Group phase 1 consortium study", *Pediatric blood & cancer*, vol. 60, no. 9, pp. 1452-1457.

- Ilan, N., Elkin, M. & Vlodavsky, I. 2006, "Regulation, function and clinical significance of heparanase in cancer metastasis and angiogenesis", *The international journal of biochemistry & cell biology*, vol. 38, no. 12, pp. 2018-2039.
- Jager, M., Schubert, S., Ochrimenko, S., Fischer, D. & Schubert, U.S. 2012, "Branched and linear poly(ethylene imine)-based conjugates: synthetic modification, characterization, and application", *Chemical Society Reviews*, vol. 41, no. 13, pp. 4755-4767.
- Joseph, C.G., Hwang, H., Jiao, Y., Wood, L.D., Kinde, I., Wu, J., Mandahl, N., Luo, J., Hruban, R.H., Diaz, L.A.,Jr, He, T.C., Vogelstein, B., Kinzler, K.W., Mertens, F. & Papadopoulos, N. 2014, "Exomic analysis of myxoid liposarcomas, synovial sarcomas, and osteosarcomas", *Genes, chromosomes & cancer*, vol. 53, no. 1, pp. 15-24.
- Juliano, R.L. 2016, "The delivery of therapeutic oligonucleotides", *Nucleic acids research*, vol. 44, no. 14, pp. 6518-6548.
- Kaczmarek, J.C., Kowalski, P.S. & Anderson, D.G. 2017, "Advances in the delivery of RNA therapeutics: from concept to clinical reality", *Genome medicine*, vol. 9, no. 1, pp. 60-017-0450-0.
- Kastner, E., Kaur, R., Lowry, D., Moghaddam, B., Wilkinson, A. & Perrie, Y. 2014, "High-throughput manufacturing of size-tuned liposomes by a new microfluidics method using enhanced statistical tools for characterization", *International journal of pharmaceutics*, vol. 477, no. 1-2, pp. 361-368.
- Kastner, E., Verma, V., Lowry, D. & Perrie, Y. 2015, "Microfluidic-controlled manufacture of liposomes for the solubilisation of a poorly water soluble drug", *International journal of pharmaceutics*, vol. 485, no. 1-2, pp. 122-130.
- Kazarin, O., Ilan, N., Naroditzky, I., Ben-Itzhak, O., Vlodavsky, I. & Bar-Sela, G. 2014, "Expression of heparanase in soft tissue sarcomas of adults", *Journal of experimental & clinical cancer research : CR*, vol. 33, pp. 39-9966-33-39.

- Kelly, T., Miao, H.Q., Yang, Y., Navarro, E., Kussie, P., Huang, Y., MacLeod, V., Casciano, J., Joseph, L., Zhan, F., Zangari, M., Barlogie, B., Shaughnessy, J. & Sanderson, R.D. 2003, "High heparanase activity in multiple myeloma is associated with elevated microvessel density", *Cancer research*, vol. 63, no. 24, pp. 8749-8756.
- Kerl[a], K., Holsten, T. & Fruhwald, M.C. 2013, "Rhabdoid tumors: clinical approaches and molecular targets for innovative therapy", *Pediatric hematology and oncology*, vol. 30, no. 7, pp. 587-604.
- Kerl[b], K., Ries, D., Unland, R., Borchert, C., Moreno, N., Hasselblatt, M., Jurgens, H., Kool, M., Gorlich, D., Eveslage, M., Jung, M., Meisterernst, M. & Fruhwald, M. 2013, "The histone deacetylase inhibitor SAHA acts in synergism with fenretinide and doxorubicin to control growth of rhabdoid tumor cells", *BMC cancer*, vol. 13, pp. 286-2407-13-286.
- Kerl, K., Moreno, N., Holsten, T., Ahlfeld, J., Mertins, J., Hotfilder, M., Kool, M., Bartelheim, K., Schleicher, S., Handgretinger, R., Schuller, U., Meisterernst, M. & Fruhwald, M.C. 2014, "Arsenic trioxide inhibits tumor cell growth in malignant rhabdoid tumors in vitro and in vivo by targeting overexpressed Gli1", *International journal of cancer*, vol. 135, no. 4, pp. 989-995.
- Khaled, S.Z., Cevenini, A., Yazdi, I.K., Parodi, A., Evangelopoulos, M., Corbo, C., Scaria, S., Hu, Y., Haddix, S.G., Corradetti, B., Salvatore, F. & Tasciotti, E. 2016, "One-pot synthesis of pH-responsive hybrid nanogel particles for the intracellular delivery of small interfering RNA", *Biomaterials*, vol. 87, pp. 57-68.
- Khvorova, A. & Watts, J.K. 2017, "The chemical evolution of oligonucleotide therapies of clinical utility", *Nature biotechnology*, vol. 35, no. 3, pp. 238-248.
- Kim, H.S., Kim, J.H., Oh, J.H., Lee, M.R., Seol, S.M. & Lee, S.H. 2006, "Expression and clinical significance of heparanasein osteosarcoma", *J Korean Orthop Assoc*, Feb;41(1):43-51.
- Kim, V.N. 2005, "MicroRNA biogenesis: coordinated cropping and dicing", *Nature reviews.Molecular cell biology*, vol. 6, no. 5, pp. 376-385.
- Koga, Y., Matsuzaki, A., Suminoe, A., Hatano, M., Saito, Y., Kinoshita, Y., Tajiri, T., Taguchi, T., Kohashi, K., Oda, Y., Tsuneyoshi, M. & Hara, T. 2009, "Long-term survival after autologous peripheral blood stem cell transplantation in two

patients with malignant rhabdoid tumor of the kidney", *Pediatric blood & cancer,* vol. 52, no. 7, pp. 888-890.

- Kovalszky, I., Hjerpe, A. & Dobra, K. 2014, "Nuclear translocation of heparan sulfate proteoglycans and their functional significance", *Biochimica et biophysica acta,* vol. 1840, no. 8, pp. 2491-2497.
- Kumar, R.M. & Fuchs, B. 2015, "Hedgehog signaling inhibitors as anti-cancer agents in osteosarcoma", *Cancers,* vol. 7, no. 2, pp. 784-794.
- Kurmasheva, R.T., Sammons, M., Favours, E., Wu, J., Kurmashev, D., Cosmopoulos, K., Keilhack, H., Klaus, C.R., Houghton, P.J. & Smith, M.A. 2017, "Initial testing (stage 1) of tazemetostat (EPZ-6438), a novel EZH2 inhibitor, by the Pediatric Preclinical Testing Program", *Pediatric blood & cancer,* vol. 64, no. 3, pp. 10.1002/pbc.26218. Epub 2016 Aug 24.
- Kussie, P.H., Hulmes, J.D., Ludwig, D.L., Patel, S., Navarro, E.C., Seddon, A.P., Giorgio, N.A. & Bohlen, P. 1999, "Cloning and functional expression of a human heparanase gene", *Biochemical and biophysical research communications,* vol. 261, no. 1, pp. 183-187.
- Kwok, A. & Hart, S.L. 2011, "Comparative structural and functional studies of nanoparticle formulations for DNA and siRNA delivery", *Nanomedicine : nanotechnology, biology, and medicine,* vol. 7, no. 2, pp. 210-219.
- Laemmli, U.K. 1970, "Cleavage of structural proteins during the assembly of the head of bacteriophage T4", *Nature,* vol. 227, no. 5259, pp. 680-685.
- Lam, J.K., Chow, M.Y., Zhang, Y. & Leung, S.W. 2015, "siRNA Versus miRNA as Therapeutics for Gene Silencing", *Molecular therapy.Nucleic acids,* vol. 4, pp. e252.
- Lange, S.E.S., Kremer, J.C., Schenone, A.D., Schultze, M.B. & Van Tine B.A. 2014, "Current Management and Molecular Targets of Synovial Sarcoma", *Austin J Cancer Clin Res*;1(2): 1008.
- Lanzi, C., Zaffaroni, N. & Cassinelli, G. 2017, "Targeting Heparan Sulfate Proteoglycans and their Modifying Enzymes to Enhance Anticancer Chemotherapy Efficacy and Overcome Drug Resistance", *Current medicinal chemistry,* vol. 24, no. 26, pp. 2860-2886.

- Lanzi, C. & Cassinelli, G. 2018, "Heparan Sulfate Mimetics in Cancer Therapy: The Challenge to Define Structural Determinants and the Relevance of Targets for Optimal Activity", *Molecules (Basel, Switzerland),* vol. 23, no. 11, pp. 10.3390/molecules23112915.
- Lee, S., Cimica, V., Ramachandra, N., Zagzag, D. & Kalpana, G.V. 2011, "Aurora A is a repressed effector target of the chromatin remodeling protein INI1/hSNF5 required for rhabdoid tumor cell survival", *Cancer research,* vol. 71, no. 9, pp. 3225-3235.
- Leong, F.J. & Leong, A.S. 1996, "Malignant rhabdoid tumor in adults--heterogenous tumors with a unique morphological phenotype", *Pathology, research and practice,* vol. 192, no. 8, pp. 796-807.
- Lewis, J.J., Antonescu, C.R., Leung, D.H., Blumberg, D., Healey, J.H., Woodruff, J.M. & Brennan, M.F. 2000, "Synovial sarcoma: a multivariate analysis of prognostic factors in 112 patients with primary localized tumors of the extremity", *Journal of clinical oncology : official journal of the American Society of Clinical Oncology,* vol. 18, no. 10, pp. 2087-2094.
- Li, W., Guo, L., Rathi, P., Marinova, E., Gao, X., Wu, M.F., Liu, H., Dotti, G., Gottschalk, S., Metelitsa, L.S. & Heczey, A. 2017, "Redirecting T Cells to Glypican-3 with 4-1BB Zeta Chimeric Antigen Receptors Results in Th1 Polarization and Potent Antitumor Activity", *Human Gene Therapy,* vol. 28, no. 5, pp. 437-448.
- Liu, C.J., Chang, J., Lee, P.H., Lin, D.Y., Wu, C.C., Jeng, L.B., Lin, Y.J., Mok, K.T., Lee, W.C., Yeh, H.Z., Ho, M.C., Yang, S.S., Yang, M.D., Yu, M.C., Hu, R.H., Peng, C.Y., Lai, K.L., Chang, S.S. & Chen, P.J. 2014, "Adjuvant heparanase inhibitor PI-88 therapy for hepatocellular carcinoma recurrence", *World journal of gastroenterology,* vol. 20, no. 32, pp. 11384-11393.
- Liu, H., Chen, X., Gao, W. & Jiang, G. 2012, "The expression of heparanase and microRNA-1258 in human non-small cell lung cancer", *Tumour biology : the journal of the International Society for Oncodevelopmental Biology and Medicine,* vol. 33, no. 5, pp. 1327-1334.
- Madia, V.N., Messore, A., Pescatori, L., Saccoliti, F., Tudino, V., De Leo, A., Bortolami, M., Scipione, L., Costi, R., Rivara, S., Scalvini, L., Mor, M., Ferrara, F.F., Pavoni, E., Roscilli, G., Cassinelli, G., Milazzo, F.M., Battistuzzi, G., Di

Santo, R. & Giannini, G. 2018, "Novel Benzazole Derivatives Endowed with Potent Antiheparanase Activity", *Journal of medicinal chemistry,* vol. 61, no. 15, pp. 6918-6936.

- Madigan, C.E., Armenian, S.H., Malogolowkin, M.H. & Mascarenhas, L. 2007, "Extracranial malignant rhabdoid tumors in childhood: the Childrens Hospital Los Angeles experience", *Cancer,* vol. 110, no. 9, pp. 2061-2066.
- Maki, R.G., Jungbluth, A.A., Gnjatic, S., Schwartz, G.K., D'Adamo, D.R., Keohan, M.L., Wagner, M.J., Scheu, K., Chiu, R., Ritter, E., Kachel, J., Lowy, I., Old, L.J. & Ritter, G. 2013, "A Pilot Study of Anti-CTLA4 Antibody Ipilimumab in Patients with Synovial Sarcoma", *Sarcoma,* vol. 2013, pp. 168145.
- Mancuso, T., Mezzelani, A., Riva, C., Fabbri, A., Dal Bo, L., Sampietro, G., Perego, P., Casali, P., Zunino, F., Sozzi, G., Pierotti, M.A. & Pilotti, S. 2000, "Analysis of SYT-SSX fusion transcripts and bcl-2 expression and phosphorylation status in synovial sarcoma", *Laboratory investigation; a journal of technical methods and pathology,* vol. 80, no. 6, pp. 805-813.
- Manon-Jensen, T., Itoh, Y. & Couchman, J.R. 2010, "Proteoglycans in health and disease: the multiple roles of syndecan shedding", *The FEBS journal,* vol. 277, no. 19, pp. 3876-3889.
- Mantovani, A., Allavena, P., Sica, A. & Balkwill, F. 2008, "Cancer-related inflammation", *Nature,* vol. 454, no. 7203, pp. 436-444.
- Martinez, J.O., Molinaro, R., Hartman, K.A., Boada, C., Sukhovershin, R., De Rosa, E., Kirui, D., Zhang, S., Evangelopoulos, M., Carter, A.M., Bibb, J.A., Cooke, J.P. & Tasciotti, E. 2018, "Biomimetic nanoparticles with enhanced affinity towards activated endothelium as versatile tools for theranostic drug delivery", *Theranostics,* vol. 8, no. 4, pp. 1131-1145.
- Masola, V., Maran, C., Tassone, E., Zin, A., Rosolen, A. & Onisto, M. 2009, "Heparanase activity in alveolar and embryonal rhabdomyosarcoma: implications for tumor invasion", *BMC cancer,* vol. 9, pp. 304-2407-9-304.
- Masola, V., Bellin, G., Gambaro, G. & Onisto, M. 2018, "Heparanase: A Multitasking Protein Involved in Extracellular Matrix (ECM) Remodeling and Intracellular Events", *Cells,* vol. 7, no. 12, pp. 10.3390/cells7120236.

- Mason, S.D. & Joyce, J.A. 2011, "Proteolytic networks in cancer", *Trends in cell biology*, vol. 21, no. 4, pp. 228-237.
- Maugis, D. 2013, "Contact, Adhesion and Rupture of Elastic Solids", Vol. 130. *Berlin: Springer Science & Business Media*.
- McBride, M.J., Pulice, J.L., Beird, H.C., Ingram, D.R., D'Avino, A.R., Shern, J.F., Charville, G.W., Hornick, J.L., Nakayama, R.T., Garcia-Rivera, E.M., Araujo, D.M., Wang, W.L., Tsai, J.W., Yeagley, M., Wagner, A.J., Futreal, P.A., Khan, J., Lazar, A.J. & Kadoch, C. 2018, "The SS18-SSX Fusion Oncoprotein Hijacks BAF Complex Targeting and Function to Drive Synovial Sarcoma", *Cancer cell*, vol. 33, no. 6, pp. 1128-1141.e7.
- McKelvey, K.J., Powell, K.L., Ashton, A.W., Morris, J.M. & McCracken, S.A. 2015, "Exosomes: Mechanisms of Uptake", *Journal of circulating biomarkers*, vol. 4, pp. 7-Dec.
- Meirovitz, A., Goldberg, R., Binder, A., Rubinstein, A.M., Hermano, E. & Elkin, M. 2013, "Heparanase in inflammation and inflammation-associated cancer", *The FEBS journal*, vol. 280, no. 10, pp. 2307-2319.
- Mellott, A.J., Forrest, M.L. & Detamore, M.S. 2013, "Physical non-viral gene delivery methods for tissue engineering", *Annals of Biomedical Engineering*, vol. 41, no. 3, pp. 446-468.
- Messore, A., Madia, V.N., Pescatori, L., Saccoliti, F., Tudino, V., De Leo, A., Bortolami, M., De Vita, D., Scipione, L., Pepi, F., Costi, R., Rivara, S., Scalvini, L., Mor, M., Ferrara, F.F., Pavoni, E., Roscilli, G., Cassinelli, G., Milazzo, F.M., Battistuzzi, G., Di Santo, R. & Giannini, G. 2018, "Novel Symmetrical Benzazolyl Derivatives Endowed with Potent Anti-Heparanase Activity", *Journal of medicinal chemistry*, vol. 61, no. 23, pp. 10834-10859.
- Mikami, S., Oya, M., Shimoda, M., Mizuno, R., Ishida, M., Kosaka, T., Mukai, M., Nakajima, M. & Okada, Y. 2008, "Expression of heparanase in renal cell carcinomas: implications for tumor invasion and prognosis", *Clinical cancer research : an official journal of the American Association for Cancer Research*, vol. 14, no. 19, pp. 6055-6061.
- Mitelman, F., Johansson, B. & Mertens, F. 2007, "The impact of translocations and gene fusions on cancer causation", *Nature reviews.Cancer*, vol. 7, no. 4, pp. 233-245.

- Molinaro, R., Wolfram, J., Federico, C., Cilurzo, F., Di Marzio, L., Ventura, C.A., Carafa, M., Celia, C. & Fresta, M. 2013, "Polyethylenimine and chitosan carriers for the delivery of RNA interference effectors", *Expert opinion on drug delivery*, vol. 10, no. 12, pp. 1653-1668.
- Molinaro, R., Corbo, C., Martinez, J.O., Taraballi, F., Evangelopoulos, M., Minardi, S., Yazdi, I.K., Zhao, P., De Rosa, E., Sherman, M.B., De Vita, A., Toledano Furman, N.E., Wang, X., Parodi, A. & Tasciotti, E. 2016, "Biomimetic proteolipid vesicles for targeting inflamed tissues", *Nature materials*, vol. 15, no. 9, pp. 1037-1046.
- Molinaro, R., Evangelopoulos, M., Hoffman, J.R., Corbo, C., Taraballi, F., Martinez, J.O., Hartman, K.A., Cosco, D., Costa, G., Romeo, I., Sherman, M., Paolino, D., Alcaro, S. & Tasciotti, E. 2018, "Design and Development of Biomimetic Nanovesicles Using a Microfluidic Approach", *Advanced materials (Deerfield Beach, Fla.)*, vol. 30, no. 15, pp. e1702749.
- Moreno, N. & Kerl, K. 2016, "Preclinical Evaluation of Combined Targeted Approaches in Malignant Rhabdoid Tumors", *Anticancer Research*, vol. 36, no. 8, pp. 3883-3887.
- Nadir, Y., Brenner, B., Zetser, A., Ilan, N., Shafat, I., Zcharia, E., Goldshmidt, O. & Vlodavsky, I. 2006, "Heparanase induces tissue factor expression in vascular endothelial and cancer cells", *Journal of thrombosis and haemostasis : JTH*, vol. 4, no. 11, pp. 2443-2451.
- Nakajima, M., Irimura, T., Di Ferrante, N. & Nicolson, G.L. 1984, "Metastatic melanoma cell heparanase. Characterization of heparan sulfate degradation fragments produced by B16 melanoma endoglucuronidase", *The Journal of biological chemistry*, vol. 259, no. 4, pp. 2283-2290.
- Natarajan, V., Ramanathan, P., Gopisetty, G., Ramachandran, B., Thangarajan, R. & Kesavan, S. 2018, "In silico and in vitro screening of small molecule Inhibitors against SYT-SSX1 fusion protein in synovial sarcoma", *Computational biology and chemistry*, vol. 77, pp. 36-43.
- Nemes, K. & Fruhwald, M.C. 2018, "Emerging therapeutic targets for the treatment of malignant rhabdoid tumors", *Expert opinion on therapeutic targets*, vol. 22, no. 4, pp. 365-379.

- Ngoune, R., Peters, A., von Elverfeldt, D., Winkler, K. & Putz, G. 2016, "Accumulating nanoparticles by EPR: A route of no return", *Journal of controlled release : official journal of the Controlled Release Society*, vol. 238, pp. 58-70.
- Nikam, R.R. & Gore, K.R. 2018, "Journey of siRNA: Clinical Developments and Targeted Delivery", *Nucleic acid therapeutics*, vol. 28, no. 4, pp. 209-224.
- Nobuhisa, T., Naomoto, Y., Okawa, T., Takaoka, M., Gunduz, M., Motoki, T., Nagatsuka, H., Tsujigiwa, H., Shirakawa, Y., Yamatsuji, T., Haisa, M., Matsuoka, J., Kurebayashi, J., Nakajima, M., Taniguchi, S., Sagara, J., Dong, J. & Tanaka, N. 2007, "Translocation of heparanase into nucleus results in cell differentiation", *Cancer science*, vol. 98, no. 4, pp. 535-540.
- Noujaim, J., Thway, K., Sheri, A., Keller, C. & Jones, R.L. 2016, "Histology-Driven Therapy: The Importance of Diagnostic Accuracy in Guiding Systemic Therapy of Soft Tissue Tumors", *International journal of surgical pathology*, vol. 24, no. 1, pp. 5-15.
- Ogren, S. & Lindahl, U. 1975, "Cleavage of macromolecular heparin by an enzyme from mouse mastocytoma", *The Journal of biological chemistry*, vol. 250, no. 7, pp. 2690-2697.
- Oliveto, S., Mancino, M., Manfrini, N. & Biffo, S. 2017, "Role of microRNAs in translation regulation and cancer", *World journal of biological chemistry*, vol. 8, no. 1, pp. 45-56.
- Orbach, D., Mc Dowell, H., Rey, A., Bouvet, N., Kelsey, A. & Stevens, M.C. 2011, "Sparing strategy does not compromise prognosis in pediatric localized synovial sarcoma: experience of the International Society of Pediatric Oncology, Malignant Mesenchymal Tumors (SIOP-MMT) Working Group", *Pediatric blood & cancer*, vol. 57, no. 7, pp. 1130-1136.
- Osada, H. & Takahashi, T. 2007, "MicroRNAs in biological processes and carcinogenesis", *Carcinogenesis*, vol. 28, no. 1, pp. 2-12.
- Pack, D.W., Hoffman, A.S., Pun, S. & Stayton, P.S. 2005, "Design and development of polymers for gene delivery", *Nature reviews.Drug discovery*, vol. 4, no. 7, pp. 581-593.
- Panagopoulos, I., Mertens, F., Isaksson, M., Limon, J., Gustafson, P., Skytting, B., Akerman, M., Sciot, R., Dal Cin, P., Samson, I., Iliszko, M., Ryoe, J., Debiec-

Rychter, M., Szadowska, A., Brosjo, O., Larsson, O., Rydholm, A. & Mandahl, N. 2001, "Clinical impact of molecular and cytogenetic findings in synovial sarcoma", *Genes, chromosomes & cancer,* vol. 31, no. 4, pp. 362-372.

- Parham, D.M., Weeks, D.A. & Beckwith, J.B. 1994, "The clinicopathologic spectrum of putative extrarenal rhabdoid tumors. An analysis of 42 cases studied with immunohistochemistry or electron microscopy", *The American Journal of Surgical Pathology,* vol. 18, no. 10, pp. 1010-1029.
- Parish, C.R., Freeman, C., Brown, K.J., Francis, D.J. & Cowden, W.B. 1999, "Identification of sulfated oligosaccharide-based inhibitors of tumor growth and metastasis using novel in vitro assays for angiogenesis and heparanase activity", *Cancer research,* vol. 59, no. 14, pp. 3433-3441.
- Petrovic, N. & Ergun, S. 2018, "miRNAs as Potential Treatment Targets and Treatment Options in Cancer", *Molecular diagnosis & therapy,* vol. 22, no. 2, pp. 157-168.
- Pollack, S.M. 2018, "The potential of the CMB305 vaccine regimen to target NY-ESO-1 and improve outcomes for synovial sarcoma and myxoid/round cell liposarcoma patients", *Expert review of vaccines,* vol. 17, no. 2, pp. 107-114.
- Przybyl, J., Jurkowska, M., Rutkowski, P., Debiec-Rychter, M. & Siedlecki, J.A. 2012, "Downstream and intermediate interactions of synovial sarcoma-associated fusion oncoproteins and their implication for targeted therapy", *Sarcoma,* vol. 2012, pp. 249219.
- Purushothaman, A., Chen, L., Yang, Y. & Sanderson, R.D. 2008, "Heparanase stimulation of protease expression implicates it as a master regulator of the aggressive tumor phenotype in myeloma", *The Journal of biological chemistry,* vol. 283, no. 47, pp. 32628-32636.
- Purushothaman, A., Hurst, D.R., Pisano, C., Mizumoto, S., Sugahara, K. & Sanderson, R.D. 2011, "Heparanase-mediated loss of nuclear syndecan-1 enhances histone acetyltransferase (HAT) activity to promote expression of genes that drive an aggressive tumor phenotype", *The Journal of biological chemistry,* vol. 286, no. 35, pp. 30377-30383.
- Ramani, V.C., Purushothaman, A., Stewart, M.D., Thompson, C.A., Vlodavsky, I., Au, J.L. & Sanderson, R.D. 2013, "The heparanase/syndecan-1 axis in cancer: mechanisms and therapies", *The FEBS journal,* vol. 280, no. 10, pp. 2294-2306.

- Ratner, B.D. & Hoffman, A.S., 1976, "Synthetic hydrogels for biomedical applications", *Hydrogels for Medical and Related Applications, ACS Symposium Series*, vol. 31, American Chemical Society, Washington, DC, pp. 1–36.
- Renwick, P.J., Reeves, B.R., Dal Cin, P., Fletcher, C.D., Kempski, H., Sciot, R., Kazmierczak, B., Jani, K., Sonobe, H. & Knight, J.C. 1995, "Two categories of synovial sarcoma defined by divergent chromosome translocation breakpoints in Xp11.2, with implications for the histologic sub-classification of synovial sarcoma", *Cytogenetics and cell genetics*, vol. 70, no. 1-2, pp. 58-63.
- Riaz, A., Ilan, N., Vlodavsky, I., Li, J.P. & Johansson, S. 2013, "Characterization of heparanase-induced phosphatidylinositol 3-kinase-AKT activation and its integrin dependence", *The Journal of biological chemistry*, vol. 288, no. 17, pp. 12366-12375.
- Robbins, P.F., Morgan, R.A., Feldman, S.A., Yang, J.C., Sherry, R.M., Dudley, M.E., Wunderlich, J.R., Nahvi, A.V., Helman, L.J., Mackall, C.L., Kammula, U.S., Hughes, M.S., Restifo, N.P., Raffeld, M., Lee, C.C., Levy, C.L., Li, Y.F., El-Gamil, M., Schwarz, S.L., Laurencot, C. & Rosenberg, S.A. 2011, "Tumor regression in patients with metastatic synovial cell sarcoma and melanoma using genetically engineered lymphocytes reactive with NY-ESO-1", *Journal of clinical oncology : official journal of the American Society of Clinical Oncology*, vol. 29, no. 7, pp. 917-924.
- Rong, R., Doxtader, E.E., Tull, J., de la Roza, G. & Zhang, S. 2009, "Metastatic poorly differentiated monophasic synovial sarcoma to lung with unknown primary: a molecular genetic analysis", *International journal of clinical and experimental pathology*, vol. 3, no. 2, pp. 217-221.
- Rosenfeldt, M.T. & Ryan, K.M. 2011, "The multiple roles of autophagy in cancer", *Carcinogenesis*, vol. 32, no. 7, pp. 955-963.
- Rosson, G.B., Hazen-Martin, D.J., Biegel, J.A., Willingham, M.C., Garvin, A.J., Oswald, B.W., Wainwright, L., Brownlee, N.A. & Wright, C.F. 1998, "Establishment and molecular characterization of five cell lines derived from renal and extrarenal malignant rhabdoid tumors", *Modern pathology : an official journal of the United States and Canadian Academy of Pathology, Inc*, vol. 11, no. 12, pp. 1228-1237.

- Saito, T., Nagai, M. & Ladanyi, M. 2006, "SYT-SSX1 and SYT-SSX2 interfere with repression of E-cadherin by snail and slug: a potential mechanism for aberrant mesenchymal to epithelial transition in human synovial sarcoma", *Cancer research*, vol. 66, no. 14, pp. 6919-6927.
- Saito, T. 2013, "The SYT-SSX fusion protein and histological epithelial differentiation in synovial sarcoma: relationship with extracellular matrix remodeling", *International journal of clinical and experimental pathology*, vol. 6, no. 11, pp. 2272-2279.
- Sanderson, R.D., Elkin, M., Rapraeger, A.C., Ilan, N. & Vlodavsky, I. 2017, "Heparanase regulation of cancer, autophagy and inflammation: new mechanisms and targets for therapy", *The FEBS journal*, vol. 284, no. 1, pp. 42-55.
- Sarrazin, S., Lamanna, W.C. & Esko, J.D. 2011, "Heparan sulfate proteoglycans", *Cold Spring Harbor perspectives in biology*, vol. 3, no. 7, pp. 10.1101/cshperspect.a004952.
- Schott, J.W., Morgan, M., Galla, M. & Schambach, A. 2016, "Viral and Synthetic RNA Vector Technologies and Applications", *Molecular therapy : the journal of the American Society of Gene Therapy*, vol. 24, no. 9, pp. 1513-1527.
- Schubert, S.Y., Ilan, N., Shushy, M., Ben-Izhak, O., Vlodavsky, I. & Goldshmidt, O. 2004, "Human heparanase nuclear localization and enzymatic activity", *Laboratory investigation; a journal of technical methods and pathology*, vol. 84, no. 5, pp. 535-544.
- Schwartz, D.L., Einck, J., Hunt, K., Bruckner, J., Conrad, E., Koh, W.J. & Laramore, G.E. 2002, "The effect of delayed postoperative irradiation on local control of soft tissue sarcomas of the extremity and torso", *International journal of radiation oncology, biology, physics*, vol. 52, no. 5, pp. 1352-1359.
- Secchi, M.F., Masola, V., Zaza, G., Lupo, A., Gambaro, G. & Onisto, M. 2015, "Recent data concerning heparanase: focus on fibrosis, inflammation and cancer", *Biomolecular concepts*, vol. 6, no. 5-6, pp. 415-421.
- Setsu, N., Kohashi, K., Fushimi, F., Endo, M., Yamamoto, H., Takahashi, Y., Yamada, Y., Ishii, T., Yokoyama, K., Iwamoto, Y. & Oda, Y. 2013, "Prognostic impact of the activation status of the Akt/mTOR pathway in synovial sarcoma", *Cancer*, vol. 119, no. 19, pp. 3504-3513.

- Shafat, I., Vlodavsky, I. & Ilan, N. 2006, "Characterization of mechanisms involved in secretion of active heparanase", *The Journal of biological chemistry*, vol. 281, no. 33, pp. 23804-23811.
- Shafat, I., Barak, A.B., Postovsky, S., Elhasid, R., Ilan, N., Vlodavsky, I. & Arush, M.W. 2007, "Heparanase levels are elevated in the plasma of pediatric cancer patients and correlate with response to anticancer treatment", *Neoplasia (New York, N.Y.)*, vol. 9, no. 11, pp. 909-916.
- Shafat, I., Ben-Arush, M.W., Issakov, J., Meller, I., Naroditsky, I., Tortoreto, M., Cassinelli, G., Lanzi, C., Pisano, C., Ilan, N., Vlodavsky, I. & Zunino, F. 2011, "Pre-clinical and clinical significance of heparanase in Ewing's sarcoma", *Journal of Cellular and Molecular Medicine*, vol. 15, no. 9, pp. 1857-1864.
- Sheng, N., Zhang, L. & Yang, S. 2018, "MicroRNA-429 decreases the invasion ability of gastric cancer cell line BGC-823 by downregulating the expression of heparanase", *Experimental and therapeutic medicine*, vol. 15, no. 2, pp. 1927-1933.
- Shi, J., Chen, P., Sun, J., Song, Y., Ma, B., Gao, P., Chen, X. & Wang, Z. 2017, "MicroRNA-1258: An invasion and metastasis regulator that targets heparanase in gastric cancer", *Oncology letters*, vol. 13, no. 5, pp. 3739-3745.
- Shteingauz, A., Boyango, I., Naroditsky, I., Hammond, E., Gruber, M., Doweck, I., Ilan, N. & Vlodavsky, I. 2015, "Heparanase Enhances Tumor Growth and Chemoresistance by Promoting Autophagy", *Cancer research*, vol. 75, no. 18, pp. 3946-3957.
- Siegel, R.L., Miller, K.D. & Jemal, A. 2018, "Cancer statistics, 2018", *CA: a cancer journal for clinicians*, vol. 68, no. 1, pp. 7-30.
- Skoda, A.M., Simovic, D., Karin, V., Kardum, V., Vranic, S. & Serman, L. 2018, "The role of the Hedgehog signaling pathway in cancer: A comprehensive review", *Bosnian journal of basic medical sciences*, vol. 18, no. 1, pp. 8-20.
- Su, J.M., Li, X.N., Thompson, P., Ou, C.N., Ingle, A.M., Russell, H., Lau, C.C., Adamson, P.C. & Blaney, S.M. 2011, "Phase 1 study of valproic acid in pediatric patients with refractory solid or CNS tumors: a children's oncology group report", *Clinical cancer research : an official journal of the American Association for Cancer Research*, vol. 17, no. 3, pp. 589-597.

- Sultan, I., Rodriguez-Galindo, C., Saab, R., Yasir, S., Casanova, M. & Ferrari, A. 2009, "Comparing children and adults with synovial sarcoma in the Surveillance, Epidemiology, and End Results program, 1983 to 2005: an analysis of 1268 patients", *Cancer,* vol. 115, no. 15, pp. 3537-3547.
- Sultan, I., Casanova, M., Al-Jumaily, U., Meazza, C., Rodriguez-Galindo, C. & Ferrari, A. 2010, "Soft tissue sarcomas in the first year of life", *European journal of cancer (Oxford, England : 1990),* vol. 46, no. 13, pp. 2449-2456.
- Sun, Y., Gao, D., Liu, Y., Huang, J., Lessnick, S. & Tanaka, S. 2006, "IGF2 is critical for tumorigenesis by synovial sarcoma oncoprotein SYT-SSX1", *Oncogene,* vol. 25, no. 7, pp. 1042-1052.
- Takenaka, S., Ueda, T., Naka, N., Araki, N., Hashimoto, N., Myoui, A., Ozaki, T., Nakayama, T., Toguchida, J., Tanaka, K., Iwamoto, Y., Matsumine, A., Uchida, A., Ieguchi, M., Kaya, M., Wada, T., Baba, I., Kudawara, I., Aoki, Y. & Yoshikawa, H. 2008, "Prognostic implication of SYT-SSX fusion type in synovial sarcoma: a multi-institutional retrospective analysis in Japan", *Oncology reports,* vol. 19, no. 2, pp. 467-476.
- Tang, D., Zhang, Q., Zhao, S., Wang, J., Lu, K., Song, Y., Zhao, L., Kang, X., Wang, J., Xu, S. & Tian, L. 2013, "The expression and clinical significance of microRNA-1258 and heparanase in human breast cancer", *Clinical biochemistry*, vol. 46, no. 10-11, pp. 926-932.
- Tang, Y., Gholamin, S., Schubert, S., Willardson, M.I., Lee, A., Bandopadhayay, P., Bergthold, G., Masoud, S., Nguyen, B., Vue, N., Balansay, B., Yu, F., Oh, S., Woo, P., Chen, S., Ponnuswami, A., Monje, M., Atwood, S.X., Whitson, R.J., Mitra, S., Cheshier, S.H., Qi, J., Beroukhim, R., Tang, J.Y., Wechsler-Reya, R., Oro, A.E., Link, B.A., Bradner, J.E. & Cho, Y.J. 2014, "Epigenetic targeting of Hedgehog pathway transcriptional output through BET bromodomain inhibition", *Nature medicine,* vol. 20, no. 7, pp. 732-740.
- Tatiparti, K., Sau, S., Kashaw, S.K. & Iyer, A.K. 2017, "siRNA Delivery Strategies: A Comprehensive Review of Recent Developments", *Nanomaterials (Basel, Switzerland),* vol. 7, no. 4, pp. 10.3390/nano7040077.
- Tekautz, T.M., Fuller, C.E., Blaney, S., Fouladi, M., Broniscer, A., Merchant, T.E., Krasin, M., Dalton, J., Hale, G., Kun, L.E., Wallace, D., Gilbertson, R.J. & Gajjar, A. 2005, "Atypical teratoid/rhabdoid tumors (ATRT): improved survival in

children 3 years of age and older with radiation therapy and high-dose alkylator-based chemotherapy", *Journal of clinical oncology : official journal of the American Society of Clinical Oncology*, vol. 23, no. 7, pp. 1491-1499.

- Thiemann, M., Oertel, S., Ehemann, V., Weichert, W., Stenzinger, A., Bischof, M., Weber, K.J., Perez, R.L., Haberkorn, U., Kulozik, A.E., Debus, J., Huber, P.E. & Battmann, C. 2012, "In vivo efficacy of the histone deacetylase inhibitor suberoylanilide hydroxamic acid in combination with radiotherapy in a malignant rhabdoid tumor mouse model", *Radiation oncology (London, England)*, vol. 7, pp. 52-717X-7-52.
- Thomas, D.M., Savage, S.A. & Bond, G.L. 2012, "Hereditary and environmental epidemiology of sarcomas", *Clinical sarcoma research*, vol. 2, no. 1, pp. 13-3329-2-13.
- Thompson, C.A., Purushothaman, A., Ramani, V.C., Vlodavsky, I. & Sanderson, R.D. 2013, "Heparanase regulates secretion, composition, and function of tumor cell-derived exosomes", *The Journal of biological chemistry*, vol. 288, no. 14, pp. 10093-10099.
- Torres-Martinez, S. & Ruiz-Vazquez, R.M. 2017, "The RNAi Universe in Fungi: A Varied Landscape of Small RNAs and Biological Functions", *Annual Review of Microbiology*, vol. 71, pp. 371-391.
- Torri, A., Carpi, D., Bulgheroni, E., Crosti, M.C., Moro, M., Gruarin, P., Rossi, R.L., Rossetti, G., Di Vizio, D., Hoxha, M., Bollati, V., Gagliani, C., Tacchetti, C., Paroni, M., Geginat, J., Corti, L., Venegoni, L., Berti, E., Pagani, M., Matarese, G., Abrignani, S. & de Candia, P. 2017, "Extracellular MicroRNA Signature of Human Helper T Cell Subsets in Health and Autoimmunity", *The Journal of biological chemistry*, vol. 292, no. 7, pp. 2903-2915.
- Toyoshima, M. & Nakajima, M. 1999, "Human heparanase. Purification, characterization, cloning, and expression", *The Journal of biological chemistry*, vol. 274, no. 34, pp. 24153-24160.
- Trautmann, M., Sievers, E., Aretz, S., Kindler, D., Michels, S., Friedrichs, N., Renner, M., Kirfel, J., Steiner, S., Huss, S., Koch, A., Penzel, R., Larsson, O., Kawai, A., Tanaka, S., Sonobe, H., Waha, A., Schirmacher, P., Mechtersheimer, G., Wardelmann, E., Buttner, R. & Hartmann, W. 2014, "SS18-SSX fusion protein-

induced Wnt/beta-catenin signaling is a therapeutic target in synovial sarcoma", *Oncogene*, vol. 33, no. 42, pp. 5006-5016.

- Valadi, H., Ekstrom, K., Bossios, A., Sjostrand, M., Lee, J.J. & Lotvall, J.O. 2007, "Exosome-mediated transfer of mRNAs and microRNAs is a novel mechanism of genetic exchange between cells", *Nature cell biology*, vol. 9, no. 6, pp. 654-659.
- van Balkom, B.W., Pisitkun, T., Verhaar, M.C. & Knepper, M.A. 2011, "Exosomes and the kidney: prospects for diagnosis and therapy of renal diseases", *Kidney international*, vol. 80, no. 11, pp. 1138-1145.
- van de Ven, A.L., Abdollahi, B., Martinez, C.J., Burey, L.A., Landis, M.D., Chang, J.C., Ferrari, M. & Frieboes, H.B. 2013, "Modeling of nanotherapeutics delivery based on tumor perfusion", *New journal of physics*, vol. 15, pp. 55004-2630/15/5/055004.
- van de Water, F.M., Boerman, O.C., Wouterse, A.C., Peters, J.G., Russel, F.G. & Masereeuw, R. 2006, "Intravenously administered short interfering RNA accumulates in the kidney and selectively suppresses gene function in renal proximal tubules", *Drug metabolism and disposition: the biological fate of chemicals*, vol. 34, no. 8, pp. 1393-1397.
- van der Ree, M.H., van der Meer, A.J., van Nuenen, A.C., de Bruijne, J., Ottosen, S., Janssen, H.L., Kootstra, N.A. & Reesink, H.W. 2016, "Miravirsen dosing in chronic hepatitis C patients results in decreased microRNA-122 levels without affecting other microRNAs in plasma", *Alimentary Pharmacology & Therapeutics*, vol. 43, no. 1, pp. 102-113.
- van Gool, S.W., Holm, S., Rachor, J., Adamson, L., Technau, A., Maass, E., Fruhwald, M.C., Schlegel, P.G. & Eyrich, M. 2016, "Immunotherapy in atypical teratoid-rhabdoid tumors: Data from a survey of the HGG-Immuno Group", *Cytotherapy*, vol. 18, no. 9, pp. 1178-1186.
- Versteege, I., Sevenet, N., Lange, J., Rousseau-Merck, M.F., Ambros, P., Handgretinger, R., Aurias, A. & Delattre, O. 1998, "Truncating mutations of hSNF5/INI1 in aggressive paediatric cancer", *Nature*, vol. 394, no. 6689, pp. 203-206.
- Vlodavsky, I., Friedmann, Y., Elkin, M., Aingorn, H., Atzmon, R., Ishai-Michaeli, R., Bitan, M., Pappo, O., Peretz, T., Michal, I., Spector, L. & Pecker, I. 1999,

"Mammalian heparanase: gene cloning, expression and function in tumor progression and metastasis", *Nature medicine,* vol. 5, no. 7, pp. 793-802.

- Vlodavsky, I. & Friedmann, Y. 2001, "Molecular properties and involvement of heparanase in cancer metastasis and angiogenesis", *The Journal of clinical investigation,* vol. 108, no. 3, pp. 341-347.
- Vlodavsky, I., Elkin, M. & Ilan, N. 2011, "Impact of heparanase and the tumor microenvironment on cancer metastasis and angiogenesis: basic aspects and clinical applications", *Rambam Maimonides medical journal,* vol. 2, no. 1, pp. e0019.
- Vlodavsky, I., Beckhove, P., Lerner, I., Pisano, C., Meirovitz, A., Ilan, N. & Elkin, M. 2012, "Significance of heparanase in cancer and inflammation", *Cancer microenvironment : official journal of the International Cancer Microenvironment Society,* vol. 5, no. 2, pp. 115-132.
- Vlodavsky, I., Singh, P., Boyango, I., Gutter-Kapon, L., Elkin, M., Sanderson, R.D. & Ilan, N. 2016, "Heparanase: From basic research to therapeutic applications in cancer and inflammation", *Drug resistance updates : reviews and commentaries in antimicrobial and anticancer chemotherapy,* vol. 29, pp. 54-75.
- Vreys, V. & David, G. 2007, "Mammalian heparanase: what is the message?", *Journal of Cellular and Molecular Medicine,* vol. 11, no. 3, pp. 427-452.
- Wagner, E. 2014, "Polymers for nucleic acid transfer-an overview", *Advances in Genetics,* vol. 88, pp. 231-261.
- Wakamatsu, T., Naka, N., Sasagawa, S., Tanaka, T., Takenaka, S., Araki, N., Ueda, T., Nishizawa, Y., Yoshikawa, H. & Itoh, K. 2014, "Deflection of vascular endothelial growth factor action by SS18-SSX and composite vascular endothelial growth factor- and chemokine (C-X-C motif) receptor 4-targeted therapy in synovial sarcoma", *Cancer science,* vol. 105, no. 9, pp. 1124-1134.
- Wasungu, L. & Hoekstra, D. 2006, "Cationic lipids, lipoplexes and intracellular delivery of genes", *Journal of controlled release : official journal of the Controlled Release Society,* vol. 116, no. 2, pp. 255-264.
- Wei, S., Henderson-Jackson, E., Qian, X. & Bui, M.M. 2017, "Soft Tissue Tumor Immunohistochemistry Update: Illustrative Examples of Diagnostic Pearls to Avoid Pitfalls", *Archives of Pathology & Laboratory Medicine,* vol. 141, no. 8, pp. 1072-1091.

- Weissmann, M., Arvatz, G., Horowitz, N., Feld, S., Naroditsky, I., Zhang, Y., Ng, M., Hammond, E., Nevo, E., Vlodavsky, I. & Ilan, N. 2016, "Heparanase-neutralizing antibodies attenuate lymphoma tumor growth and metastasis", *Proceedings of the National Academy of Sciences of the United States of America*, vol. 113, no. 3, pp. 704-709.
- Weissmann, M., Bhattacharya, U., Feld, S., Hammond, E., Ilan, N. & Vlodavsky, I. 2018, "The heparanase inhibitor PG545 is a potent anti-lymphoma drug: Mode of action", *Matrix biology : journal of the International Society for Matrix Biology*, .
- Werth, S., Urban-Klein, B., Dai, L., Hobel, S., Grzelinski, M., Bakowsky, U., Czubayko, F. & Aigner, A. 2006, "A low molecular weight fraction of polyethylenimine (PEI) displays increased transfection efficiency of DNA and siRNA in fresh or lyophilized complexes", *Journal of controlled release : official journal of the Controlled Release Society*, vol. 112, no. 2, pp. 257-270.
- Wetmore, C., Boyett, J., Li, S., Lin, T., Bendel, A., Gajjar, A. & Orr, B.A. 2015, "Alisertib is active as single agent in recurrent atypical teratoid rhabdoid tumors in 4 children", *Neuro-oncology*, vol. 17, no. 6, pp. 882-888.
- Whitehead, K.A., Langer, R. & Anderson, D.G. 2009, "Knocking down barriers: advances in siRNA delivery", *Nature reviews.Drug discovery*, vol. 8, no. 2, pp. 129-138.
- Wilson, B.G., Wang, X., Shen, X., McKenna, E.S., Lemieux, M.E., Cho, Y.J., Koellhoffer, E.C., Pomeroy, S.L., Orkin, S.H. & Roberts, C.W. 2010, "Epigenetic antagonism between polycomb and SWI/SNF complexes during oncogenic transformation", *Cancer cell*, vol. 18, no. 4, pp. 316-328.
- Wu, L., Viola, C.M., Brzozowski, A.M. & Davies, G.J. 2015, "Structural characterization of human heparanase reveals insights into substrate recognition", *Nature structural & molecular biology*, vol. 22, no. 12, pp. 1016-1022.
- Wu, X., Dagar, V., Algar, E., Muscat, A., Bandopadhayay, P., Ashley, D. & Wo Chow, C. 2008, "Rhabdoid tumour: a malignancy of early childhood with variable primary site, histology and clinical behaviour", *Pathology*, vol. 40, no. 7, pp. 664-670.
- Wu, Y., Bi, W., Han, G., Jia, J. & Xu, M. 2017, "Influence of neoadjuvant chemotherapy on prognosis of patients with synovial sarcoma", *World journal of surgical oncology*, vol. 15, no. 1, pp. 101-017-1165-9.

- Xie, Y., Skytting, B., Nilsson, G., Brodin, B. & Larsson, O. 1999, "Expression of insulin-like growth factor-1 receptor in synovial sarcoma: association with an aggressive phenotype", *Cancer research,* vol. 59, no. 15, pp. 3588-3591.
- Xiong, Z., Lu, M.H., Fan, Y.H., Cao, Y.L., Hu, C.J., Wu, Y.Y., Wang, S.M., Luo, G., Fang, D.C., Li, C. & Yang, S.M. 2012, "Downregulation of heparanase by RNA interference inhibits invasion and tumorigenesis of hepatocellular cancer cells in vitro and in vivo", *International journal of oncology,* vol. 40, no. 5, pp. 1601-1609.
- Xu, Y. & Szoka, F.C.,Jr 1996, "Mechanism of DNA release from cationic liposome/DNA complexes used in cell transfection", *Biochemistry,* vol. 35, no. 18, pp. 5616-5623.
- Yahalom, J., Eldor, A., Fuks, Z. & Vlodavsky, I. 1984, "Degradation of sulfated proteoglycans in the subendothelial extracellular matrix by human platelet heparitinase", *The Journal of clinical investigation,* vol. 74, no. 5, pp. 1842-1849.
- Yang, J., Deng, L.H., Han, C.R., Duan, J.F., Ma, M.G., Zhang, X.M., Xu, F. & Sun, R.C. 2013, "Synthetic and viscoelastic behaviors of silica nanoparticle reinforced poly(acrylamide) core–shell nanocomposite hydrogels"*, Soft Matter*, 9 , 1220 -1230.
- Yang, Y., Gorzelanny, C., Bauer, A.T., Halter, N., Komljenovic, D., Bauerle, T., Borsig, L., Roblek, M. & Schneider, S.W. 2015, "Nuclear heparanase-1 activity suppresses melanoma progression via its DNA-binding affinity", *Oncogene,* vol. 34, no. 47, pp. 5832-5842.
- Zahm, S.H. & Fraumeni, J.F.,Jr 1997, "The epidemiology of soft tissue sarcoma", *Seminars in oncology,* vol. 24, no. 5, pp. 504-514.
- Zcharia, E., Jia, J., Zhang, X., Baraz, L., Lindahl, U., Peretz, T., Vlodavsky, I. & Li, J.P. 2009, "Newly generated heparanase knock-out mice unravel co-regulation of heparanase and matrix metalloproteinases", *PloS one,* vol. 4, no. 4, pp. e5181.
- Zetser, A., Levy-Adam, F., Kaplan, V., Gingis-Velitski, S., Bashenko, Y., Schubert, S., Flugelman, M.Y., Vlodavsky, I. & Ilan, N. 2004, "Processing and activation of latent heparanase occurs in lysosomes", *Journal of cell science,* vol. 117, no. Pt 11, pp. 2249-2258.

- Zhang, L., Sullivan, P.S., Goodman, J.C., Gunaratne, P.H. & Marchetti, D. 2011, "MicroRNA-1258 suppresses breast cancer brain metastasis by targeting heparanase", *Cancer research,* vol. 71, no. 3, pp. 645-654.
- Zhang, P., An, K., Duan, X., Xu, H., Li, F. & Xu, F. 2018, "Recent advances in siRNA delivery for cancer therapy using smart nanocarriers", *Drug discovery today,* vol. 23, no. 4, pp. 900-911.
- Zhang, S., Zhao, B., Jiang, H., Wang, B. & Ma, B. 2007, "Cationic lipids and polymers mediated vectors for delivery of siRNA", *Journal of controlled release : official journal of the Controlled Release Society,* vol. 123, no. 1, pp. 1-10.
- Zheng, L.D., Jiang, G.S., Pu, J.R., Mei, H., Dong, J.H., Hou, X.H. & Tong, Q.S. 2009, "Stable knockdown of heparanase expression in gastric cancer cells in vitro", *World journal of gastroenterology,* vol. 15, no. 43, pp. 5442-5448.
- Zheng, L.D., Jiang, G.S., Mei, H., Pu, J.R., Dong, J.H., Hou, X.H. & Tong, Q.S. 2010, "Small RNA interference-mediated gene silencing of heparanase abolishes the invasion, metastasis and angiogenesis of gastric cancer cells", *BMC cancer,* vol. 10, pp. 33-2407-10-33.
- Zhou, H., Roy, S., Cochran, E., Zouaoui, R., Chu, C.L., Duffner, J., Zhao, G., Smith, S., Galcheva-Gargova, Z., Karlgren, J., Dussault, N., Kwan, R.Y., Moy, E., Barnes, M., Long, A., Honan, C., Qi, Y.W., Shriver, Z., Ganguly, T., Schultes, B., Venkataraman, G. & Kishimoto, T.K. 2011, "M402, a novel heparan sulfate mimetic, targets multiple pathways implicated in tumor progression and metastasis", *PloS one,* vol. 6, no. 6, pp. e21106.
- Zhuge, Y., Cheung, M.C., Yang, R., Perez, E.A., Koniaris, L.G. & Sola, J.E. 2010, "Pediatric non-Wilms renal tumors: subtypes, survival, and prognostic indicators", *The Journal of surgical research,* vol. 163, no. 2, pp. 257-263.

PUBLICATIONS

Publications related to my PhD project

- Parodi, A., Molinaro, R., Sushnitha, M., Evangelopoulos, M., Martinez, J.O., **Arrighetti, N.,** Corbo, C. & Tasciotti, E. 2018, "Bio-inspired engineering of cell- and virus-like nanoparticles for drug delivery", *Biomaterials*, Sep 22;147:155-168.
- **Arrighetti, N.,** Corbo, C., Evangelopoulos, M., Pasto, A., Zuco, V. & Tasciotti, E. 2018, "Exosome-like nanovectors for drug delivery in cancer", *Curr Med Chem*, In press.
- Parodi, A., **Arrighetti, N.,** Evangelopoulos, M., Cevenini, A., Livingston, M., Khaled, S.Z., Taraballi, F., Brown, B.S., Yazdi, I.K., Campa-Carranza, J.N. & Tasciotti, E. 2019, "Biological impact of nanoparticle endosomal escape and re-compartmentalization in multilamellar bodies", submitted at *Small.*

Other publications

- Gatti, L., De Cesare, M., Ciusani, E., Corna, E., **Arrighetti, N.,** Cominetti, D., Belvisi, L., Potenza, D., Moroni, E., Vasile, F., Lecis, D., Delia, D., Castiglioni, V., Scanziani, E., Seneci, P., Zaffaroni, N. & Perego P. 2014, "Antitumor activity of a novel homodimeric SMAC mimetic in ovarian carcinoma", *Mol Pharm*, 11:283-93.
- Gatti, L., Cossa, G., Tinelli, S., Carenini, N., **Arrighetti, N.,** Pennati, M., Cominetti, D., De Cesare, M., Zunino, F., Zaffaroni, N. & Perego P. 2014, "Improved apoptotic cell death in drug-resistant non small cell lung cancer cells by TRAIL-based treatment", *J Pharmacol Exp Ther*, 348:360–371.
- Cossa, G., Lanzi, C., Cassinelli, G., Carenini, N., **Arrighetti, N.,** Gatti, L., Corna, E., Zunino, F., Zaffaroni, N. & Perego, P. Differential outcome of MEK1/2 inhibitor-platinum combinations in platinum-sensitive and -resistant ovarian carcinoma cells. *Cancer Lett*, 2014 Jun 1;347(2):212-24.
- Gatti, L., Sevko, A., De Cesare, M., **Arrighetti, N.,** Manenti, G., Ciusani, E., Verderio, P., Ciniselli, C.M., Cominetti, D., Carenini, N., Corna, E., Zaffaroni, N., Rodolfo, M., Rivoltini, L., Umansky, V. & Perego, P. 2014, "Histone deacetylase inhibitor-temozolomide co-treatment inhibits melanoma growth through suppression of Chemokine (C-C motif) ligand 2-driven signals", *Oncotarget*, Jun 30;5(12):4516-28.

- Gabrielli, L., Calloni, I., Donvito, G., Costa, B., **Arrighetti, N.,** Perego, P., Colombo, D., Ronchetti, F., Nicotra, F. & Cipolla, L. 2014, "Phosphatidylinositol 3-Phosphate Mimics Based on a Sulfoquinovose Scaffold: Synthesis and Evaluation as Protein Kinase B Inhibitors", *Eur. J. Org. Chem*, 5962–5967.
- Vetro, M., Costa, B., Donvito, G., **Arrighetti, N.,** Cipolla, L., Perego, P., Compostella, F., Ronchetti, F. & Colombo, D. 2015, "Anionic glycolipids related to glucuronosyldiacylglycerol inhibit protein kinase Akt", *Org Biomol Chem*, Jan 28;13(4):1091-9
- **Arrighetti, N.,** Corno, C. & Gatti, L. 2015, "Drug Combinations with HDAC Inhibitors in Antitumor Therapy", *Crit Rev Oncog*, 20(1-2):83-117.
- **Arrighetti, N.,** Cossa, G., De Cecco, L., Stucchi, S., Carenini, N., Corna, E., Gandellini, P., Zaffaroni, N., Perego, P. & Gatti, L.2016, "PKC alpha modulationby miR-483-3p in platinum-resistant ovarian carcinoma cells", *Toxicol Appl Pharmacol*, 1;310:9-19.
- El Bezawy, R., Cominetti, D., Fenderico, N., Zuco, V., Beretta, G.L., Dugo, M., **Arrighetti, N.,** Stucchi, C., Rancati, T., Valdagni, R., Zaffaroni, N. & Gandellini, P. 2017, "miR-875-5p counteracts epithelial-to-mesenchymal transition and enhances radiation response in prostate cancer through repression of the EGFR-ZEB1 axis", *Cancer Lett*, Mar 6. S0304-3835(17)30150-7
- Corno, C., Gatti, L., **Arrighetti, N.,** Carenini, N., Zaffaroni, N., Lanzi, C. & Perego, P. 2017, "Axl molecular targeting counteracts aggressiveness but not platinum-resistance of ovarian carcinoma cells", *Biochem Pharmacol*, Apr 9. pii: S0006-2952(17)30191-0.
- Lanzi, C., Dal Bo, L., Favini, E., Tortoreto, M., Beretta, G.L., **Arrighetti, N.,** Zaffaroni, N. & Cassinelli, G. 2019, "Overactive IGF1/Insulin receptors and NRASQ61R mutation drive mechanisms of resistance to pazopanib and define rational combination strategies to treat synovial sarcoma", *Cancers*, 11, 408.

DECLARATION OF AUTHORSHIP

This dissertation is submitted for the degree of Doctor of Philosophy at The Open University (Milton Keynes, UK).

I hereby certify that the thesis I am submitting is entirely my own original work, except for part of the work carried out at the HMRI:

- The synthesis of HNPs was performed by Dr. Francesca Taraballi from the Center for Biomimetic Medicine.
- The characterisation of HNPs was performed in collaboration with Dr. Francesca Taraballi.
- The synthesis and physico-chemical characterisation of leukosomes were performed by Kelly Hartman and Roberto Molinaro from the Center for Biomimetic Medicine.
- The FACS analyses of HNPs and leukosomes were performed in collaboration with Dr. Francesca Taraballi.
- The preparation of samples and the TEM were performed by Clair Haueter from the Electron Microscopy Core.
- The confocal microscopy analyses were performed in collaboration with Dr. Francesca Taraballi.
- The IVM experiments and analyses were performed by Dr. Enrica De Rosa, from the Intravital Microscopy Core.